UNIVERSITY OF PISA

Ph.D. *in* **CHEMICAL SCIENCES** - *XXII Cycle*

Ecocompatible, Biodegradable Polymers.
Plastic Items
Preparation & Characterization

Arianna Barghini

Supervisor: Prof./Dr. Emo Chiellini

Tutor: Dr. Elizabeth Grillo Fernandes

Department of Chemistry and Industrial Chemistry

SSD: CHIM/05

ACKNOWLEDGEMENTS

During the work on this Thesis, my life was characterized by some events that modified it.

My marriage, the born of a child and the discover of a thyroid carcinoma weren't loss many time to imagine the moment in which I would get to this part.

Only now I realize this situation, looking back at this period of my life with pleasure and gratitude.

Finally, this moment will come. The examiners will evaluate the results of this work, but I can certainly say that the process will be pleasant. So I am glad to complete it by remembering many wonderful people who have contributed to it in various ways.

My firsts thanks goes to God, for its constant presence in my life, for guiding my choices and for the comfort in the difficult moments.

Sincere thanks to my supervisor, Prof. Emo Chiellini, who gave me the opportunity to achieve this important objective.

I also thank the reading committee members who kindly agreed to read my manuscript and to participate in this discussion.

Special thanks to Maria Viola, Michela Bianchi and Maria Caccamo.

Persons that help me in all situations!

Very special thanks to my tutor Dr: Elizabeth Grillo Fernandes (Beth) and the Prof. Syed Imam; they had been so generous with their time. For all the teachings, friendship, trust and patience I am truly grateful.

I would also like to thank several people from the DCCI and BIOLAB for all time we spent together in these years; for share the good times and for the help that gave me in the moments I needed. great colleagues like Elisa, Matteo, Sara, Federica, Ahmed, Federica, Cristiano, Veska, Marcella, Antonella, Sangram, Mamoni, Chiara, Andrea, Silvia, Patrizia, Giulia and all the others that are too long to list.

Finally, I am greatly indebted to my family. A huge thanks to my parents, Sauro and Vittoria, to my sister Lisa and her husband Roberto. Finally, a truthful thanks to my husband Gabriele, for allowing me the time and space to realize this project, for its love, support, advices and faith. A grateful thanks to Aurora, my daughter, that she is the scope of my life and she always gives me the forces and hopes to continue and to complete this work.

INDEX

LIST OF ABBREVIATIONS

ASH	Alkaline-Peroxide Soluble Hemicellulose
ASL	Alkaline-Peroxide Soluble Lignin
Bn	Bionolle
CA	Cellulose Acetate
ΔC_p	Specific Heat
$CaCO_3$	Calcium Carbonate
$CaSO_4$	Calcium Sulphate
C-SCB	Chopped Sugar Cane Bagasse
C-RS	Chopped Rice Straw
DAGA	Department of Agronomy and Agrosystem Management
DSC	Differential Scanning Calorimetry
DC-SCB	Dewaxed Chopped Sugar Cane Bagasse
DM-SCB	Dewaxed Milled Sugar Cane Bagasse
DC-RS	Dewaxed Chopped Rice Straw
DM-RS	Dewaxed Milled Rice Straw
DS	Degree of Substitution
DTGA	Derivative Thermogravimetric Analysis
EC	European Community
EEA	European Energy Agency
El	Elastic Modulus
Fc	Flour
FeO	Iron Oxide
FR	Ground Rice
FTIR	Transmission Fourier Transform Infrared Spectroscopy
FU	Function Unit
GPC	Gel Permeation Cromatography
ΔH_{cc}	Cold Crystallization Enthalpy
ΔH_m	Enthalpy of Fusion
ICTA	International Confederation for Thermal Analysis

LCA	Lyfe Cycle Assessment
LFT	Hydrolene
Min	Minutes
Mn	Number Average Molecular Weight
Mw	Weight Average Molecular Weight
Mw/Mn	Polydispersivity Index
M-RS	Milled Rice Straw
M-SCB	Milled Sugar Cane Bagasse
NMR	Nuclear Magnetic Resonance
OMW	Olive Oil Mills Wastewater
P	Pressure
PAR	Pilot Aerobic Reactor
PCL	Poly-Caprolactone
PET	Poly-(ethylene)-terephalate
PFc	Chaff-Flour Mixture
PHAs	Poly-(Hydroxy)-Alkanoates
PHB	Poly-(hydroxy)-butirrate
PLA	Poly-Lactic Acid
PP	Pilot Plant
PS	Polystyrene
PVA	Poly-(Vinyl)-Alcohol
R	Residue
RS	Rice Straw
SAR	Small Aerobic Reactor
SCB	Sugar Cane Bagasse
SEM	Scanning Electron Microscopy
StDv	Standard Deviation
T	Temperature
T_{cc}	Cold Crystallization Temperature
T_d	Decomposition Temperature
T_{on}	Onset Temperature
T_p	Degradation Temperature

$T_{2\%}$	Degradation Temperature Corresponding 2 % Weight Loss in the Sample
T_g	Glass Transition Temperature
T_m	Melting Temperature
TGA	Thermogravimetric Analysis
U	Ulva
UTS	Ultimate Tensile Strenght
V	Speed
ΔW	Weight Loss
WAXS	Wide Angle X-Ray Spectroscopy
WSFR	Water Soluble Free Residue
WSH	Water Soluble Hemicellulose
WSL	Water Soluble Lignin
ZnO	Zinc Oxide
YM	Young Modulus

LIST OF TABLES

LIST OF FIGURES

ABSTRACT

The study of this thesis was focused on natural materials of marine origin such as algae or seaweeds and lignocellulosic materials such as sugar cane bagasse (SCB) and rice straw (RS).

The aim was to make an improve for the mechanical properties of the polymer blending it with the selected natural fillers to obtain composites and objects that can be competitive with the conventional ones and so introduced on the market.

This work was structured in three chapters, where the latter reports all the obtained results divided in six sections. In the first section, the polyhydroxyalkanoates (PHAs) production from olive oil mills wastewater, their characterization and Lyfe Cycle Assessment (LCA) were studied.

For this purpose, a screening of the traditional methods and carbon source to obtain PHAs from biomasses, was conducted, in order to plan a POLYVER technology.

The variables selected were four bacterial strains processed in a Pilot Aerobic Reactor (PAR), in a Small Aerobic Reactor (SAR) and in a Pilot Plant (PP) in accord to the LABOR (Rome) protocol.

The PHAs were characterized by means of thermal analysis (TGA and DSC), gel permeation chromatography (GPC) and Fourier Transform Infrared Spectroscopy (FTIR).

In the second section, the cellulose extracted from sugar cane bagasse and rice straw was modified by the acetylation process obtaining cellulose acetate.

The starting raw materials were dried and submitted to a dewaxing process using a Kumagawa extractor and toluene/ethanol (2:1) as a solvent mixture.

SCB and RS, before and after dewaxing, were characterized by means of scanning electron microscopy (SEM), TGA, DSC and FTIR.

Some chemical procedures were used to isolate the material components (cellulose, alkaline peroxide soluble hemicellulose, alkaline peroxide soluble lignin, WSFR). The cellulose and its acetylated product that is cellulose acetate were characterized by means of SEM, TGA, DSC, FTIR and wide angle x-ray scattering (WAXS).

The FTIR technique was used for the determination of the substitution degree (DS) of the acetylated product (DS=2.7).

The third section comprises two series of experiments concerning the production of blends based on biodegradable polymers, natural and synthetic.

Two different types of blends were produced: polylactic acid-Bionolle (PLABn) and cellulose acetate-polyhydroxybutirrate (CA/PHB) blends.

The first type was obtained by compression moulding and the second was produced by film casting.

PLABn blends were characterized by means of TGA, DSC and tensile test (Instron), while CA/PHB blends were characterized by means of SEM, TGA, DSC and wide angle x-ray scattering (WAXS).

The fourth section analyzed the production and the characterization of composites based on biodegradable polymers and natural organic fillers.

Some types of composites were produced using algae, ground rice and its by-products as natural fillers and PHB, PCL, hydrolene as biodegradable polymers by extrusion or compression moulding. These composites were evaluated for dimensional (ASTM distribution), morphological (SEM, FTIR), thermal (TGA, DSC) and mechanical properties.

The obtained results showed that the ground rice improved the adhesion between the filler and the polymeric matrix. The mechanical properties of the Ulva family showed an increase for the Young Modulus and a decrease for the Elongation at Break and the Ultimate Tensile Strenght.

The fifth and sixth sections reported the background for the foaming agents and the effervescent materials.

1. INTRODUCTION

The European Environmental Agency (EEA)[1] has conducted some studies concerning the achievement of the material wealth levels that are similar to today's levels in industrialised and developing countries.

Naturally, world consumption of resources would increase by a factor ranging from two to five and a huge growing municipal and industrial wastes will have to be handled.

Waste consists of a mix of very different materials, that have their own characteristics, environmental impact, recycle and re-use options.

The inevitable waste resulting from plastic goods and packaging are found all over the world. Plastics are relatively cheap, durable and versatile materials.

However, when they are transformed in waste they constitute a sizeable percentage of the litter. Besides, many of the plastics are also non-biodegradable or they are difficult to re-use and/or recycle, and they may represent risks to human health and to environment. The demand for green packaging will approach $45 billion in 2013. The largest markets for green packaging are food, consumer products and beverages, that together represented two thirds of total green packaging demand in 2008.

However, the fastest growing markets through 2013 will be the foodservice and shipping markets[2].

1.1. Waste Disposal Issues and Legislative Background

The greatest environmental pressure for the packaging chain comes from legislation. According to the European Environmental Agency[1,5-9], packaging waste is the major and growing waste stream. Its amounts has increased in most European countries despite the agreed objective of the waste prevention. The projections show that packaging waste amounts will arrive at 77 million tonnes in 2008.

A well-known example at European level is the EC Directive on Packaging Wastes. This directive stipulates that "packaging shall mean all products made of any materials of any nature to be used for the containment, protection, handling, delivery and presentation of goods, from raw materials to processed goods, from the producer to the user or the consumer.

Non–returnable items used for the same purposes shall also be considered to constitute packaging"[(3)]. "Packaging waste shall mean any packaging material covered by the definition of waste in Directive 75/442/EEC, excluding production residues" and "waste means any substance or object which the holder disposes of or it is required to dispose of pursuant to the provisions of national law in force"[(4)].

The solid waste is disposed in open dumps and landfills and it generates methane and other gases. Many countries regularly capture LFG as a strategy to improve landfill safety, generate electricity, reduce greenhouse gas emissions, and to earn carbon emission reduction credits[(159)].

The volatility of the market and the energy prices[(168)], the declining production rates, and the recent geopolitical acts of war and terrorism were underscored the vulnerability of the current global energy system to supply disruptions.

According to World Energy Outlook (2008), current energy supplies were unsustainable from environmental, economic, and societal standpoints.

In addition, it was projected that world energy demands will continue to expand by 45 % from 2008 to 2030, with an increased average rate of 1.6 %/yr.

In 2007, the intergovernmental panel on climate change (IPCC 2007) released its fourth assessment report confirming that the climate change was accelerating and if the current trends continued, energy-related emissions of carbon dioxide (CO_2) and other greenhouse gases will rise inexorably, pushing up average global temperature by as much as 6°C in the long term.

Recent floods, cyclones, tsunamis, sea rise, droughts, and famines throughout the world were implicated as a part of climate change resulting from unabated burning of fossil fuels (IPCC 2008). This situation had a strong impact on the threatens water, the food production, the human health and the quality of land on a global scale (OCC 2006; IPCC 2008). Preventing catastrophic and irreversible damage to the global climate ultimately required a major decarbonization drive.

Globally, 80 % of total primary energy supply depended on the fossil fuels coal, gas, and petroleum-based oils. Renewable energy sources represented only 13 % of total primary energy supply currently, with biomass (the material derived from living organisms) dominating with 10 % in renewable sector (IEA 2007a).

Traditional biomass, including fuel wood, charcoal, and animal dung, continued to provide important sources of bio-energy for most of the world population who live in extreme poverty and who used this energy mainly for cooking. More advanced and efficient conversion technologies now allow the extraction of bio-fuels in solid, liquid, and gaseous forms from a wide range of biomass sources such as woods crops and biodegradable plant and animal wastes. Bio-fuels can be classified according to source, type and technological process of conversion under the categories of first, second, third and fourth generation bio-fuels.

First generation of bio-fuels are products made from biomass consisting of sugars, starch, vegetable oils, animal fats, or biodegradable output wastes from industry, agriculture, forestry, and households using conventional technologies. Second generation is derived from lignocellulosic biomass using a liquid technology, including cellulosic bio-fuels from non-food crops such as the stalks of wheat, corn, wood, and energy-dedicated biomass crops, such as miscanthus.

Many of them are under development such as bio-hydrogen, bio-methanol,

dimethyl furan, dimethyl ether, Fischer–Tropsch diesel, bio-hydrogen diesel, mixed alcohols, and wood diesel.

Third generation is in the nascent stage of development and it is derived from low input/high output production organisms such as algal biomass.

Fourth generation is derived from the bioconversion of living organisms (micro-organisms and plants) using biotechnological tools[169,170].

National governments are setting targets and developing strategies, policies, and investment plans in bio-fuels to enhance energy security and exploit alternative energy to mitigate CO_2 emission. The recent increase of oil prices, energy security fears, and the domestic reform of agricultural policies give cause for a more serious consideration of bio-fuel in most of countries. USA, Europe, and Brazil are leading proponents of these initiatives. Mandates for blending bio-fuel into vehicle fuels were enacted in at least 37 countries[171]. In developed countries, government support for the domestic production of energy crops for bio-fuel seemed to be the rule[172].

In the USA, estimated subsidies to the bio-fuel industry might reach US $13 billion in 2008 and federal tax credit could cost US $19 billion/yr by 2022[173] while in the European Union (EU), bio-fuel support of €0.52/l will end up costing its tax payers €34 billion/yr[174-176].

These initiatives contributed to the rapid growth of liquid bio-fuels in terms of volume and share of transport fuels. Since 2001, bio-fuel production was increased almost six fold to 6 billion litres in 2006 and it was projected to grow to 3.0–3.5 % of total global transport energy by 2030 from the present 1.9 %[177,178]. However, environmental groups were raising concerns about the trade-off in food vs. fuel and effectiveness of bio-fuels in mitigating green house gas emissions.

Recent rise in food prices, shortage of food, conflicting demands of arable land, heavy use of fertilizers for bio-fuel production, and deforestation of rain forests escalated the debate to a global scale[170,176,178-181]. On the other hand,

several studies showed that bio-fuel production can be significantly increased without affecting food crops. Further reports suggested that Brazil's sugar-based ethanol production had not contributed to the food crisis[182-185].

Others suggested that the success of second and third generation technologies dealing with non-food biomass will play much bigger role than expected in coming years[171,186].

Another legislation example is the Norwegian Public Roads Administration, which has been chosen a way to obtain more practical acceptance criteria for recycled materials in road construction[236].

The approach was based on a combination of the European standard for characterization of waste, ENV 12920, and Guidelines for evaluating impact on health and ecosystem; SFT 99:01, issued by the Norwegian Pollution Control Authority.

Norwegian conditions concerning natural resources and waste were described with the aim of pointing out major differences from European countries that had achieved high recycling levels.

One reason for the low level of recycling in this area was the abundance of high quality and relatively low cost natural aggregates and the ambitious environmental policy settted high standards for pollution control and raised concern regarding potential damage caused by long-term leaching.

However, implementation of uniform acceptance criteria according the methods described might increase the rate of recycled materials used in road construction.

1.2. Disposal of Algae and Ground Rice

Anaerobic degradation or digestion is a biological process where organic carbon is converted by subsequent oxidations and reductions to its most oxidized state (CO_2), and its most reduced state (CH_4). A wide range of micro-organisms can catalyze the process in the absence of oxygen; so the main products of the process are carbon dioxide and methane, but minor quantities of nitrogen, hydrogen, ammonia and hydrogen sulfide (usually less than 1 % of the total gas volume) are also generated[163].

The mixture of gaseous products is termed biogas and the anaerobic degradation process is often also termed the biogas process. As the result of the removal of carbon, organic bound minerals and salts are released to their soluble inorganic form. The biogas process is a natural process and it occurs in a variety of anaerobic environments, such as marine and fresh water sediment, sewage sludge, mud, etc.

The interest in this process is mainly due to the following two reasons, that are an high degree of reduction of organic matter that is achieved with a small increase, compared to the aerobic process, in the bacterial biomass;
the production of biogas, that can be utilized to generate different forms of energy (heat and electricity) or be processed for automotive fuel.

The biogas process was known and utilized for many years, but especially after the rise of energy prices in the 1970s, the process received renewed attention due to the need to find alternative energy sources to reduce the dependency on fossil fuels. Although the price of fossil fuels decreased in 1985, the interest in the biogas process still remained due to the environmental benefits of anaerobic waste degradation. Additionally, the biomass used for biogas production was originally produced by photosynthetic fixation of carbon dioxide from the atmosphere, and

combustion of biogas thus did not add extra carbon dioxide to the atmosphere as it did when combusting fossil fuels formed millions of years ago.

The anaerobic degradation process was used for years for energy production and waste treatment. It was used in closed systems where optimal and controlled conditions can be maintained for the micro-organisms.

The process can be utilized for the fast and efficient degradation of different waste materials. The anaerobic process is today mainly utilized in four sectors of waste treatment:

1. Treatment of primary and secondary sludge produced during the aerobic treatment of municipal sewage. The process is utilized to stabilize and reduce the final amount of the sludge and at the same time biogas is produced, that can be used to partly cover the need for energy in the sewage treatment plant.

This application is widespread in the industrialized world connected with the establishment of the advanced treatment systems for domestic wastewater.

2. Treatment of industrial wastewater produced from biomass, food processing or fermentation industries. These wastewater types are often highly loaded and they can successfully be treated anaerobically before disposal directly to the environment or sewage system. The produced biogas can often be utilized to cover the need for process energy. With the environmental concerns and cost of alternative disposal this application of the anaerobic process is increasing.

3. Treatment of livestock waste in order to produce energy and improve the fertilizing qualities of manure. Due to more strict rules concerning the usage, distribution, and storage of manure this application is growing especially in countries with an high animal production density.

4. A relatively new sector for use of the anaerobic processes on an industrial scale is the treatment of the organic fraction of municipal solid waste (OFMSW).

The aim of this process is first of all to reduce the amount of waste in the other treatment systems, i.e. landfills and incineration plants, and secondly to recycle the nutrients from this type of waste to the agricultural sector.

European Community must find a resolution for two environmental problems that are the algal proliferations and the elimination of the plastic waste.

Sudden growth and uncontrolled proliferation of algae and sea weeds was occurred in several costal regions due to many environmental factors such as climate changes and particularly the eutrophyzation of sea water induced by the agriculture and the farmers practices. Collection and storing of the algal material represent a problem for many communities.

Very limited prior art has been found on the use of algae for the production of bio-composite materials. US56564103A and WO00/1106 patents dealt with the use of algae for the production of respectively films and foamed articles for packaging applications.

Some articles studying algae structure considered their applications as filler in composite materials. Extracts from algae were used as emulsifier and flow agents [(68)].

Ground rice is an italian material based on starch, easily processable and characterized by a low cost. It is used as food resource for the animals.

1.3. Polymers from Renewable Resources

The term "polymers from renewable resources" refers to natural products that are polymeric in character as grown or they can be converted to polymeric materials by conventional or enzymatic synthetic procedures[104].

Thus under that heading one can include *natural polymers* used as direct feedstock for plastic production as well as *artificial polymers* as those obtained by chemical modification of preformed natural polymers or by polymerization of monomers deriving from renewables[105,106].

The compostability is independent of the resources used as raw materials.

The "biodegradability" of plastics is dependent on the chemical structure of the material and on the constitution of the final product, but not on the resources used for its production. This fact is proven both scientifically and technically. Therefore, the market should decide which raw material is best for the respective biodegradable plastics application[107].

By the way there is an increasing pressure for a wider utilization of biomass feed-stocks for speciality items. The total biomass produced on earth is estimated as approximately 170 billion tons, and it consists of 75 % carbohydrates, 20 % lignin and 5 % other natural products such as oils, fats, proteins, terpenes, alkaloids and nucleic acids. Only about 3.5 % of this biomass are used by man world-wide, with one-third being wood, one-third cereals and one-third other products like oil seeds, sugar beets and sugar cane, fruits and vegetables[108,109].

The major options for the production of polymeric materials specifically meant to be converted to plastic items that should eventually experience environmental degradation after the service life, are pointed out in Figure 1.1.

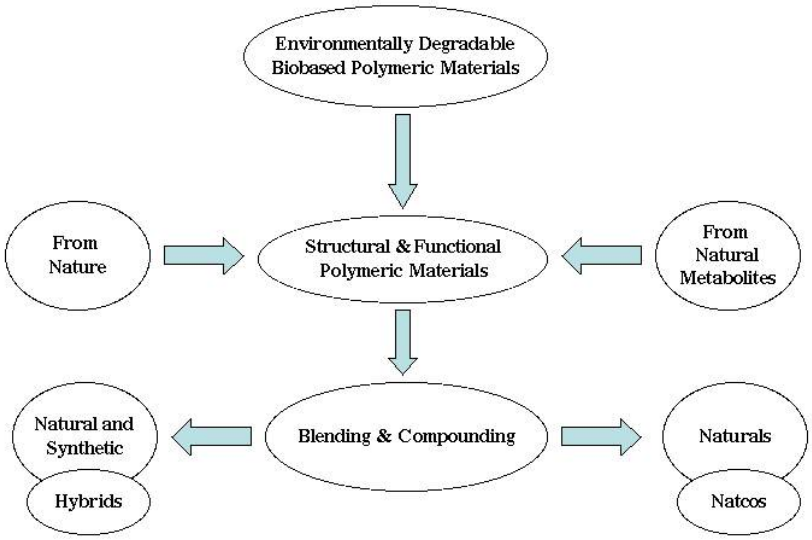

Figure 1.1. Main Options for the Production of Environmentally Degradable Bio-Based Polymeric Materials and Plastics.

1.4. Polyesters

Biodegradable polyesters and aliphatic or aromatic co-polyesters, comprising aromatic poly-functional acid and aliphatic acid, as azelaic (≥ 50 %), sebacic (≥ 70 %), brassylic acid (≥ 90 %) and a diol component selected from C3, C4, C6 diols[103], were also used in food packaging applications.

Chemical and mechanical properties of poly-hydroxybutirate (PHB), wheat and corn starch were extensively investigated. Permeability O_2/CO_2 was 1:7 for poly-lactic acid (PLA) and 1:12 for PHB so it made possible to render these materials suitable for packaging of food with high respiration[110].

PLA has received much attention in the last decade because of its originating from renewable resources and its potential biodegradability.

The packaging industry's requirements are the realization of rigid objects and soft films if a plasticizer is added to PLA[111].

The obtained films were studied by tensile testing, differential scanning calorimetry (DSC), permeation of carbon dioxide, oxygen and water vapour[100], showing that the choice of plasticizers was limited by the requirements of the application in food packaging, like being non-toxic substances approved for food contact, low migration rates and good miscibility with PLA by creating an homogeneous blend[112].

PLA films have better UV light barrier properties than polyethylene but they are worse than those of cellophane, polystyrene (PS) and polyethyleneterephtalate (PET). NatureWorks PLA is suitable as food packaging material and it can be recycled back to a monomer and into polymers. It is fully compostable in industrial facilities, where it breaks down like other matter derived from plants[113]. Recycled PLA provides an opportunity for full material utilization and lower costs in applications concerning the maintenance of fresh food.[98].

The effect of moisture sorption on stability of PLA films at food packaging conditions obtained at different humidity and temperature was investigated by decrease in numeral average molecular weight and loss of tensile strength. PLA was expected to be mechanically stable when packaging foods covering the region from dry to moist food and storage conditions from chill to ambient temperatures[114].

PLA biopolymer showed an improvement of packaged food quality and safety by increasing the barrier properties to oxygen of an ethylene-vinyl alcohol copolymer in dry and under humid conditions[115]. PLA treatments inhibited the growth of E.coli by a spray method[116].

The extrusion polymerized process is a catalytic system that can be used to produce PLA continuously in larger quantities with lower costs[117].

Blends of a non crystalline PLA polymer and a crystalline PLA polymer were suitable for blister containers, food and packaging containers[97].

PLA was used for the production of plastic bags for household for bio waste, barriers for sanitary products and diapers, planting cups, disposable cups and plates[136].

1.5. Multilayer Packaging Films

Multi-layers films or laminates were produced to improve properties for single bio-based polymers as well as co-extruded laminate films had become increasingly important for many applications expecially in food industry (packaging of fresh pasta, meats and cut vegetables) to extend the shelf-life of the goods[118].

Biodegradable blends of PLA and poly-caprolacton (PCL) showed good gas barrier properties[119] and a biodegradable hot-melt adhesive was developed from PCL and soy protein isolate[120]. Cups based on PLA and PHB were used in protecting an orange juice simulant and a dressing from quality changes during storages[121].

Multilayer films composed of a soy protein isolate inner layer and PLA outer layer were prepared by a solvent casting method in order to investigate the advantageous properties of both film materials. The lamination of PLA layers on soy protein isolate (SPI) film resulted in desiderable gas barrier properties with low water vapour permeability of PLA and low oxygen permeability of SPI[122].

A biopolymer base sheet was laminated to a poly-glicolic acid resin layer through a layer of a water based adhesive to form a multilayered sheet characterized by excellent oxygen barrier properties and moisture not permeability. The sheet was suitable for use as a packaging material base for a food container[123]. Sheets were also produced by corn starch, konjaku starch, wax, oleic acid, zinc stereate, oleamide and PCL[124].

These materials were constructed by fusion/lamination of a biodegradable resin layer on a base sheet of vegetable origin. This sheet had a lamination structure made of a biodegradable material with light environmental burden at disposal. It was excellent in oxygen-barrier properties, resistant to moisture transmission and it was usable as a food container material[125].

A biodegradable laminate was also reported for use in shaped paper based articles (containers for liquid and solid, food products). Its substrate was made of paper having first and second co-polyesters layers[126].

Laminates sheets comprising a core of higher melting PLA and a surface layer of lower melting PLA were bonded together along the edge seemed to give a sachet having a nozzle at the top seam of the sachet and it was suitable for brewing coffee in the sachet. It was developed a new laminate films based on modified starch and PLA characterized by good water and gas-barrier properties.

Some laminates comprising a core coated with a PLA on the top side of the core and a polyvinylalcohol (PVA) on the bottom side of the core were developed. This material had good biodegradability, waterproofing, heat sealing properties[124].

A biodegradable packaging material was used to indicate the expiration of the shelf-life of the enclosed goods. The films was composed by a first film layer, a second biodegradable film layer and a reactive chemical interposed between the films. When the second layer was proximal to a food product, reactive stimuli might include enzymes, bacteria, or chemicals emitted by the food[125].

PLA based long fibre non-woven having mechanical properties, biodegradability and heat-seal properties were suitable for use in a biodegradable bag such as kitchen garbage bag or tea bag. The non-woven fabric consisted of a lactic acid-based polymer and an aromatic polyester copolymers[128].

Composite films from chitosan and PLA were prepared by a solution mixing and a film casting procedure. The characterization of these blends, based on bio-packaging for potential food applications, was evaluated and the study of the antifungal activity of coatings and films on three mycotoxinogen fungal strains was conducted. The hydrophobic nature of PLA reduced the

hydrophobicity of chitosan–based films and consequently improved their moisture barrier properties and decreased overall the water/matrix interactions[129].

1.6. Technology for Biobased Polymer Processing

The optimal processing for bio-based polymer, using in food packaging applications, is based on the use of conventional apparatus that is normally used in plastic factories.

By the way alternative technologies can be developed if the cost of the variations in the production line is worthy of the results. Literature and patents report studies on the trials to fit bio-based polymeric formulations for the realisation of efficient food packaging suitable for pilot plant and industrial scale productions.

There are many patents concerning the production of bio-films, characterised by the arrangement of a flexible biodegradable polyester resin (Ecoflex) between two kinds of PLA and co-extruding them through a die.

They showed an improvement in wrinkle, surface waviness, elongation and impact resistance[130]. A new material was composed of PLA or PLA copolymer in the outer layer, producing by extrusion or coating procedure[131].

A screening of a variety of food ingredients identified as pectin, pea starch, gelatine/sodium alginate blends as potential materials for the formation of stable edible films by estrusion with conventional extruders[132], were selected.

Composite bio-films based on starch/PCL were composed by three–layer PCL/starch/PCL sheets and they were prepared by a co-extrusion process[133].

There were some studies concerning the effects of biological factors on the mechanical and morphological properties of plastics composites used for

fermented food such as cottage cheese[134].

Biodegradable bags for food packaging comprised a laminate film composed of a sealant layer made of a biodegradable polymer, a barrier layer capable of blocking oxygen/vapour and a barrier layer-supporting that made of a biodegradable polymer.

Bionolle 1001 film and an Al_2O_3/Lacty9800/paper laminated films were dry-laminated using a biodegradable adhesive to give a film roll with a good O_2 and H_2O permeability which was fabricated into a snack packaging bag at a low heat-sealant temperature[135].

OBJECTIVES

In recent years, there has been an increasing trend towards more efficient utilization of agro-industrial residues, such as sugar cane bagasse (SCB)[39] and rice straw (RS). These natural fibers are gaining progressive account as renewable, environmentally acceptable, and biodegradable starting material for industrial applications, technical textiles, composites, pulp and paper, civil engineering and building activities[141], as well as a source of chemicals or building blocks[39].

Natural fibers offer a number of well-known advantages that include low cost, availability of renewable natural resources and biodegradability[141].

Sugar cane bagasse (SCB) is a low value product burned for its energy value[139] and rice straw (RS) has great potential as a lignocellulosic feedstock for making renewable fuels and chemicals. However, RS appears to be more recalcitrant than the other agricultural residues[137].

The disposal of rice straw by open-field burning frequently causes serious air pollution, hence new economical technologies for the disposal of this material and its utilization must be developed[140].

Applications of agro-industrial residues in pulping process and other chemical production on the one hand provide alternative substrates, and help in solving pollution problems, that their disposal may otherwise cause[39].

Waxes[51,138], found in rice straw and sugar cane bagasse, were removed using a Kumagawa extractor with a solvent mixture toluene/ethanol (2:1 v/v) to conduct the dewaxing process that was influenced by the particle size of the agro-waste material.

The SCB recycling is based on the chemical modification of their components, e.g. hemicellulose is used for producing xylitol, lignin for producing phenolic resins, and cellulose for producing ethanol, composites, and cellulose derivatives. The use of SCB for producing cellulose acetate (CA) as well as membranes of this produced cellulose acetate was proposed[13,46,145;153;148;150].

Cellulose acetate (CA) is one of the oldest manmade macromolecule of renewable origin[142],used extensively in the textile industry, filters, photographic films, transparent and pigmented sheeting and plastic compositions such as those used for compression, extrusion, injection moulding and to a lesser extent, surface coating[48; 151].

This product was obtained by cellulose acetylation, in which cellulose reacted with acetic anhydride that was used as acetylating agent, in the presence of acetic acid as solvent, and sulfuric acid or perchloric acid used as catalysts[13,154,144].

The CA degree of substitution (*DS*) can be defined as the number of acetyl groups per anhydroglucose unit, and it can range from 0 for cellulose to 3 for the triacetate. Higher-*DS* polymers are acetone-soluble and the CA polymers with a DS below 1.7 do not dissolve in acetone. Moreover, there is a strong link between the *DS* and the biodegradability; the lower the *DS* the more biodegradable CA becomes which will make the lower-DS polymers very important in CA copolymers and/or blends. Also, as the *DS* decreased, an increase in the cristallinity was observed due to the fact that as the acetyl content of low-*DS* decreased, a more "cellulose like", semi-crystalline structure was adopted[48].

On the other hand, poly(hydroxybutyrate) (PHB) is one of the typical natural bio-polyesters produced by many microorganisms as intracellular carbon and energy storage compounds[156,146,143]. PHB has attracted industrial attention as an environmental friendly polymer for agricultural, marine, and medical applications due to its biocompatibility and biodegradability[149;147].

However, it has several inherent deficiencies for use as a practical polymer material, such as its brittleness due to high crystallinity and thermal instability (T_m=180ºC).

To overcome the drawbacks of PHB and obtain some useful new material properties, physical blending and chemical modification were adopted[32;155].

There were many attempts to blend PHB with other flexible polymers or low molecular weight plasticizers to turn PHB into a material with improved properties in impact strength, film formation, processing, mechanical strength, amphiphilicity, biodegradability and biocompatibility[156,91,152].

In this regard, PHB was blended with the cellulose acetate (CA) obtained from the cellulose acetilation with the aim to improve the application properties of the polymeric material since the blending is a more convenient and well-developed technology with lower cost for improving polymer properties.

The second topic of this thesis analyses the production of poly(hydroxyalkanoates) (PHAs) from olive oil mills wastewater, their morphological, structural and thermal characterization and Lyfe Cycle Assessment (LCA) evaluation.

PHAs can be obtained by the fermentation from several carbon source as for example, sugar cane bagasse wastes in presence of the bacteria *Burkholderia Sacchari*[17], and by surplus whey permeate from dairy industries[18-20] from several bacterial strains such as *Variovorax, Azeobacter vinelandii, R. entropha and Haloferax mediterranei*. This latter resulted more economically efficient and ecologically feasible for the PHAs production.

The present LCA study performs a preliminary comparative evaluation of the environmental impact associated to the production of PHAs according to technology developed in the POLYVER Project[94]. The obtained results were compared to the values found in the relevant literature and they were associated with the manufacture considering the PHAs produced with technologies other than POLYVER and the oil derived commodity polymers (such as PE, PP and PS) obtained by the traditional petrochemical technologies.

The final objective of the POLYVER project was to develop and implement a technology able to permit the conversion of OMW from a

dangerous waste to a renewable source for biopolymers production. This aim was accomplished by using OMW directly as the carbon source necessary for PHAs accumulation.

The third topic was the production of blends based on biodegradable polymers such as poly-lactic acid/Bionolle (PLA/Bn) and cellulose acetate-poly (hydroxybutirate) (CA/PHB) to improve the plasticity and the biodegradability of the polymers.

The fourth topic was the production of composites based on biodegradable biomasses, such as algae, ground rice and its by-products.

Algae constitute a largely available, low value material from renewable resource of marine origin to be used for the production of eco-compatible composites. Fibers of the green alga *Ulva armoricana*, largely present on French, Spanish and Italian costs, were evaluated for the production of hybrid films with a hydrophilic, eco-compatible polymers, such as poly(hydroxy butirrate) (PHB) and polycaprolacton (PCL), as continuous matrices[71] with the aim to recycle this synthetic materials[68].

In a first screening of the material compatibility, PHB, PCL and Ulva were utilized for the production of hybrid composites by compression moulding. Positive results were obtained for composites forming properties and mechanical characteristics attesting for Ulva suitability to be introduced in industrial formulations, because of algal biomasses contain significant amounts of crystalline cellulose as a structural component of the cell walls[68].

The aim was to make plastic items competitive with the conventional ones that can be introduced in the market.

The latter topic was the background on the foaming agent and effervescent materials with the aim to give new ideas for cleansings and drain cleaners formulations.

2. EXPERIMENTAL

The experimental chapter provides the chemicals and polymers used in the formulation of composites and blends with biodegradable polymers and fillers. The commercial products were used as received if not otherwise stated.

2.1. MATERIALS

2.1.1. *Reagents and Solvents*

Hydrochloric acid, ethanol 96 %, sodium hydroxide were purchased from Carlo Erba Chemical Co. (Italy). Sulphuric acid, hydrogen peroxide (30 %), dichloromethane, chloroform, glacial acetic acid (99-100 %) were purchased from J.T. Baker (The Netherlands). Toluene was supplied by BDH while acetic anhydride was purchased from Sigma Aldrich.

2.1.2. *Additives*

Glycerol was kindly supplied by J.T. Baker (The Netherlands).

Magnesium stereate and pentaeritritol were purchased from Sigma Aldrich; polyethylene wax and erucamide were kindly provided by Idroplax, (Altopascio–LU-Italy).

2.1.3. *Fillers*

Organic fillers. Ulva (U) was supplied by Centre d'Etude et de Valorisation des Algues (CEVA) (Pleubian-France); ground rice (FR) was provided by Idroplax (Altopascio–LU- of Italy); chaff and flour were friendly supplied by Canedole rice mill (Mantova). Sugar cane bagasse (SCB) and rice straw (RS) were supplied by a sugar mill in Tanta (Egypt).

Inorganic fillers. Calcium carbonate was supplied by Omya S.p.a (Carrara-Italy); calcium sulphate was obtained from Tecno Boy (S. Piero a Grado-Pisa-Italy). Zinc oxide was purchased from Tellerini S.p.a (Castel Maggiore–Bologna-Italy); iron oxide was donated by Idroplax (Altopascio-Lucca-Italy).

2.2. Polymers

BIOCYCLE® poly(3-hydroxybutyrate) (PHB), pellets with average molecular weight (Mw)=425 kDa and polydispersivity (Mw/Mn)=2.51 and microbially produced from *Burkholderia Sacchari*, was kindly supplied by PHB Industrial S.A. (Brazil).

Poly(idroxyalkanoates) (PHAs) microbially produced from *Pseudomonas strain* and *Azotobacter sp* were supplied by LABOR (Rome-Italy).

Poly(vinyl) alcohol (PVA) with hydrolysis degree 88 % and average molecular weight (Mw)=67 kDa, was kindly provided by Erkol (Spagna).

Hydrolene LFT proprietary PVA formulations with various additives was kindly supplied by Idroplax [Altopascio (Lucca)-Italy].

Wastes from hydrolene (LFT), containing inks and other products were supplied by Idroplax [Altopascio (Lucca)-Italy].

Bionolle 1020 (succinate polybutylene) and Bionolle 1050 (polybutylene adipate), pellets with –Mw-40-300 kDa and Mw/Mn in the range 1.8–4.5, were obtained by Showa Highpolymer Co. (Japan).

Poly lactic acid (PLA), pellet –Mw-180 kDa, was supplied by Cargill Dow LLC -Moël (Montelupo Fiorentino-Italy).

Poly caprolactone (PCL), grades CAPA 6500 and CAPA 6800 were kindly provided by Solvay (UK). CAPA 6500 has a melt flow index (MFI) in

the range 6.3–7.9 and –Mw- 50 kDa. CAPA 6800 has –MFI- in the range 2.01-4.03 and –Mw- 80 kDa.

Scheme 2.1 depicts the chemical structure of various biodegradable polymers PHB, PVA, PLA, Bionolle and PCL.

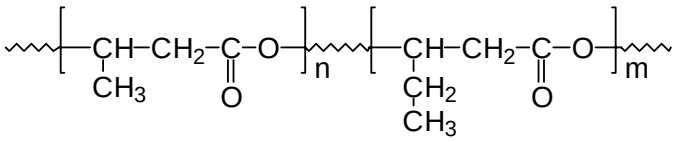

(a) PHB (m=0)

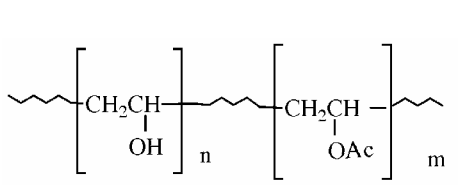

(b)

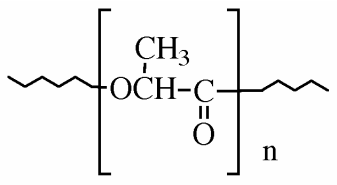

(c)

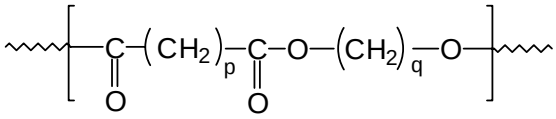

(c) p=2, q=4

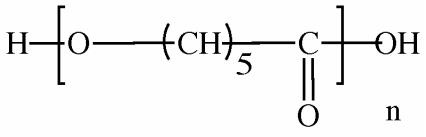

(e)

Scheme 2.1. Structure of Polymers PHB (a), PVA (b), PLA (c), Bionolle (d) and PCL (e).

2.3. Polymers–Natural Fibres Composites

2.3.1 Preparation of PHB/Ulva Composites

Before melt processing, all materials were mixed physically and dried at 45°C in a laboratory oven under vacuum for 90 minutes.

Melt processing was performed in a torque rheometer W 50 EHT (with roller blade) connected to a Plastograph Can-Bus Brabender at 170°C and 30 rpm by 7 minutes[(1)]. Films were obtained by compression moulding in a laboratory press at 180°C with a pressure of 90 bar by 6-8 minutes.

The composition and processing conditions for each formulation are reported in Table 2.1. All single components were processed in the same conditions for reference.

Table 2.1. Compositions and Processing Conditions of PHB/Ulva Composites.

Formulation	Melt mixing			Compression moulding		
	T (°C)	V (rpm)	Time (min)	T (°C)	P (bar)	Time (min)
PHB	170	30	7	180	90	6-8
PHBU5	170	30	7	180	90	6-8
PHBU10	170	30	7	180	90	6-8
PHBU20	170	30	7	180	90	6-8
PHBU30	170	30	7	180	90	6-8
PHBU40	170	30	7	180	90	6-8
PHBU50	170	30	7	180	90	6-8

Before films preparation, the mixtures were dried at 45°C in a laboratory oven under vacuum for 90 minutes. The composite PHB/Ulva (80/20) was

selected to perform an extrusion trial in a double screw extruder using a sample of 850 g. and working conditions as reported in Table 2.2.

Table 2.2. Double Screw Extruder Working Parameters.

Sample	T_1 (°C)	T_2 (°C)	T_3 (°C)	T_4 (°C)	T_{head} (°C)	Speed (rpm)
PHBU20	170	175	175	180	180	31.30

2.3.2 Preparation of PCL/Ulva Composites

PCL/Ulva composites composition and the working conditions are presented in Table 2.3. Pristine PCL was also processed in the same conditions as blank[(2)].

Table 2.3. Compositions and Working Conditions of PCL/Ulva Composites.

Formulation	Melt mixing			Compression moulding		
	T (°C)	V (rpm)	Time (min)	T (°C)	P (bar)	Time (min)
PCL	90	30	7	110	90	6-8
PCLU5	90	30	7	110	90	6-8
PCLU10	90	30	7	110	90	6-8
PCLU20	90	30	7	110	90	6-8
PCLU30	90	30	7	110	90	6-8
PCLU40	90	30	7	110	90	6-8
PCLU50	90	30	7	110	90	6-8

2.3.3. Preparation of PHBPCL blends

PHB/PCL blends composition and the working conditions are presented in Table 2.4. PHB and PCL were also processed in the same conditions as blanks[(2)].

Table 2.4. Compositions and Working Conditions of PHBPCL Blends.

Formulation	Melt mixing			Compression moulding		
	T (°C)	V (rpm)	Time (min)	T (°C)	P (bar)	Time (min)
PCL	170	30	9	180	90	6-8
PHB	170	30	9	180	90	6-8
PHB90PCL10	170	30	9	180	90	6-8
PHB80PCL20	170	30	9	180	90	6-8
PHB70PCL30	170	30	9	180	90	6-8
PHB50PCL50	170	30	9	180	90	6-8
PHB10PCL90	170	30	9	180	90	6-8
PHB20PCL80	170	30	9	180	90	6-8
PHB30PCL70	170	30	9	180	90	6-8

2.3.4 Preparation of PHBPCL/Ulva Composites

PHB/PCL/Ulva composites composition and the working conditions are presented in Table 2.5.

Table 2.5. Compositions and Working Conditions of PHBPCL/Ulva Composites.

Formulation	Melt mixing			Compression moulding		
	T (°C)	V (rpm)	Time (min)	T (°C)	P (bar)	Time (min)
PHBPCL(80/20)U10	170	30	9	180	90	7-8
PHBPCL(80/20)U20	170	30	9	180	90	7-8
PHBPCL(80/20)U30	170	30	9	180	90	7-8
PHBPCL(80/20)U10	170	30	9	180	90	7-8
PHBPCL(80/20)U20	170	30	9	180	90	7-8
PHBPCL(80/20)U30	170	30	9	180	90	7-8

2.3.5 Preparation of Hydrolene/Ground Rice Composites

Hydrolene/ground rice (LFTFR) composites composition and the working parameters are presented in Table 2.6.

Table 2.6. Compositions and Working Conditions for Hydrolene/Ground Rice Composites.

Formulation	Melt mixing			Compression moulding		
	T (°C)	V (rpm)	Time (min)	T (°C)	P (bar)	Time (min)
LFT	190	30	7	180	90	6-8
LFTFR10	190	30	7	180	90	6-8
LFTFR20	190	30	7	180	90	6-8
LFTFR30	190	30	7	180	90	6-8
LFTFR40	190	30	7	180	90	6-8
LFTFR50	190	30	7	180	90	6-8
LFTFR60	190	30	7	180	90	6-8

The blends (300 g) LFTFR containing 30 % and 40 % of ground rice were selected to conduct an extrusion in a double screw extruder using the working conditions reported in Table 2.7.

Table 2.7. Double Screw Extruder Working Parameters.

Sample	T_1 (°C)	T_2 (°C)	T_3 (°C)	T_4 (°C)	T_{head} (°C)	Speed (rpm)
LFTFR30	180	190	195	200	200	31.30
LFTFR40	180	190	195	200	200	31.30

2.3.6 Preparation of Hydrolene/Ground Rice/Calcium Carbonate Composites.

Calcium carbonate was added in an increasing quantity (from 5 % up to 35 %) to the formulation LFTFR containing 40 % of ground rice.

Hydrolene/ground rice/calcium carbonate composites composition and the working conditions are reported in Table 2.8.

Table 2.8. Compositions and Working Conditions of Hydrolene/Ground Rice/$CaCO_3$ Composites.

Formulation	Melt mixing			Compression moulding		
	T (°C)	V (rpm)	Time (min)	T (°C)	P (bar)	Time (min)
LFTFR40	180	30	7	200	90	6-8
LFTFR40C5	180	30	7	200	90	6-8
LFTFR40C10	180	30	7	200	90	6-8
LFTFR40C15	180	30	7	200	90	6-8
LFTFR40C20	180	30	7	200	90	6-8
LFTFR40C25	180	30	7	200	90	6-8
LFTFR40C30	180	30	7	200	90	6-8
LFTFR40C35	180	30	7	200	90	6-8

2.3.7 Preparation of Hydrolene/Ground Rice/Calcium Carbonate/ Calcium Sulphate Composites.

Calcium carbonate and calcium sulphate were added in the formulation LFTFR40 in the percentages of 5 and 10 %. The amount of both inorganic fillers in the formulation LFTFR30 was 15 %.

LFTFR40 was also processed in the same conditions as blank.

Composites composition and working parameters are reported in Table 2.9.

Table 2.9. Compositions and Working Parameters of Hydrolene/Ground Rice/$CaCO_3$/$CaSO_4$ Composites.

Formulation	Melt mixing			Compression moulding		
	T (°C)	V (rpm)	Time (min)	T (°C)	P (bar)	Time (min)
LFTFR40C5G5	180	30	7	210	90	6-8
LFTFR40C10G10	180	30	7	210	90	6-8
LFTFR40C15G15	180	30	7	210	90	6-8

2.3.8 Preparation of Hydrolene/Chaff and Flour Composites

Chaff and flour were mixed in the ratio 70/30, which was added to hydrolene up to 40 %. LFT was also processed in the same conditions as blank. Composites composition and working parameters are reported in Table 2.10.

Table 2.10. Compositions and Working Parameters of Hydrolene/Chaff/Flour Composites.

Formulation	Melt mixing			Compression moulding		
	T (°C)	V (rpm)	Time (min)	T (°C)	P (bar)	Time (min)
LFTPFc10	175	30	7	-	-	-
LFTPFc20	175	30	7	-	-	-
LFTPFc30	175	30	7	-	-	-
LFTPFc40	175	30	7	-	-	-

2.3.9 Preparation of Hydrolene/PFc/Calcium Carbonate/Calcium Sulphate Composites.

Composites composition and the working parameters are presented in Table 2.11.

Table 2.11. Compositions and Working Parameters of Hydrolene/PFc/$CaCO_3$/$CaSO_4$ Composites.

Formulation	Melt mixing			Compression moulding		
	T (°C)	V (rpm)	Time (min)	T (°C)	P (bar)	Time (min)
LFTPFc20	175	30	7	175	80	7
LFTPFc20C5G5	175	30	7	175	80	7
LFTPFc20C10G10	175	30	7	175	80	7
LFTPFc20C15G15	175	30	7	175	80	7

2.3.10 Preparation of Poly(lactic acid)/Bionolle Blends

Composites composition and the working parameters are reported in Table 2.12.

Table 2.12. Compositions and Working Parameters of PLABn Blends.

Formulation	Melt mixing			Compression moulding		
	T (°C)	V (rpm)	Time (min)	T (°C)	P (bar)	Time (min)
PLA	180	30	8	180	80	5-6
Bionolle	180	30	8	180	80	5-6
PLABn20	180	30	8	180	80	5-6
PLABn40	180	30	8	180	80	5-6
PLABn50	180	30	8	180	80	5-6
PLABn60	180	30	8	180	80	5-6
PLABn80	180	30	8	180	80	5-6

2.4 Poly(hydroxyalkanoates) (PHAs) Extraction and Purification

2.4.1 PHAs Pretreatment

The aqueous biomasses deriving from a fermentation of oil wastes water were centrifuged in a Rotofix 32A-1624 at speed 40x100 rpm for 30 minutes. The sedimented materials were lyophilised and stored in a refrigerator at 4°C for further purification and extraction.

The difference between purified and non purified biomass is shown in Figure 2.1.

(a) (b)

Figure 2.1. Example of Non Purified (a) and Purified (b) Biomass.

2.4.2 PHAs Purification

Five grams of lyophilised biomass was mixed with 250 mL of acetone and then stirred under reflux at 65°C for 12h under N_2 atmosphere.

The solid biomass residue was filtered under vacuum with a Büchner funnel and dried at room temperature in a desiccator.

2.4.3 PHAs Solvent Extraction

PHAs extraction was performed using a Kumagawa extractor under N_2 atmosphere. About 5 grams of biomass was extracted in 250 mL of chloroform under reflux for 7h at 55°C. Extracted PHAs solution was concentrated using a rotary evaporator up to a volume of 20 mL.

These concentrated solution was dropped slowly into 100 mL of diethyl ether at 0-4°C with constant strong stirring. Precipitated PHAs were filtered and dried at room temperature.

2.5 Dewaxing of Ligno-Cellulosic Materials

2.5.1 Sugar Cane Bagasse (SCB)

Sugar cane bagasse was exposed to the open air to sunlight and then cut into small pieces. The fibers were dried in an oven under vacuum at 55°C for 48h and finally grinded to fine powder with a blade grinder[5,8].

The powder was sieved and the fractions between the following mesh sieves were collected: 0.60 mm- 0.425 mm; 0.425 mm- 0.3 mm; 0.212 mm- 0.15 mm; 0,15 mm- 0.106 mm; 0.106 mm- 0.053 mm.

Wax was removed from milled and chopped sugar cane bagasse (SCB) by using a Kumagawa extractor (Figure 2.2). The solvent was a mixture of toluene/ethanol (2:1). When the extraction was completed, dewaxed sugar cane bagasse (DSCB) was dried under vacuum at room temperature overnight. A sample of extracted solvent in the dean stark stopcock was taken every three hours and evaporated using a rotavapor to check the progress of extraction process and to dissolved wax (Scheme 2.2).

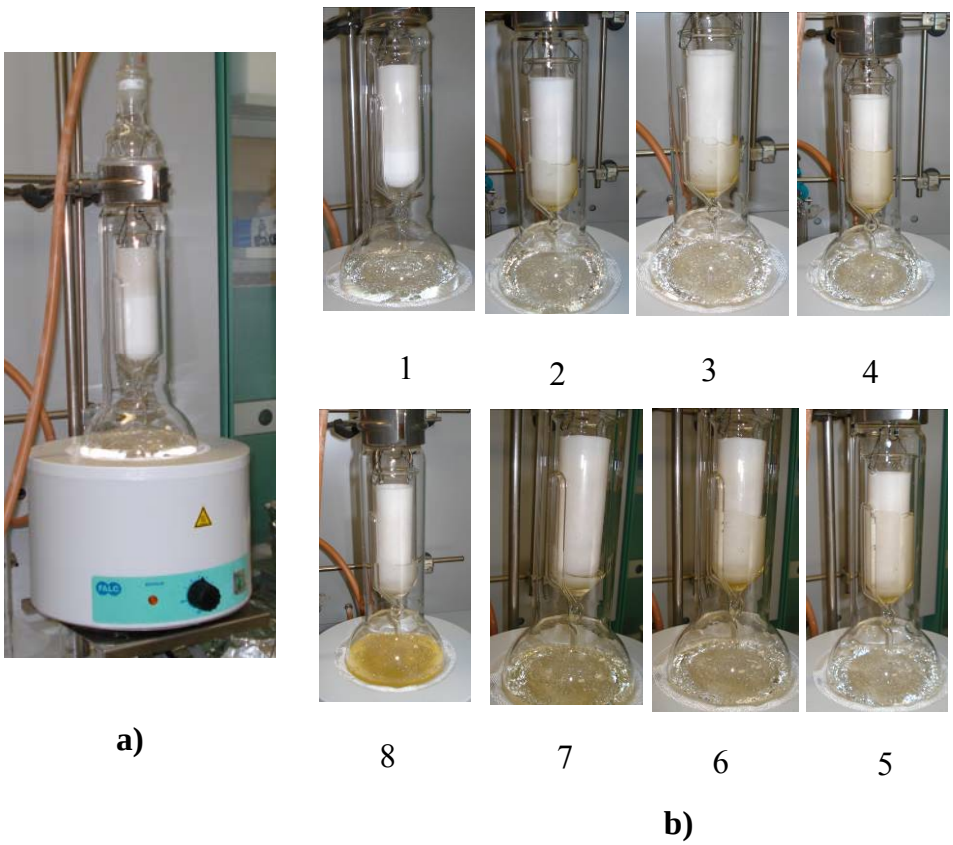

Figure 2.2. Dewaxing of Sugar Cane Bagasse (SCB) Using a Kumagawa Extractor (a) and Dewaxing Step-by-Step (b).

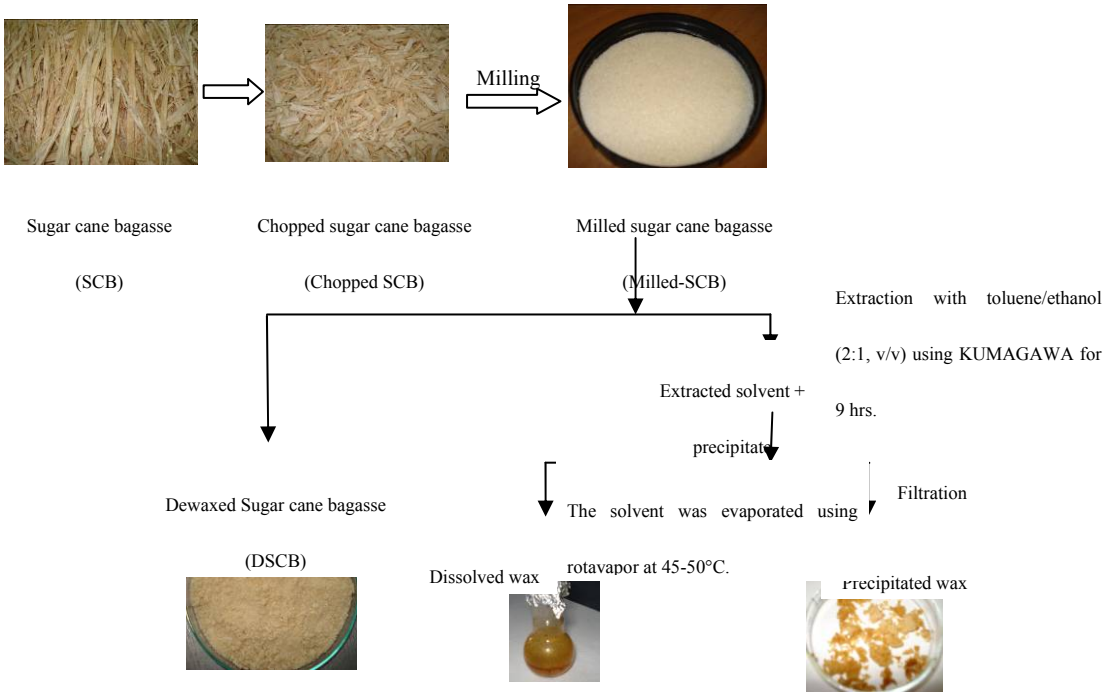

Scheme 2.2. Dewaxing of Sugar Cane Bagasse (SCB).

2.5.2 Rice Straw (RS)

The rice straw (RS) was grossly dried by exposition open air to sunlight and then cut to small pieces that were dried in an oven under vacuum at 55°C for 48h and then pulverized with a blade grinder.

The chopped rice straw was sieved and the fractions between the following mesh sieves were collected: 0.60 mm- 0.425 mm; 0.425 mm- 0.3 mm; 0.212 mm- 0.15 mm; 0,15 mm- 0.106 mm; 0.106 mm- 0.053 mm.

Wax was removed from rice straw (25 g) using a Kumagawa extractor in which a mixture of toluene/ethanol (2:1) has been introduced.

A sample of extracted solvent in the dean stark stopcock was taken every two hours and evaporated using rotavapor to check the progress of extraction process.

After the extraction was completed, dewaxed rice straw (DRS) was dried under vacuum at room temperature overnight.

The precipitate wax was filtered off and the filtrate was evaporated using rotavapor to get the dissolved wax (Scheme 2.3).

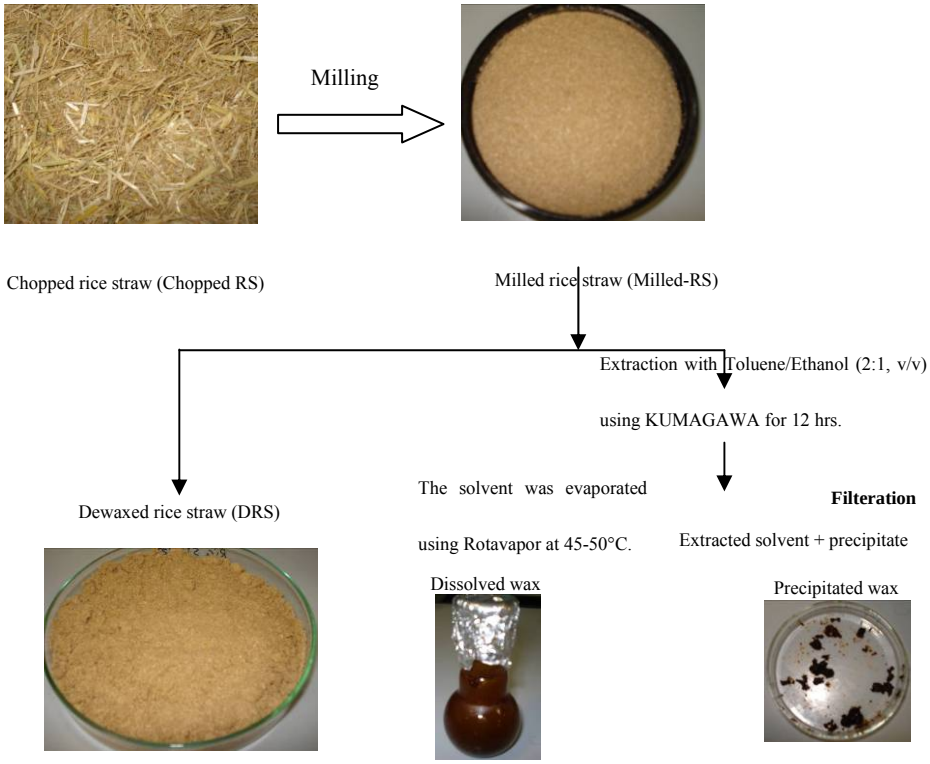

Scheme 2.3. Dewaxing of Rice Straw (RS).

2.6 Isolation of Water-Soluble Hemicellulose (WSH) Water-Soluble Lignin (WSL)

2.6.1 Sugar Cane Bagasse (SCB)

The dewaxed sugar cane bagasse (DSCB) (10 g) was soaked in 300 mL distilled water at 55°C for 2h with stirring as shown in Figure 2.3.

The water-soluble free residue (WSFR) was recovered by vacuum filtration, washed with distilled water, and it was dried under vacuum at 50°C for 48h.

The filtrate and supernatant were collected and concentrated on rotavapor at 40°C to 30 mL. Water-soluble hemicellulose (WSH) was obtained by precipitation of the concentrated aqueous extract in 4 volumes of 95 % ethanol (120 mL) and the mixture was left with stirring at room temperature for 1h. The precipitated water-soluble hemicellulose (WSH) was recovered by filtration, was washed with 70 % ethanol and was air-dried.

After filtration, the filtrate and the supernatant were collected and were acidified to pH 1.5, as adjusted by 6M HCl.

Water-soluble lignin (WSL) was obtained by evaporation on rotavapor till dryness and it was freeze-dried (Scheme 2.4).

Figure 2.3. Apparatus for the Sugar Cane Bagasse Dewaxing.

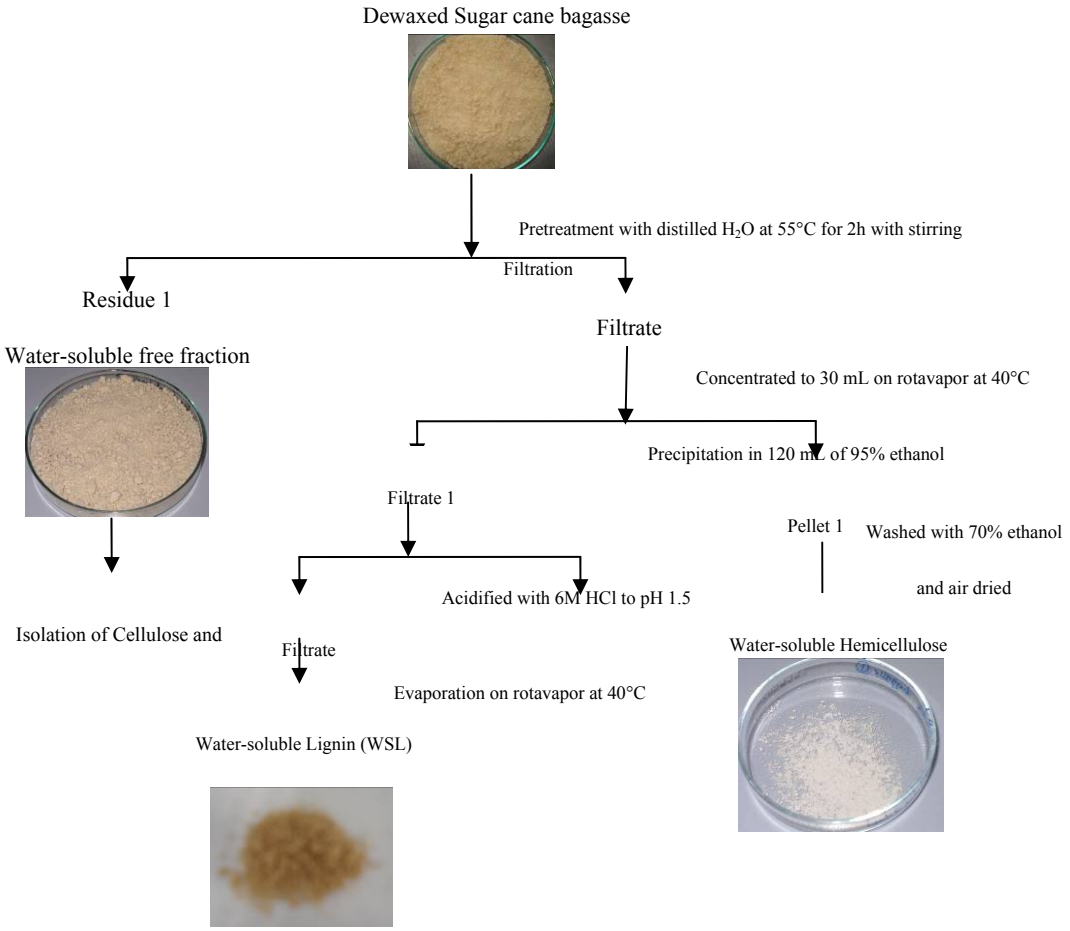

Scheme 2.4. Isolation of Water-Soluble Hemicelluose (WSH) and Water-Soluble Lignin (WSL) from Dewaxed Sugar Cane Bagasse (DSCB).

2.7 Isolation of Cellulose, Alkaline-Peroxide-Soluble Hemicellulose (APSH) and Alkaline-Peroxide-Soluble Lignin (ASL) from Water-Soluble Free Dewaxed Sugar Cane Bagasse (WSFR)

2.7.1 Sugar Cane Bagasse (SCB)

Water-soluble free dewaxed sugar cane bagasse (WSFR) was dried under vacuum at 50°C for 48h and soacked in the following solution: 20 g of 30 % H_2O_2 was diluted to 300 mL with distilled water and the pH was adjusted to 11.5 with 4M NaOH.

The residue (cellulose) was recovered by vacuum filtration, it washed with distilled water till neutral (pH 6-7) and it was dried under vacuum at 50°C for 48h.

The filtrate and the supernatant were collected and the pH adjusted to 5.5-6 using 6M HCl. The filtrate was concentrated on rotavapor at 40°C to 200 mL.

Alkaline-peroxide-soluble hemicellulose (APSH) was obtained by precipitation of the concentrated aqueous extract in 4 volumes of 95 % ethanol (800 mL) and the mixture was left with stirring at room temperature for 1h. The precipitated alkaline-peroxide-soluble hemicellulose (APSH) was recovered by filtration, washed with 70 % ethanol and was air-dried.

After filtration, the filtrate and the supernatant were collected. Ethanol was evaporated on rotavapor and then acidified to pH 1.0-1.5 using 6M HCl.

Alkaline-peroxide-soluble lignin (ASL) was obtained by evaporation of water on rotavapor at 40°C till dryness and it was freeze-dried (Scheme 2.5).

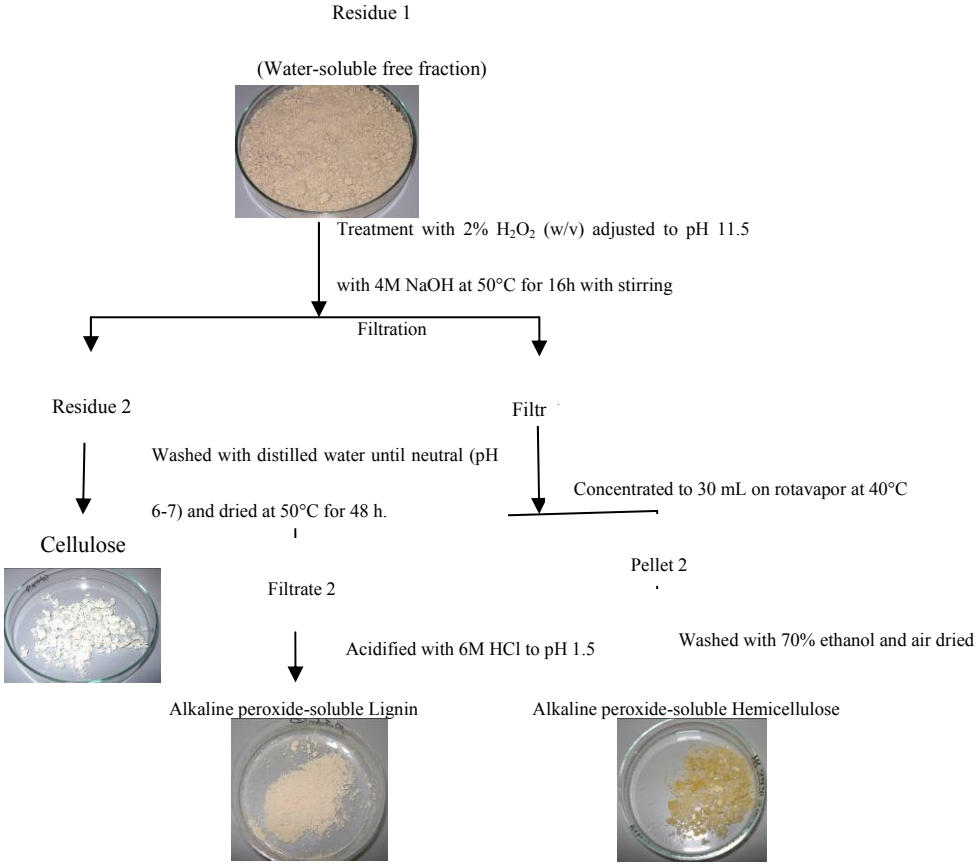

Scheme 2.5. Isolation of Alkaline-Peroxide-Soluble Hemicellulose (APSH) and Alkaline-Peroxide-Soluble Lignin (ASL) from Water-Soluble Free Dewaxed Sugar Cane Bagasse (WSFR).

2.7.2 Rice Straw (RS)

Dewaxed rice straw (D-RS) was dried under vacuum at 50°C for 48h, then 2 % (w/v) H_2O_2 (pH 11.5) was prepared as previously.

Isolation of cellulose from D-RS takes place as in two steps as following: the elimination of the organosolv-soluble fractions (OSH and OSL) was performed soaking 10 g of DRS in 195 mL of a mixture of ethanol/distilled water (2:1) and adding 5 mL of 0.2 N HCl, at 70°C for 4h with stirring.

The organosolv-soluble free residue (OSFR) was recovered by filtration using a piece of cloth, washed with a mixture of ethanol/distilled water, and was dried under vacuum at 50°C for 48h.

Alkaline-peroxide-soluble fractions, (APSH and ASL), were removed by soaking the organosolv-soluble free dewaxed rice straw (9 g) in 300 mL of 2 % (w/v) H_2O_2 adjusted to pH 11.5 with 4M NaOH at 45°C for 16h with stirring. The residue (cellulose) was recovered by vacuum filtration, washed with distilled water till neutral pH and was dried under vacuum at 50°C for 48h.

2.8 PHB–Natural Fibers Blends

2.8.1 Acetylation of Cellulose

Acetylation of cellulose was carried out according to the following procedure[9]. Cellulose (3.0 g) was soaked in 75 mL of glacial acetic acid and was stirred at room temperature for 30 min in a 250 mL round bottom-flask.

Then, 0.24 mL of conc. H_2SO_4 in 27 mL of glacial acetic acid was added and stirring was continued for further 30 min at room temperature. Cellulose pulp solution was separated by tilting the flask and pouring it into a beaker.

An amount of 96 mL of acetic anhydride was added to the solution, that was poured back into the flask containing the cellulose. The reaction mixture was stirred for 90 min and the flask was covered and left to stand at room temperature for 17h. The reaction mixture was stirred at 30°C for 6h and then was stood at room temperature for 16h.

The undissolved material was removed by filtration, and water was added to the filtrate to stop the reaction and precipitate cellulose acetate (CA). The produced cellulose acetate (CA) was filtered and washed with distilled water till neutral pH acid and then dried at room temperature for 48h.

2.8.2 Production of Films by Casting

Cellulose acetate was dissolved in 5 mL of dichloromethane with stirring for one week at room temperature (20°C), and PHB was dissolved in 5 mL of chloroform by heating for 1h. The solution of cellulose acetate (CA) and dichloromethane was added to that of PHB one and the mixture was stirred for further 1-2h, to give a total concentration of 2.5 % in a mixture of dichloromethane/chloroform (1:1). The solution was cast on a glass Petri dish and the solvent was left evaporate.

After the evaporation of the solvent, the films were dried under vacuum at room temperature till constant weight. Blends CA/PHB were produced in the following amounts of CA: 20, 40, 60, 80, and 100 w/w, are referred as PHB, PHB80, PHB60, PHB50, PHB40, PHB20, and CA, respectively[10,14].

2.9 Characterization of Building Blocks, Polymers and Relative Blends and Composites

2.9.1 Thermogravimetric Analysis (TGA)

TGA experiments were performed in the thermogravimetric analyzer Series Q500 of the TA Instruments. Generally, sample size was between 10-20 mg. Two different range of temperatures were scanned at 10°C·min^{-1} under nitrogen atmosphere at 60 mL·min^{-1} flow rate. These range of temperatures were from 30°C to 800°C and from 30°C to 600°C depending on the type of filler (organic or inorganic) in the formulations, respectively.

2.9.2 Differential Scanning Calorimetry (DSC)

A DSC instrument from Mettler-Toledo was used. a system consisting of the DSC-822 module with FRS5 sensor and operated by means of STAR^e software for making experiments and for the evaluation of the thermodynamic parameters of polymers–natural fibres composites.

Samples of 5-10 mg were weighed in 40 μL aluminium pan and an empty pan was used as reference. DSC temperature calibration was performed using indium, lead and zinc standards and energy calibration by using indium standard.

For the formulations containing poly(hydroxybutyrate), poly(caprolactone) or hydrolene, the measurements were performed under nitrogen flow rate of 80 mL·min^{-1} according to the following protocol:

1. First heating scan from 0°C to 210°C at 10°C·min^{-1} and 2 min of isotherm at the end;
2. Cooling scan from 210°C to 0°C at 10°C·min^{-1};
3. Second heating scan from 0°C to 210°C at 10°C·min^{-1}

For the formulations based on poly(lactic acid) and Bionolle, the measurements were performed under nitrogen flow rate of 160 mL·min^{-1} according to the following protocol:

1. First heating scan from -50°C to 210°C at 10°C·min^{-1} and 2 min of isotherm at the end;

2. Cooling scan from 210°C to -50°C at 10°C·min^{-1};
3. Second heating scan from -50°C to 210°C at 10°C·min^{-1}.

For the formulations families containing ligno-cellulosic materials, the measurements were performed under nitrogen flow rate of 160 $mL \cdot min^{-1}$ according to the following protocol:

1. First heating scan from 25°C to 200°C at $10°C \cdot min^{-1}$ and 3 min of isotherm at the end;
2. Cooling scan from 200°C to 25°C at $10°C \cdot min^{-1}$;
3. Second heating scan from 25°C to 200°C at $10°C \cdot min^{-1}$;

2.9.3 Scanning Electron Microscopy (SEM)

The cross-section morphologies of films were recorded using a JEOL (JSM-5600LV) scanning electron microscope (SEM) at the required magnification and with accelerating voltage of 14kV. The film samples frozen in liquid nitrogen were fractured and sputtered with gold before SEM observation.[a]

2.9.4 Wide Angle X-ray Scattering (WAXS)

Wide-angle X-ray diffraction patterns were performed at room temperature with a Kristalloflex 810 diffractometer (SIEMENS) using a Cu Kα (λ=1.5406 Å) as X-ray source. Scans were run in the high angle region from 5° to 40° at scan rate of 0.016°/min and a dwell time of 1s.

[a)] SEM and WAXS were performed in the Department of Chemical Engineering, Industrial Chemistry and Materials Science, University of Pisa by Mr. Piero Narducci, to whom a grateful acknowledgement is described.

2.9.5 Gel Permeation Chromatography (GPC)

GPC traces were performed using a Jasco PU-1580 HPLC liquid chromatograph connected to Jasco 830-RI and Perkin-Elmer LC-75 spectrophotometric (λ=260 nm) detectors and equipped with two PLgel 5 μ mixed-C columns (linear range of MW: 200-2,000,000) was used to obtain average molecular weights. Chloroform stabilized with amylene was used as eluent at 1.0 mL/min flow rate. The average molecular weight of the samples were calculated using the calibration curve established from standard samples of monodisperse polystyrene.

2.9.6 Transmission Fourier Transform Infrared Spectroscopy (FTIR)

Transmission infrared spectra of all samples were recorded with a Jasco FT-IR Spectrometer mod. FT/IR-410 in the mid-IR region (4000-400 cm^{-1}) at 4 cm^{-1} resolution using 32 scans. Samples were casted from $CHCl_3$ solutions on a KBr crystal plate.

2.9.7 Nuclear Magnetic Resonance (NMR)

^{1}H-NMR spectra were obtained by means of a Varian Gemini VRX 200 (200 MHz) from deuterated chloroform ($CDCl_3$) solutions.

2.9.8 Mechanical Tests

The tensile tests were performed on the specimens (ASTM D638) according to the standard test method using a universal testing machine Instron (model 5564) with a load cell of 2 kN and pneumatic grips.

Specimens were preconditioned inside desiccators containing saturated solutions of magnesium nitrate (≈ 50 % RH) by 48h at 23°C (ASTM E104-02)[14]. At least 7 specimens for each sample formulation were tested and the average value has been reported. A digital micrometer was used to monitor film thickness. Measurements were performed with a crosshead speed set at 10 mm·min$^{-1.}$

2.9.9 Fiber Analyzer

The instrument used for the determination of the chemical composition of used lignocellulosic materials is a FIBER ANALYZER MOD. ANCOM located in Department of Agronomy and Agrosystem Management (DAGA) University of Pisa, Pisa, Italy.

The system is a pressure pot with a stirrer where the pouches similar to tea-bags and made of synthetic material are immersed in a boiling solution and stirred for 1h.

After that the solvent is unloaded and the sample is washed with distilled water, acetone and dried in a ventilated oven. For the non dissolved fibres (NDF) determination, α-amylase is used for eliminating starches. The sample incineration is made by a muffola oven and the material is brought at constant weight with an analytic balance.

2.9.10 Mill

Natural fibres and polymers were grinded using a grind Brabender Wiley with a tri-phase motive power (0.75 keV), equipped with four static mechanical shovels and six rotary ones. The mill has three interchangeable sieves ((2 mm, 3 mm, and 4 mm).

2.9.11 Brabender

The selected mixtures were worked using a torque rheometer Brabender W 50 EHT (with a roller blade) connected with a Plastograph can-Bus-Brabender.

2.9.12 Lab-Scale Double Screw Extruder

Materials granules were obtained mixing polymers and natural fibres in a laboratory double screw (length=18L, D=2x25 mm), extruder (TEACH–LINE ZK 25 T)-Collin.

2.9.13 Pilot-Scale Double Screw Extruder

The mixtures more promising were introduced in a double screw (D=20 mm) extruder (PRISM TSE 24 HC).

2.9.14 Compression Moulding

Compression moulding was performed using a press Collin P 200E (D=196x196 mm, compression force ≤ 125 kN, hydraulic pressure ≤ 240 bar. The plates have a maximum heating temperature around of 300°C

2.9.15 Density Measurements

Density measurements were performed using a picnometer[9].

A series of weights were performed: empty picnometer; picnometer+water (32.52 g.), material+picnometer.

The difference in weight between the water with or without the material represents the volume occupied by the material.

3 RESULTS

The results chapter has been divided in six parts as indicated by following:

1. Poly(hydroxyalkanoates) from olive oil mills wastewater: characterization and LCA;
2. Modification of cellulose extracted from sugar cane bagasse (SCB) and rice straw (RS);
3. Blends based on biodegradable polymers of natural and synthetic origin;
4. Composites based on biodegradable materials and natural organic fillers.
5. Background on the foaming agents
6. Background on the effervescent materials

3.1 Poly(hydroxyalkanoates) from Olive Oil Mills Wastewater: Characterization and LCA

Poly(hydroxyalkanoates) are fully biodegradable polyesters of hydroxyalkanoates (HAs) that are accumulated by several micro-organisms[24].

Bacteria synthesize and accumulate PHAs as carbon and energy storage materials or as a sink for redundant reducing power under the condition of limiting nutrients in the presence of excess carbon source. When the supply of the limiting nutrient is restored, the PHAs can be degraded by intracellular depolymerases and subsequently metabolized as carbon and energy source[15,16].

Once extracted from the cells, PHAs exhibit thermoplastic and elastomeric properties. PHAs are recyclable, natural materials and they can be easily degraded to carbon dioxide and water. They are excellent replacements for petroleum-derived plastics in terms of processability, physical characteristics and biodegradability. In addition, these polymers are biocompatible and they

have several medical applications.

All of the monomeric units of PHAs are enantiomerically pure and in the R-configuration. R-hydroxyalkanoic acids produced by the hydrolysis of PHAs can also be widely used as chiral starting materials in fine chemical, pharmaceutical and medical industries.

PHAs can be obtained by the fermentation of several carbon source as for example, sugar cane bagasse wastes in presence of the bacteria *Burkholderia Sacchari*[17], and by surplus whey permeate from dairy industries [18-20] from several bacterial strains such as *Variovorax, Azeobacter vinelandii, R. entropha and Haloferax mediterranei*. This latter resulted more economically efficient and ecologically feasible for the PHAs production.

Finally PHAs can be extracted from bacterial strains that live in the olive oil mills wastewater such as *Pseudomonas* and *Azotobacter Sp*, *Azotobacter Vinelandii* and *Azotobacter ChR*[22], that were characterized in this study.

Tables 3.1 shows the identification codes and the preparation methods of the samples produced using a Pilot Aerobic Reactor by Pseudomonas strain.

Table 3.1. Samples Produced by *Pseudomonas* Strain.

Sample	Initial Quantity (ml)	Final Quantity (ml)
PAR-1	16000	16000
PAR-2	2000	1000
PAR-4	200	80
PAR-5	200	80
PAR-7	3000	2100
PAR-9	30	5[a]
PAR-10	370	15[a]

a) Quantity in grams.

The treatment for these samples consisted in a cooling at –80°C for 30 minutes for PAR-1, in an addition of $Al_2(SO_4)_3$ for the precipitation for PAR-2, in a biomass sedimentation, sampling, cooling at -80°C for 30 min and sedimentation for PAR-4 and PAR-5.

The treatment for PAR-7 and PAR-9 was a biomass sedimentation to 10 lit, 10 lit of 3D water for washing followed by a biomass sedimentation to approx 4 lit and a cooling at 80°C for 30 minutes, an addition of H_2SO_4 at 85°C for 40 minutes and the NaOH ones up to pH 10, the centrifugation at 10000 RPM x 15 min, a bleach solution 1:2 vol and a centrifugation after a day.

Table 3.2 shows the identification codes and the preparation methods of the samples produced using a small aerobic reactor by *Azotobacter Sp*.

Table 3.2. Samples Produced by *Azotobacter Sp* with a Small Aerobic Reactor.

Sample	Initial Quantity (ml)	Final Quantity (ml)
SAR-1	500	50
SAR-2	100	100
SAR-3	100	100
SAR-4	100	100

The treatment for these samples was a cooling at –80°C for 30 minutes followed by a biomass sedimentation using 6 g/l of $Al_2(SO_4)_3$ and an extraction with the HClO method.

Table 3.3 shows the identification codes and the preparation methods of the samples produced using a pilot plant by *Azotobacter Sp.*

Table 3.3. Samples produced by *Azotobacter Sp* with a Pilot Plant.

Sample	Initial Quantity (lt)	Final Quantity (ml)
PP-1	30	100
PP-2	1	50
PP-4	30	400

The treatment was a series of the same steps used for producing the SAR samples.

Polyhydroxyalkanoates found a large number of applications in many areas such as medicine, agriculture, tissue engineering, nanocomposites, polymer blends and chiral synthesis[158].

The agricultural applications regards principally the production of mulch films. In recent years Procter & Gamble have produced Nodax, that can be used to manufacture biodegradable agricultural film. This material is a copolymer containing mainly 3(HB) and small quantities of medium chain length (MCL) monomers. It can degrade anaerobically and hence it can be used as a coating for urea fertilizers to be used in rice fields or for herbicides and insecticides.

Other applications of P(3HB-3HV) in agriculture concerned the controlled release of insecticides and the bacterial inoculants used to enhance nitrogen fixation in plants as confirmed by some experiments conducted in Mexico using maize and wheat.

Increased and accelerated global economic activities over the past century led to interlink problems that require urgent attention[188].

Greater emphasis was put on the concept of sustainable economic systems that relied on technologies based on and supporting renewable sources of energy and materials. Average UK households produce around 3.2 million

tonnes of packaging waste annually whereas 150 million tonnes of packaging waste is generated annually by industries in the UK. The development of biologically derived biodegradable polymers is one important element of the new economic development.

3.1.1 Gel Permeation Cromatography

Typical GPC traces of PHAs produced by *Pseudomonas* strain, *Azotobacter Sp* using a small aerobic reactor, *Azotobacter Vinelandii* and *Azotobacter ChR* are shown in Figures 3.1-3.3.

The PAR-7 sample showed a monomodal (Fig.3.1). The weight average molecular weight (Mw) of the sample was around 490 kDa with a polydispersion index (Mw/Mn) of 5.15.

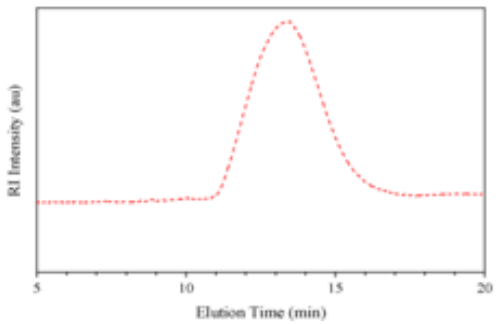

Figure 3.1 GPC Trace (RI detector) of PAR-7.

GPC traces of SAR-1, SAR-2, SAR-3 and SAR-4 samples are shown in Figure 3.2. All sample solutions were prepared with the same concentration.

However, peak intensity between 11-16 min of elution time were very different. Besides, that of samples SAR-1 and SAR-2 the signal was very near to baseline. This was, probably due to the fermentation condition and/or extraction method..

The values of Mw and Mw/Mn of SAR-3 and SAR-4 samples are reported

in Table 3.4. The highest value of Mw was found in the case of SAR-4 sample (higher than 1000 kDa), that presented the lower Mw/Mn value too.

Peaks observed at higher retention time can be attributed to the presence of oligomers and/or impurities.

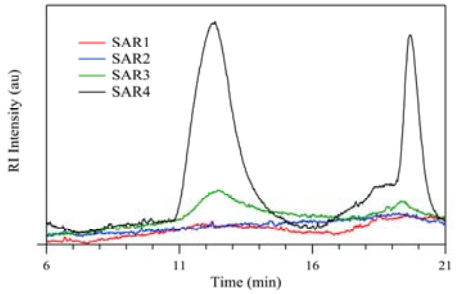

Figure 3.2 GPC Traces of SAR-1, SAR-2, SAR-3 and SAR-4.

Table 3.4. Mw (kDa) of SAR-3 and SAR-4.[a]

Sample	Mw (kDa)	Mw/Mn
SAR-3	714	3.74
SAR-4	1068	2.32

[a)] Mw is the weight average molecular weight; Mw/Mn is the polydispersity index.

GPC traces of 72h and 96h samples are shown in Figure 3.3. The first sample was prepared by *Azotobacter Vinelandii* UWD as fermentation microorganism and 60 % digested alperujo as culture medium for 72 hours while the second one was prepared using *Azotobacter ChR* as fermentation microorganism and 40 % digested alpeorujo as culture medium for 96 hours.

The values of Mw and Mw/Mn are reported in Table 3.5. The highest value of Mw was found in the case of 96h (216 kDa) compared to 72h (188 kDa). Mw/Mn was basically the same for both samples and it was around 2.4.

Table 3.5. Mw (kDa) of *72h* and *96h*.

Sample	Mw (kDa)	Mw/Mn
72h	188	2.37
96h	216	2.39

[a)] Mw is the weight average molecular weight; Mw/Mn is the polydispersity index.

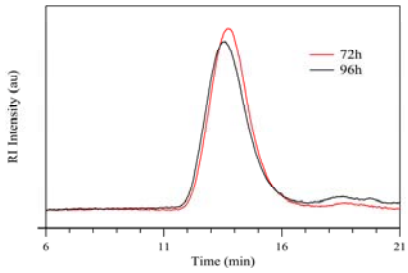

Figure 3.3 GPC Traces of *72h* and *96h*.

3.1.2 Thermal Properties

Thermal characterization of polymers gave several important information as for example degradation temperature (T_d), processing temperature and the miscibility between components of polymer blends and composites[7,23].

In the present study, thermal properties of PHAs were assessed by thermogravimetry (TGA) and differential scanning calorimetry (DSC).

3.1.2.1 Thermogravimetry (TGA)

TGA provided important data parameters relating to thermal stability of polymers[25]. One of them was the decomposition temperature (T_d), which was defined as the onset temperature at the beginning of the weight loss. In the present study, T_d was defined as the temperature at 2 wt-% of weight loss.

Another parameter was the peak degradation temperature (T_p), which was related to the reaction mechanism. The T_p data were obtained from the first

derivate of TGA (DTGA) trace and they corresponded to the temperature at the maximum degradation rate.

The experiments of this study were conducted under nitrogen atmosphere in the range temperature of 25-500°C and the recovered residue was

measured at 500°C. The selected materials were the PHAs produced by the bacterial strains in LABOR (Roma) facilities.

TGA data of PHAs produced by Pseudomonas strain using a Pilot Aerobic Reactor are presented in Table 3.6.

The $T_{2\%}$ values of PAR-1, PAR-2, PAR-4, PAR-5, PAR-7, PAR-9 were 235°C, 182°C, 151°C, 244°C, 239°C and 241°C, respectively. T_{p2} value was evident only for the PAR-2 sample; for the other samples it wasn't possible to determine this parameter, because of the ΔW_2 was a shoulder of the main degradation effect (ΔW_1).

Table 3.6. TGA Parameters in Nitrogen Atmosphere of PHAs Produced by *Pseudomonas* Strain[a].

Sample	$T_{2\%}$ (°C)	T_{on} (°C)	T_{p1} (°C)	T_{p2} (°C)	R_{500} (wt-%)
PAR-1	235.4	242.3	264.9	-	2.4
PAR-2	182.3	235.9	260.8	328.42	8.8
PAR-4	151.3	221.9	244.1	-	4.0
PAR-5	244.7	256.6	279.7	-	1.5
PAR-7	239.5	242.6	272.9	-	0.4
PAR-9	241.8	248.3	264.9	-	1.5

[a)] $T_{2\%}$ is the degradation temperature corresponding to 2% weight loss in the sample, ΔW is the weight loss, T_{on} is the temperature corresponding to the beginning of the material degradation, T_p is the temperature corresponding to the maximum weight loss rate, R_{500} is the residual weight measured at 500°C.

TGA traces coming from thermogravimetric analysis (TGA) and their corresponding DTGA ones of *PAR* samples under nitrogen flow are shown in Figure 3.4.

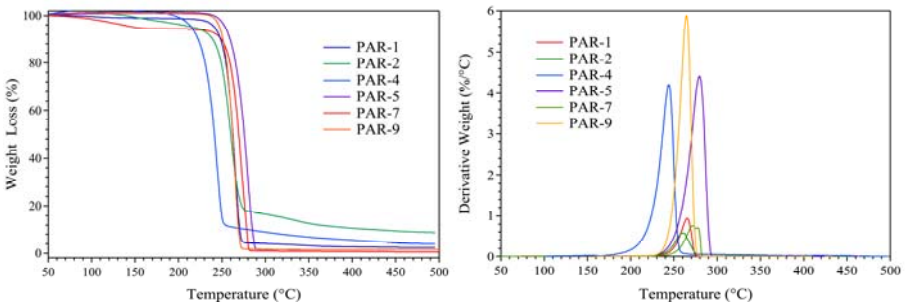

(a) (b)

Figure 3.4 TGA (a) and DTGA (b) Traces Produced by *Pseudomonas* Strain.

The first weight loss between 30°C-150°C probably was due to the evaporation of some residual solvent used in the polymer purification.

The temperatures of maximum weight loss rate (T_p), corresponding to the main weight loss step (ΔW_1), was observed in the range 260-280°C.

This step, which should correspond to polymer decomposition, can provide an estimation of the real PHAs content in the samples and the presence of impurity considering that pure PHAs didn't leave residues after pyrolysis. In particular, ΔW_1 was calculated in around 96, 80 and 93 wt-% for PAR-1, PAR-2 and PAR-7 respectively and 91 and 99 wt-% for PAR-4, PAR-5 and PAR-9.

Values of $T_{2\%}$ and T_p were in good agreement with the data commonly reported in literature for PHAs[26-28]. Another minor decomposition step (ΔW_2) was observed at higher temperatures, calculated in around 2-9 wt-%.

Residual weight at 500°C (R_{500}), was estimated in the range 0-9 wt-%.

These data indicated that PAR-2 (and partially PAR-1 and PAR-4)

contained a relatively large amount of impurities that might derive from the culture medium and not properly removed during the purification.

For the PHAs produced by *Azotobacter sp* using a Small Aerobic Reactor (Fig. 3.5), the only $T_{2\%}$ value was calculated only for SAR-4 sample.

Thermogravimetric data are presented in Table 3.7.

Table 3.7. TGA Parameters in Nitrogen Atmosphere of PHAs Produced by *Azotobacter Sp* Using a Small Aerobic Reactor[a].

Sample	$T_{2\%}$ (°C)	T_{on} (°C)	T_{p1} (°C)	R_{500} (%)
SAR-1	-	-	-	89.5
SAR-2	-	-	-	91.2
SAR-3	-	-	-	72.4
SAR-4	180.1	210.6	241.0	7.1

[a)] $T_{2\%}$ is the degradation temperature corresponding to 2% weight loss in the sample, Δ_w is the weight loss, T_p is the temperature corresponding to the maximum weight loss rate, R_{500} is the residual weight measured at 500°C.

Figure 3.5 shows the TGA and DTGA traces for the SAR samples.

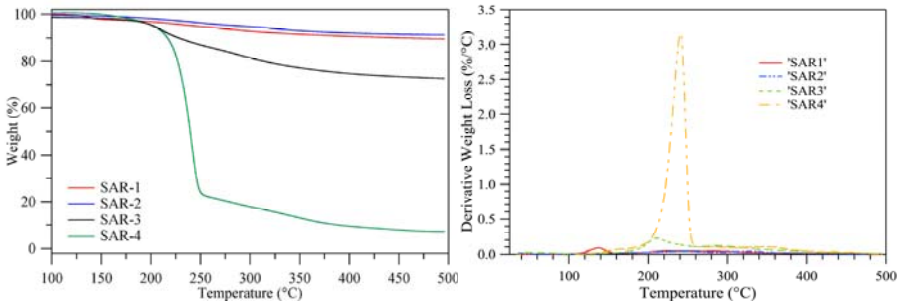

(a) (b)

Figure 3.5 TGA (a) and DTGA (b) Traces in Nitrogen Atmosphere of Produced by *Azotobacter Sp* Using a Small Aerobic Reactor.

Samples SAR-1, SAR-2 and SAR-3 still contained an high amount of impurities, as indicated by the high value of residual weight at 500°C (R_{500}).

These values ranged from 91 wt% for SAR-2 to 72 wt-% for SAR-3. With regard to SAR-4, the onset of thermal degradation, calculated as the initial 2 % weight loss ($T_{2\%}$) and the temperature of maximum weight loss rate (T_p) were found at 180°C and 241°C respectively. The main weight loss step (ΔW_1), which should provide an estimation of the real PHAs content in the sample, was around 77.6 wt-%. Residual weight at 500°C was estimated in around 7 wt-%.

In Table 3.8 are shown the data relative to the PP-1 sample, that is a PHA produced by *Azotobacter sp* using a pilot plant and Figure 3.6 reports its TGA (a) and DTGA (b) traces.

Table 3.8. TGA Parameters in Nitrogen Atmosphere of PHAs Produced by *Azotobacter Sp* Using a Pilot Plant (PP-1)[a].

Sample	$T_{2\%}$ (°C)	T_{on} (°C)	T_{p1} (°C)	T_{p2} (°C)	R_{500} (wt-%)
PP-1	99.9	223.9	303.4	-	53.5

[a] $T_{2\%}$ is the degradation temperature corresponding to 2% weight loss in the sample, T_{on} is the temperature corresponding to the beginning of the PHA degradation, ΔW is the weight loss, T_p is the temperature corresponding to the maximum weight loss rate, R_{500} is the residual weight measured at 500°C.

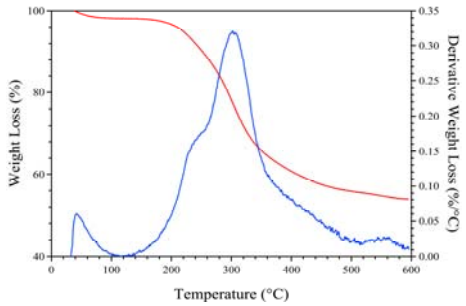

Figure 3.6 TGA and DTGA Traces of PP-1 Sample.

The onset temperature and the recovered residue at 500°C showed that PP-1 sample presents an high quantity of impurities after purification.

TGA data of PHAs produced by *Azotobacter Vinelandii* and *Azotobacter ChR* are reported in Table 3.9.

Table 3.9. TGA Parameters in Nitrogen Atmosphere of PHAs Produced by *Azotobacter Sp*. at 72h and 96h[a].

Sample	$T_{2\%}$ (°C)	T_{on} (°C)	T_{p1} (°C)	T_{p2} (°C)	R_{500} (wt-%)
72h	211.0	263.5	295.5	325.1	3.6
96h	252.0	258.8	94.8	284.1	2.3

[a)] $T_{2\%}$ is the degradation temperature corresponding to 2% weight loss in the sample, T_{on} is the temperature corresponding to the beginning of the material degradation, Δw is the weight loss, T_p is the temperature corresponding to the maximum weight loss rate, R_{500} is the residual weight measured at 500°C.

Figure 3.7 shows TGA (a) and DTGA (b) traces for these two samples.

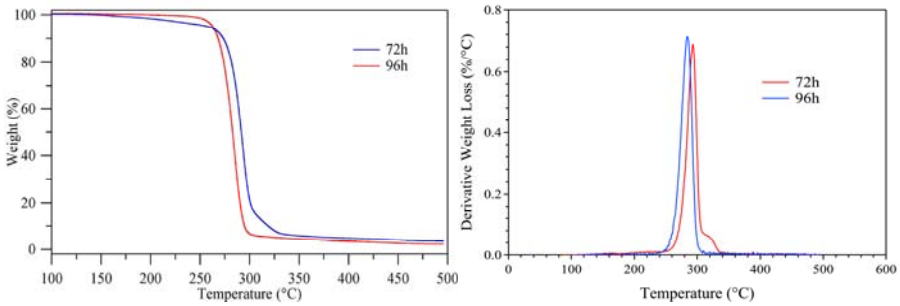

(a) (b)

Figure 3.7 TGA (a) and DTGA (b) Traces in Nitrogen Atmosphere of *72h* and *96h* Samples.

$T_{2\%}$ ranged from ca. 211°C (*72h*) to 252°C (*96h*), while the temperatures of maximum weight loss rate (T_p), was observed in the range 285-295°C. On the other hand, the values of the main weight loss step ΔW_1 (85-95 wt-%) and the residual weight at 500°C R_{500} (2-4 wt-%) indicated that the polymers still contain impurities.

3.1.2.2 Differential Scanning Calorimetry (DSC)

DSC analysis was performed in four scans. Figure 3.8 illustrates the typical DSC trace of the PHAs produced by *Pseudomonas* strain using a pilot plant reactor (a) and that of the PHAs produced by *Azotobacter sp Vinelandii* and *ChR* (b).

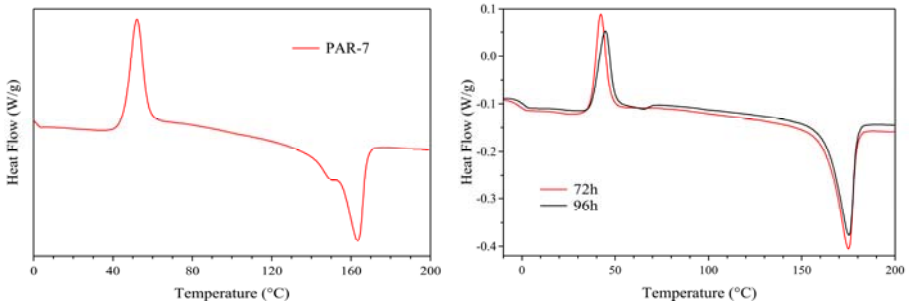

(a) (b)

Figure 3.8 Second Heating DSC Traces of PAR-7 (a) and 72h-96h (b).

The thermodynamic parameters of PAR-7 are reported in Table 3.10. The presence of a double melting peak at ca. 150°C and 163°C confirmed the copolymeric nature of this sample. In fact, these values were typical of 3(HB) copolymerized with 3-hydroxyvalerate 3(HV) units[26].

Table 3.10. Thermodynamic parameters of PAR-7 (second heating).[a)]

	T_g (°C)	ΔH_{cc1} (J/g)	T_{cc1} (°C)	ΔH_{cc2} (J/g)	T_{cc2} (°C)	ΔH_t (J/g)	T_{m1} (°C)	T_{m2} (°C)
PAR-7	0.4	50.9	52.7	21.6	62.2	24.3	150.5	163.3

a) T_g is the glass transition temperature, ΔH_{cc} is the cold crystallization enthalpy, T_{cc} is the cold crystallization temperature, ΔH_m is the enthalpy of fusion, T_m is the melting temperature.

3.1.3 FTIR Analysis

FT-IR spectra of PAR samples are reported in Figure 3.9.

The wavenumbers of the main PHAs FT-IR peaks reported in literature are in Table 3.11. More relevant peaks were observed in the ranges 3400-2850 cm^{-1} (CH_3 and CH_2 stretching) and 1500-1000 cm^{-1} (CH_3 bending, CH_2 wagging, C-O, C-C and C-O-C stretching), in addition to the very strong carbonyl signal found around at 1724 cm^{-1}.

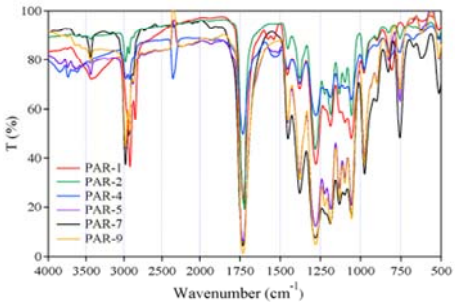

Figure 3.9 FT-IR Spectra of PHAs Produced by *Pseudomonas* Strains..

Table 3.11. Assignments of PHAs main FT-IR Absorption Bands[29-32].

Wavenumber (cm^{-1})	*Assignment*
3437	OH stretching (H bridges)
2976	CH_3 (asymmetric stretching)
2934	CH_2 (asymmetric stretching)
2875	CH_3 (symmetric stretching)
2855	CH_2(symmetric stretching)
1724	C=O stretching
1453	CH_3 (asymmetric bending)
1379	CH_3 (symmetric bending)
1289	CH_2 wagging
1278	CH_2 wagging
1228	Conformational band of the helical chains
1184	C-O-C asymmetric stretching
1132	C-O-C symmetric stretching
1100	OH stretching
1057	C-O symmetric stretching
979	C-C stretching
929	CH_2 rocking
896	CH_3 rocking
825	CH_3 rocking

FT-IR spectra of *72h* and *96h* are reported in Figure 3.10. Both polymers showed the typical absorption peaks reported in Table 3.8, confirming that they belong to the PHAs family.

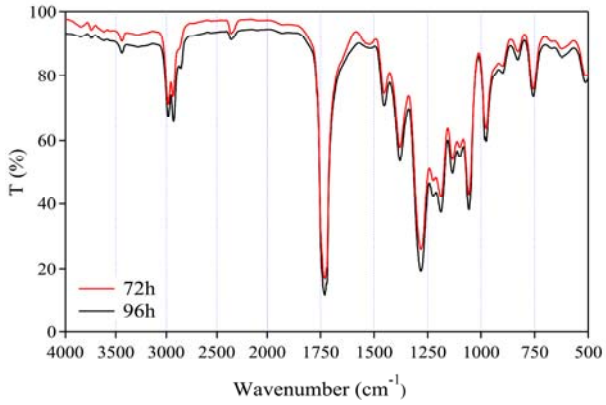

Figure 3.10 FT-IR Spectra of PHAs Produced by *Azotobacter Sp* at 72h and 96h**.**

3.2 LCA Evaluation for the PHAs Obtained from Wastewaters of Olive Oil Mill

The goal of the present LCA study was to perform a preliminary comparative evaluation of the environmental impact associated to the production of PHAs according to technology developed in the POLYVER Project[(94)].

The Functional Unit (FU) chosen in order to compare results from different sources was 1 kg of polymer, and the LCA was based on a *cradle-to-factory gate* approach.

Since POLYVER is still a technology under development, the two impact categories that will be considered are Gross Energy Use (GEU) and Global Warming Potential (GWP)[(233,234)].

These categories considered the relevant environmental impact regarding

human health, plants and animals (ecological health), or the future availability of natural resources (resource depletion).

In the work from *Akiyama et al.*[233], based on experimental results on lab scale, the production of P(3HB-co-3HHx) and P(3HB) from the *recombinant strain of PHA-negative harboring the aeromonas cavie PHA synthase* was considered. The substrates were soybean oil for P(3HB-co-3HHx) and glucose from corn for P(3HB). The reactor was a fed batch typo, with a production rate 5000 tonnes per year. Fermentation step was accomplished growing the cells in a mineral medium containing the substrate until nitrogen is exhausted, followed by the production of PHA from the substrate in the absence of nitrogen source. Assumed fermentation conditions were as follows: fermenter volume: 300-750 m^3, fermentation time: 30-50h, and fermentation temperature: 34°C. The downstream process was accomplished distruping the cells by sodium dodecylsulfate (SDS) pretreatment and followed by sodium hypochlorite (NaOCl) washing, while PHAs were dried by means of a spray dryer.

These experimental conditions leads to a cell concentration of 100-200 g/l with a PHA content of 75-85 wt-%.

On the other hand, the report from *Harding et al.*[234] concerned the production of P(3HB) starting from the experimental results obtained from *Harrison et al.*[235] on a pilot plant scale using *cupriavidus necator* as microorganism and sugar cane glucose as substrate. The reactor, operating at 30°C for 80h, was a fed batch type with a production rate of 1000 kg. In particular, the sucrose feed was initiated after batch production of biomass, and PHB started to accumulate with the onset of phosphate limitation.

After cell distruption, solid PHB was removed by centrifugation and re-suspended with alkaline serine protease. Furthermore, PHB was treated with non-ionic detergents and hydrogen peroxide (H_2O_2), both steps followed by water dilution and centrifuge cycles. Finally, P(3HB) drying was performed

by means of a spray dryer. In these experimental conditions, cell concentration of 150 g/l with a polymer content of 71 % was claimed.

Concerning relevant LCA issues, it was worth of notice that both studies considered the carbon sources used for PHAs accumulation (soybean oil and glucose from corn and sugar cane) as produced specifically for this purpose.

This was reflected in the fact that the whole environmental load due to carbon source production was included in PHAs final impact. However, both studies concluded that carbon sources production accounts only for a limited share, and the processes contributing most to LCA impacts (Energy Use and Global Warming Potential) were electricity and steam generation.

System boundaries of traditional and POLYVER technologies for PHAs production and Olive Oil Mills Wastewater (OMW) are showed in Figures 3.11 and 3.12 respectively. *Processes* and *Products* were indicated with blue and red colour respectively. Olive oil was assumed to be produced with a three-phases process.

With the traditional technologies (Fig. 3.11), PHAs production and OMW treatment belong to different process. From a general point of view, PHAs production was typically composed of two different macro-steps: the production of the carbon source followed by the polymer fermentation and recovery. On the other hand, OMW was generated as by-product in olive oil industry. Infact, the three phases milling technology, very common in Italy and Greece but not in Spain, gave rise to three products: olive oil, olive husk and OMW. On the other hand, OMW was found to be very rich of organic matter (e.g. organic acids, lipids, alcohols and polyphenols), that increased its phytotoxicity to very high levels. Due to this reasons, in order to reduce its environmental impact, OMW had to treat with special techniques (e.g. evaporation, physico-chemical treatments or biotechnological transformations)[33,,34].

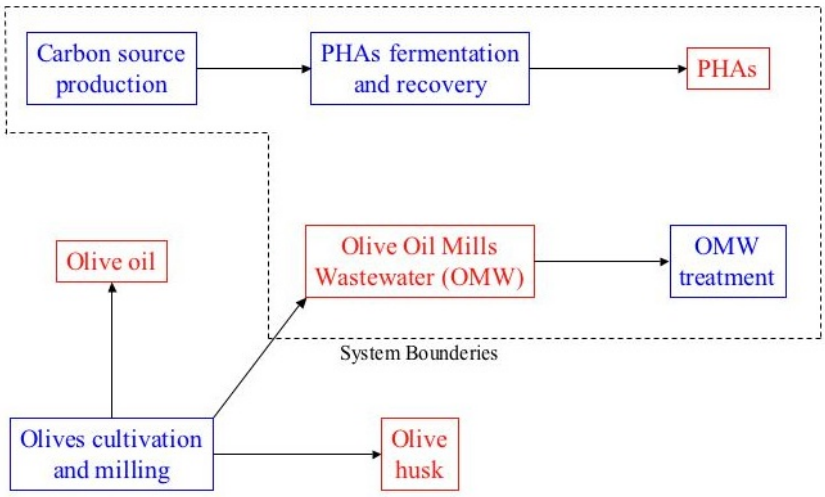

Figure 3.11 System Boundaries of Traditional Technologies for PHAs Production and OMW Treatment**.**

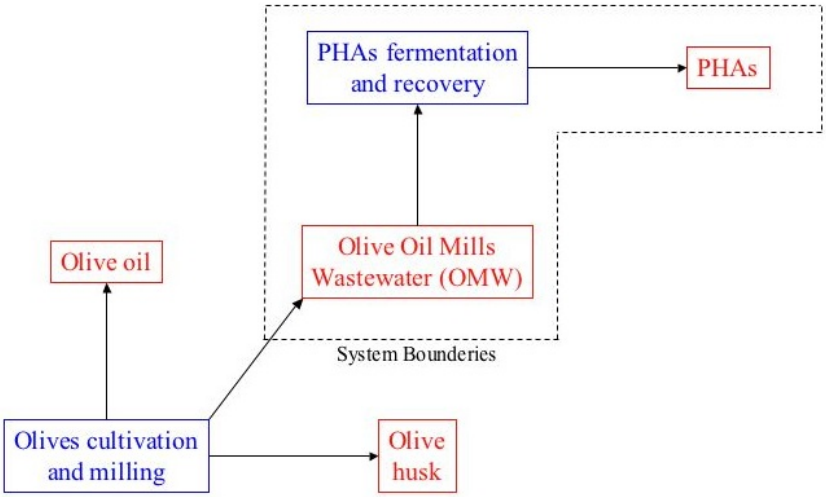

Figure 3.12 System Boundaries of POLYVER Technologies for PHAs Production and OMW Treatment.

The final objective of the POLYVER project was to develop and implement a technology able to permit the conversion of OMW from a dangerous waste to a renewable source for biopolymers production. This aim

was accomplished by using OMW directly as the carbon source necessary for PHAs accumulation. In this view, in comparison with the traditional one, in the POLYVER scenario the two steps regarding the production of carbon source and the treatment of OMW did not need to be performed anymore.

In order to render the two scenarios comparable, the *System Expansion* method was applied. The system expansion approach (Fig. 3.13) broadened the system boundaries and introduced a new functional unit to make the two systems being compared equal in scope.

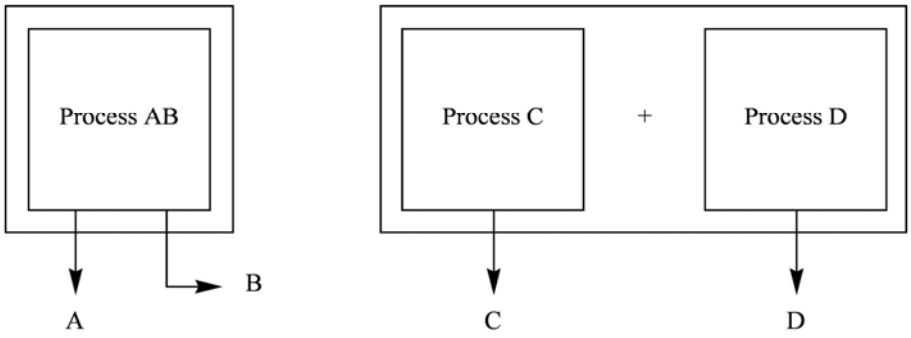

Figure 3.13 Schematization of System Expansion Approach.

For example, product A was produced by Process AB along with product B. Product A was to be compared to product C which was the only product to be produced by process C. Using system expansion, an alternative way to produce product B was added to process C. The comparison now was between Process AB and Process C plus Process D [(34)]. Another approach to applying system expansion was by subtracting the environmental burdens of an alternative way of producing Product B so that only Product A was compared to product C. This approach was also referred to as the "avoided burden" approach since it was reasoned that the production of any alternative products was no longer needed and the resultant environmental burdens were avoided.

The environmental burdens allocated to the product of interest were then calculated as the burdens from the process minus the burdens of an alternative co-product[34].

Since the output considered as FU was 1 kg of PHAs, this approach had to be applied to the OMW management process, which can be treated in two different ways: either added to PHAs impact in traditional technology or subtracted from PHAs impact in POLYVER scenario. This second approach was the one chosen for the present LCA. System Expansion was not applied to the carbon source production since this step was just replaced by OMW production in olive oil mills.

Data regarding the final yields of PHAs obtained by means of POLYVER technology, in terms of biomass and polymer concentration in the culture media, polymer content in the biomass and culture media needed for 1 kg of PHAs are reported in Table 3.12.

Table 3.12. Biomass and Polymer Concentration in the Culture Media, Polymer Content in the Biomass and Culture Media Needed for 1 kg of PHAs.

Sample	Biomass Concentration (kg/m^3)	Polymer Content (%)	Polymer Concentration (kg/m^3)	Medium needed for 1 kg PHAs (l)
PAR-1	17.90	1.38	0.25	4050
PAR-2	11.90	0.44	0.05	19270
PAR-4	22.00	0.49	0.11	9340
PAR-5	10.00	0.18	0.02	56090
PAR-7	31.13	1.02	0.32	3160
PAR-9	12.25	24.07	2.95	340

Taking the culture media needed for 1kg of PHAs as representative factor, the run that gave best yield results is PAR-9, with a value of 340 l/kg PHAs.

For this reason, the run PAR-9 will be taken as model to develop the present LCA study. However, from a first comparison with the values listed in Table 3.12, the yields obtained with POLYVER technology were much lower than those reported in literature for other fermentation technologies.

Since OMW was used directly for PHAs production, it was assumed that both olive oil mill and bioreactor were integrated in the same industrial plant.

In this way, no OMW transportation was required, leading to fuel savings.

As already illustrated, OMW was not produced specifically as PHAs substrated, but it was generated as unwanted by-product in olives milling. In this view, the impact arising from OMW production assumed to be negligible. POLYVER process examined in detail was the purification and extraction step. Input/output analysis of this step are schematized in Figure 3.14. The inputs related to this step were electricity and water consumption, along with the utilization of acetone, chloroform and diethyl ether. On the other hand, the three abovementioned solvents represented also the main outputs.

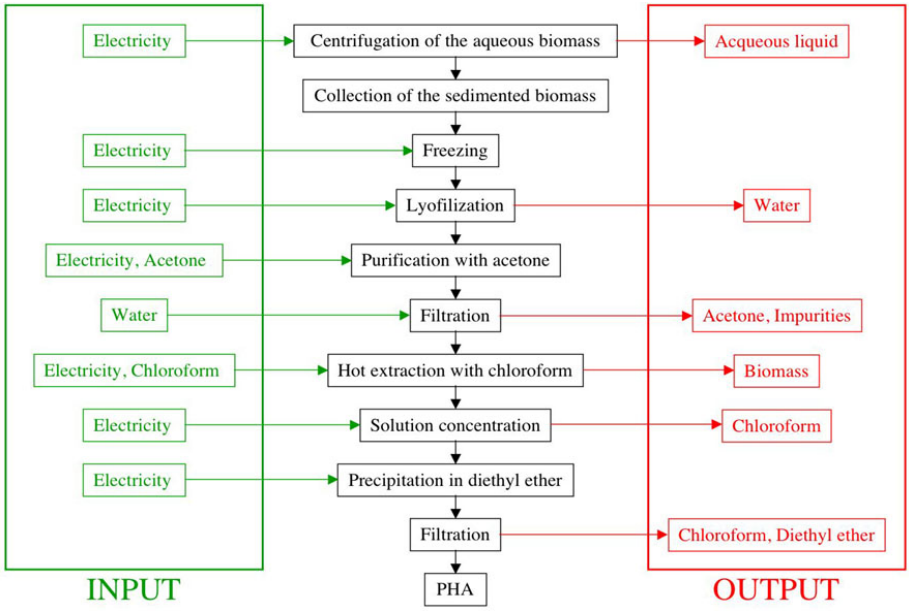

Figure 3.14 Input/Output Analysis of PHAs Purification and Extraction.

3.3 Conclusions

PHAs Produced by Pseudomonas Strain: From TGA analysis, purification efficiency in the samples increased with the following order: *PAR-9* > *PAR-7* > *PAR-1* > *PAR-4* > *PAR-2* > *PAR-5*. All polymers are most likely composed by ca. 90 % of P(3HB) copolymerized with other HA units. This hypothesis seems to be confirmed, in the case of *PAR-7*, from the double melting peak detected by DSC. However, the molecular weight of *PAR-7* was lower when compared with PHAs produced with Small Aerobic Reactor.

PHAs Produced by Azotobacter Sp with Small Aerobic Reactor: Among these samples, *SAR-4* showed a relatively high value of molecular weight (more than 1000 KDa). From TGA, *SAR-4* was the sample containing less impurities (ca. 7 wt-%). The residual weight of other 3 samples measured at 500°C ranged between 72 and 91 wt-%.

PHAs Produced by Azotobacter Sp with Pilot Plant: Among these samples, PP-1 is the only sample that gave an available polymer concentration (0.13 g/l). From TGA, PP-1 was the sample containing a large quantities of impurities (ca. 53.5 wt-%).

PHAs from University of Granada: NMR and DSC indicated that both *72h* and *96h* samples are almost fully composed of P(3HB) homopolymer. From TGA 72h sample showed superior thermal performances, but also a higher content of impurities. Molecular weight of *96h* (216 KDa) was higher if compared with *72h* (188 KDa).

3.4 Modification of Cellulose Extracted from Sugar Cane Bagasse (SCB) and Rice Straw (RS).

Waxes is one of the most important lipophilic extractives found in rice straw (RS) and sugar cane bagasse (SCB), in addition to fatty acids, sterols, steryl esters, and triglycerides. These extractives when liberated during the pulping process can cause significant problems for pulp and paper manufactures as they are deposited as pitch, either alone or in combination with fibers, fillers, defoaming agents, or coating binders. In recent years, there has been an increasing trend towards more efficient utilization of agro-industrial residues, such as RS and SCB. These natural fibers are gaining progressive account as renewable, environmentally acceptable, and biodegradable starting material for industrial applications, such as technical textiles, composites, pulp and paper, civil engineering and building activities as well as a source of chemicals or building blocks[39,45,141,162].

Extraction process of these two milled biomass was carried out using a Kumagawa extractor and toluene-ethanol (2:1, v/v) as solvent mixture.

The obtained materials were characterized by thermal, morphological and spectroscopic analyses.

So, the cellulosic fraction obtained from biomasses SCB and RS was derivatized to obtain cellulose acetate (CA). The chemical procedure used acetic anhydride (96 mL) as acetylating agent, in the presence of acetic acid (27 mL) as solvent, and sulfuric acid (0.24 mL) as catalyst[39,45,162].

The past 10 years has witnessed a renewed interest in cellulose research and application, sparked mostly by technological interests in renewable raw materials and more environmentally friendly and sustainable resources.

The cellulose can be considered as a smart material using for biomimetic sensor/actuator devices and micro-electromechanical systems. This smart

cellulose is termed electroactive paper (EAPap). It can produce a large bending displacement with low actuation voltage and low power consumption. Because of cellulose EAPap is ultra-lightweight, inexpensive, and biodegradable, it is advantageous for many applications such as micro-insect robots, micro-flying objects, micro-electromechanical systems, biosensors, and flexible electrical displays[237].

Cellulose acetate (CA) is one of the oldest man made macromolecules used extensively in the textile industry, filters, etc. One of its applications is the production of membranes for separation processes such as hemodialysis, reverse osmosis and gas separation.

3.4.1 Chemical Composition

Chemical composition of SCB as a function of treatment stage is reported in Table 3.13.

Table 3.13. Chemical Composition (wt-%) of Egyptian Sugar Cane Bagasse[a].

Sample	wt-%							
	Extractive		Moist	Cel.	Hecel.	Lig	Silica	Ash
	A	B						
C-SCB	-	32	3.1	31.1	27.5	8.0	0.8	2.6
DC-SCB	-	-	2.7	42.1	33.2	9.5	1.1	2.5
M-SCB	-	30	3.8	27.6	24.0	7.3	1.3	2.2
DM-SCB	-	-	2.1	39.8	32.2	13.3	1.9	2.8

[a)] A and B are water and toluene/ethanol (de-waxing) extractives, respectively; C-SCB and DC-SCB are chopped and de-waxed chopped SCB, respectively; M-SCB and DM-SCB are milled and de-waxed milled SCB pass 0.425 mm, respectively; Hcel, Cel, Lig and Si are hemicellulose, cellulose, lignin and silica, respectively following van Soest procedure[(@)]; Moist determined gravimetrically

SCB as received (C-SCB) contained about 31 wt-% of cellulose, 27 wt-% of hemicellulose and 8 wt-% of lignin. In general, these values decreased slightly for the fraction of M-SCB and collected from the sieve that pass 0.425 mm (M-SCB). Exception was verified for the amount of silica.

The behaviour of the samples as received (C-SCB) and milled (M-SCB) was some what different after de-waxing. Both samples presented higher composition values of the components analyzed in relation to undewaxed samples.

However, after milling only cellulose and hemicellulose decreased and the

other components increased. Besides the samples that were milled and after de-waxing (DM-SCB) resulted to have about 13 % of lignin that represented an increasing of 62 % compared to C-SCB.

Chemical compositions as received, M-RS and DM-RS are reported in Table 3.14.

Table 3.14. Chemical Composition (wt-%) of Egyptian Rice Straw[a].

Sample	wt-%							
	Extractive		Moist	Cel.	Hcel.	Lig	Silica	Ash
	A	B						
C-RS	-	9.4	3.3	29.7	12.6	12.7	10.7	15.1
DC-RS	-	-	4.9	39.6	15.4	7.0	12.3	15.2
M-RS	-	8.1	1.9	31.6	14.7	7.0	10.5	15.0
DM-RS	-	-	4.4	31.2	15.9	12.4	12.4	15.3

[a)] A and B are water and toluene/ethanol (de-waxing) extractives, respectively; C-SCB and DC-SCB are chopped and de-waxed chopped SCB, respectively; M-SCB and DM-SCB are milled and de-waxed milled SCB pass 0.425 mm, respectively; Hcel, Cel, Lig and Si are hemicellulose, cellulose, lignin and silica, respectively following van Soest procedure[(@)]; Moist determined gravimetrically.

The behaviour of RS as a function of milling and de-waxing was quite different to that of SCB.

RS as received (C-RS) contained 30 wt-% of cellulose, 13 wt-% of hemicellulose and 13 wt-% of lignin. After milling (M-RS), only moisture and lignin decreased of about 42 % and 45 %, respectively compared to C-RS. On the other hand, the values of cellulose and hemicellulose amounts were higher than that of C-RS about 6 % and 17 %, respectively compared to C-RS. This behaviour was contrary to that observed in M-SCB. As received RS (DC-RS) after dewaxing showed to contain more amount of the component analyzed except that of lignin in relation to C-RS. These changes

corresponded to 48 %, 33 %, 22 %, 15 % increasing in moisture, cellulose, hemicellulose and silica, respectively and 45 % decreasing in lignin.

However, for the composition of RS that was first milled (M-RS) and then de-waxed (DM-RS) only moisture and lignin amount showed significant changes with the treatment performed. These changes corresponded to an increasing of 132 % and 77 %, respectively in compared to M-RS.

Both SCB and RS showed that ash amounts were basically invariable with the milling and dewaxing treatments, which were around 3 % and 15 % respectively. On the other hand, these biomass treatments had a significant affect on their composition as previously showed.

3.4.2 Morphology of Lignocellulosic Wastes

Comparative SEM photomicrographs of chopped (C), dewaxed-chopped (DC), milled (M) and dewaxed-milled (DM) SCB and RS are presented in Figures 3.15 and 3.16, respectively.

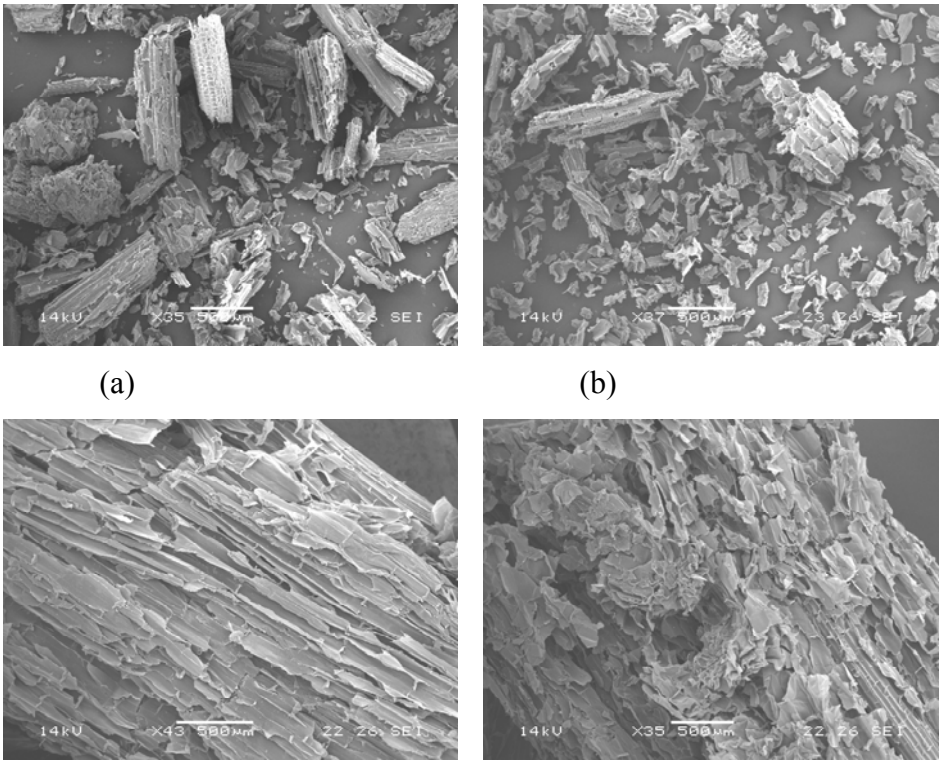

Figure 3.15 SEM Photomicrographs for M-SCB-35X (a), DM-SCB-37X (b), C-SCB-43X (c), DC-SCB-35X (d).

Pictures c) and d) in Figures 3.15 and 3.16 showed the characteristic cylinder and/or vascular bundles of the grass plants like straws and SCB.
These morphologies can also be observed in the water soluble free residue (WSFR) resulted from the acetilation of cellulose obtained from SCB (Fig.

3.17c). Moreover, the cellulose extracted from SCB (Fig. 3.17a) appeared as an agglomerate of fibre and the cellulose acetate (CA) (Fig. 3.17b) from SCB cellulose acetilation as a thick agglomerated powder.

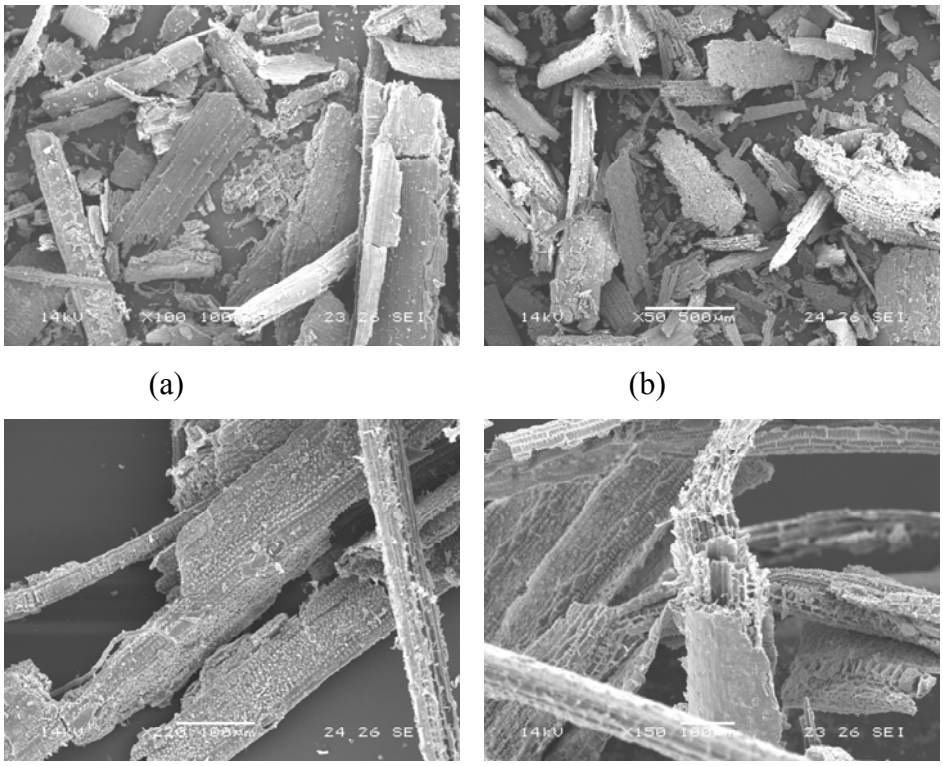

(a) (b)

(c) (d)

Figure 3.16 SEM Photomicrographs for M-RS-100X (a), DM-RS-50X (b), C-RS-220X (c), DC-RS-150X (d).

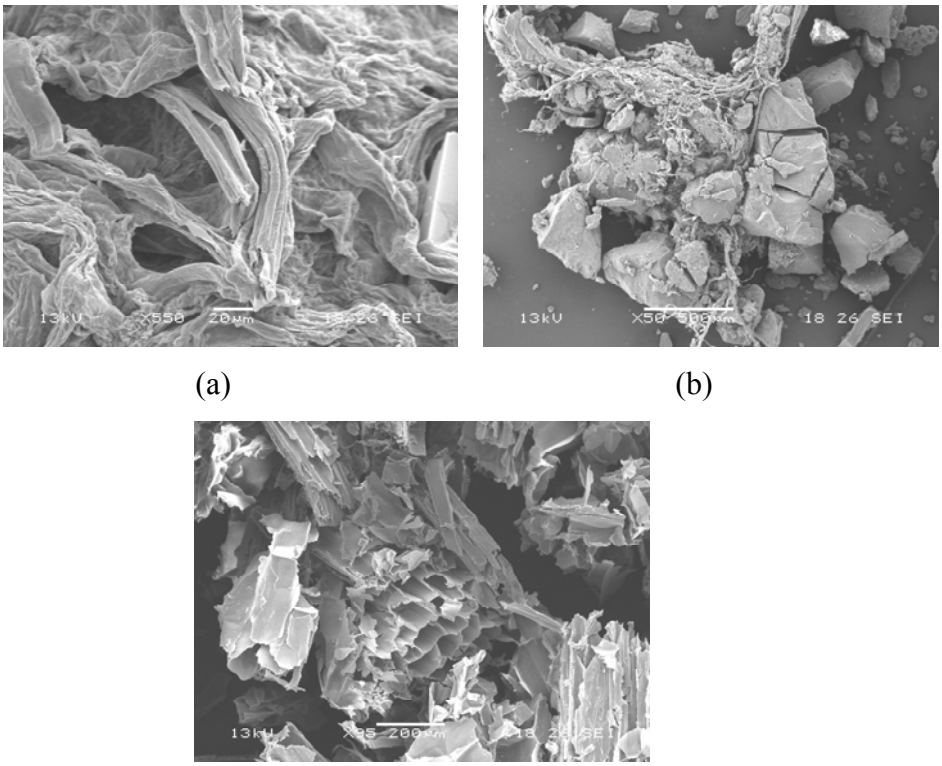

(a) (b)

(c)

Figure 3.17 SEM Photomicrographs for Cellulose from SCB-550X (a), Cellulose Acetate-50X (b), WFSR-95X (c).

3.4.3 Thermal Properties of Lignocellulosic Materials

Thermal characterization of the two ligno-cellulosic based materials (SCB and RS) and their derivative products gave informations on the degradation temperature and the processability of the materials[36,39].

Thermal properties of SCB, RS and extracted cellulose were assessed by thermogravimetry (TGA) and differential scanning calorimetry (DSC).

3.4.3.1 Thermogravimetric Analysis (TGA)

TGA pyrolysis traces and their derivatives (DTGA) of as received (C-SCB), milled (M-SCB) and dewaxed SCB (DM-SCB) are represented in Figure 3.18 and their TGA data are in Table 3.15.

The weight loss steps observed in the samples C-SCB and M-SCB (Fig. 3.18) were at least six steps, where five of them were overlapped as shown DTGA traces (Fig. 3.18b) that appeared as shoulder, peaks and tail. These samples after dewaxing, DC-SCB and DM-SCB, presented three and two weight loss steps, respectively.

The first step (25°C-120°C) of all samples corresponded to the moisture volatilization and were 3.1 %, 2.1 %, 4 %, 4.7 % in the C-SCB, DC-SCB, M-SCB, DM-SCB, respectively.

The second and third overlapped steps of weight loss in the samples C-SCB and M-SCB occurred between ca 120°C and 240°C. These steps can be assigned to the low molecular weight extractives, that in the case of SCB, can be starch, sugars (principally saccarose), phenolics and tannins[157].

As the second step seemed to be a tail of the third one, the weight loss step was calculated as a single step and corresponds to a 18.5 % and 20.1 % for C-SCB and M-SCB, respectively.

This slight increasing on extractive amounts in the sample M-SCB suggested that probably milling-sieving process concentrates something more of fragile component in the fraction that pass 0.425 mm.

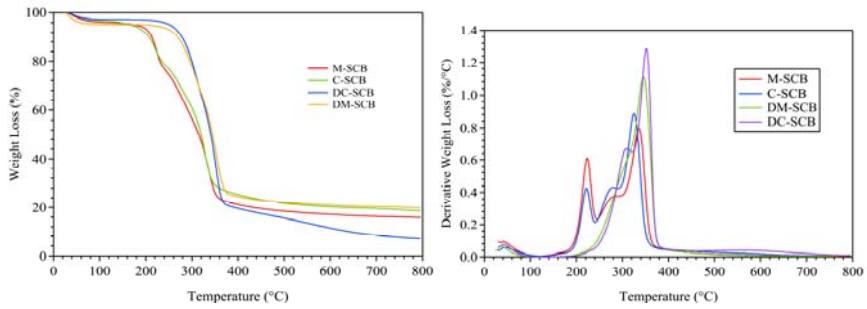

(a) (b)

Figure 3.18 TGA (a) and DTGA (b) Traces of SCB Based Materials Under Nitrogen Atmosphere.

Fourth weight loss step was measured between ca 240°C-300°C and the values for C-SCB and M-SCB were 14.2 % and 18 %, respectively. The principal chemical component of ligno-cellulosic biomass that decompose in this range of temperature was the hemicellulose[41].

The highest amount of hemicellulose among C-SCB and M-SCB, from chemical assessment (Table 3.13) was verified for the first one that apparently disagreed with the TGA results. So, this meant that with milling-sieving process changed the proportion between components, probably due to the mechanical characteristics of each components as previously proposed.

The last weight loss step was a peak followed by a tail up to the end of the experiment. The temperature range of the step corresponding to the DTGA peak was between ca. 300°C-380°C, which principal component decomposing was the cellulose. A small fraction of lignin that continue to degrade at higher temperatures was present, too. The values of weight loss for this step were 37 % and 35 % for C-SCB and M-SCB, respectively.

Finally in the temperature range of 400°C-800°C the weight loss was 6.6 % and 5.2 % leaving a recovered residue of 18.1 % and 15.3 % for C-SCB and M-SCB, respectively. This last step corresponded principally to the lignin decomposition and the residue to the inorganic materials and carbon.

Table 3.15. Thermogravimetric Data of SCB Based Materials Under Nitrogen Atmosphere.

Sample	T_{on} (°C)	T_{p1} (°C)	T_{p2} (°C)	T_{p3} (°C)	T_{p4} (°C)	T_{p5} (°C)	R_{800} (%)
DC-SCB	277	-	317	351	416	-	4.4
M-SCB	206	222	281	335	400	-	15.3
DM-SCB	275	-	306	352	447	-	19.6
C-SCB	221	220[a]	282	327	399	-	18.1

[a] overlapped weight loss, b) shoulder.

C-SCB and M-SCB after extraction with the solvent mixture toluene/ethanol (samples DC-SCB and DM-SCB, respectively) displayed no weight loss steps in the temperature range of 120°C-240°C. So, C-SCB and DM-SCB TGA traces suggested at least four weight loss steps, which the first one corresponded to the moisture volatilization, as previously reported.

The first and second degradation weight loss steps in the temperature range of ca. 200°C and 380°C were overlapped at around 320°C.

The values of these steps for DC-SCB were 30 % and 44 % and for DM-SCB were 27 % and 44 %, respectively. The last step that resulted principally from lignin pyrolysis corresponded to the weight loss in the temperature range of 380°C-800°C that was ca. 8 % and corresponding to the DTGA peak was 3 % for DC-SCB and DM-SCB, respectively. The residues recovered at 800°C were ca. 4 % and 20 %, respectively.

Table 3.15 records the TGA data of SCB based materials. The temperatures of onset pyrolysis (T_{on}) depended on both milling-sieving process and toluene/ethanol extraction. T_{on} value of C-SCB was 221°C, that decreased of ca. 15°C after milling (M-SCB) and it increased ca. 56°C for the

sample without extractives (DC-SCB).

On the other hand, both DC-SCB and DM-SCB presented equivalent T_{on} values around 276°C. Consequently the difference in the thermal stability among C-SCB and M-SCB was due to extractive composition.

The maximum rate of decomposition product volatilization (T_p) depended principally from the toluene/ethanol extraction which values were higher than that of pristine material.

TGA and DTGA experiments were conducted also under air atmosphere: the traces and the relative data are presented in Figure 3.19 and in Table 3.16.

The samples C-SCB and M-SCB (Fig. 3.19) showed at least five steps, while the same samples after dew axing process, DC-SCB and DM-SCB, had four weight loss steps.

Under air atmosphere; the first step (25°C-120°C) of all samples corresponded to the moisture and volatiles elimination and it was 2.3 %, 1.7 %, 1.6 %, 2.5 % in the C-SCB, DC-SCB, M-SCB, DM-SCB, respectively.

The second, the third and fourth steps of weight loss in the samples C-SCB and M-SCB occurred between 120°C and 500°C. The third step for M-SCB and the fourth one for C-SCB presented shoulders so as weight loss we considered the total effect finding 18.1 % (M-SCB) and 30.3 % (C-SCB).

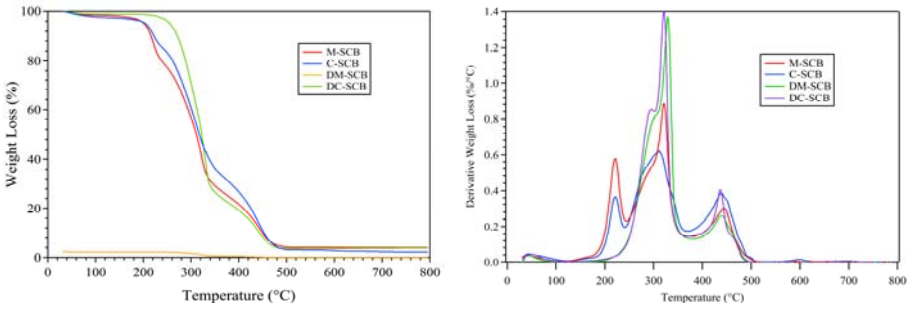

(a) (b)

Figure 3.19 TGA (a) and DTGA (b) Traces of M-SCB, C-SCB, DM-SCB, and DC-SCB Under Air Atmosphere.

For both samples, the second step felt down in the temperature range of ca. 180°C-250°C and the corresponding weight losses were 12.5 % for C-SCB and 19.9 % for M-SCB, respectively. The same trend was observed also for the fourth step that occurred between 350°C and 500°C for C-SCB and for M-SCB that corresponded to the weight losses of 30.3 % and 33 %, respectively.

A difference in the intensity of these peaks was observed, because of the milling process made the peak higher than the same one compared to the pristine material.

Finally in the temperature range of 500°C-800°C the weight losses were 0.9 % and 22.4 % leaving a residue of 2.3 % and 4 % for C-SCB and M-SCB, respectively.

Table 3.16. Thermogravimetric Data of SCB Based Materials Under Air Atmosphere.

Sample	T_{on} (°C)	T_{p1} (°C)	T_{p2} (°C)	T_{p3} (°C)	T_{p4} (°C)	T_{p5} (°C)	R_{800} (%)
DC-SCB	265	-	295	322	437	469	2.9
M-SCB	203	222	292	321	445	-	4.0
DM-SCB	259	-	224	293	325	439	3.4
C-SCB	229	222	310	440	600	-	2.3

C-SCB and M-SCB after extraction with the solvent mixture toluene/ethanol (samples DC-SCB and DM-SCB, respectively) displayed no weight loss steps in the temperature range of 120°C-240°C.

So, C-SCB and DM-SCB TGA traces suggested at least four weight loss steps, which the first one corresponded to the moisture and volatiles elimination, as previously reported.

The shoulder in the first degradation weight loss step was more evident for

DC-SCB respect to DM-SCB and the values were 37.5 % and 25.1 %, respectively.

The weight losses for the real step were 32.8 % and 45.1 %. The same effect was also evident in the second degradation weight loss step, mainly due to the decomposition of cellulose and lignin. The values were 23.8 % for DC-SCB and 21 % for DM-SCB. The residues recovered at 800°C were ca. 3 % and 3.4 %, respectively.

Table 3.16 reports the onset temperatures for the SCB based materials before and after extraction when the TGA experiments were conducted under air atmosphere.

The onset temperature for C-SCB was 229°C and it decreased of ca. 16°C after milling (M-SCB) and it increased of ca. 36°C for the sample without extraction (DC-SCB).

DC-SCB and DM-SCB had similar onset temperatures: the difference of 6°C suggested that the thermal stability depended on the extractive composition.

Figure 3.20 reports the TGA (a) and DTGA (b) traces for RS before and after milling and dew axing processes.

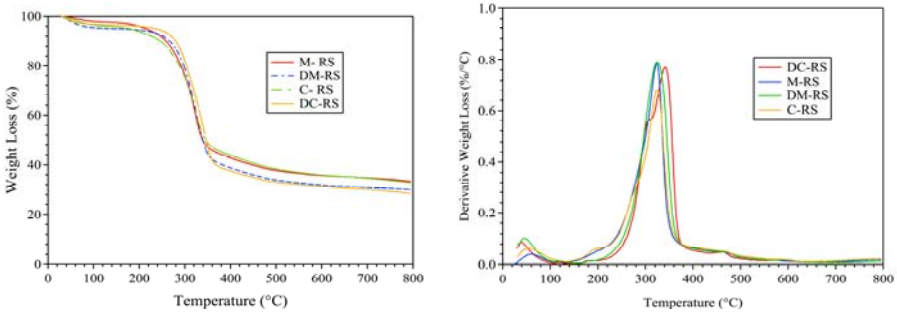

(a) (b)

Figure 3.20 TGA (a) and DTGA (b) Traces of M-RS, C-RS, DM-RS, and DC-RS Under Nitrogen Atmosphere.

The first step (25°C-120°C) of all samples corresponded to the moisture volatilization and were 3.3 %, 3 %, 1.9 %, 4.4 % in the C-RS, DC-RS, M-RS, DM-RS, respectively.

The second and third steps of weight loss in the samples C-RS and M-RS occurred between ca 120°C and 240°C and the corresponding values were 4.7 % and 18.5 % for C-RS and 6.8 % and 46.7 % for M-RS. The residues recovered at 800°C were ca. 31.8 % and 32.2 %, respectively.

The extraction process shifted the shoulder of the chopped material from around 200°C to ca. 300°C and a third peak around at 480°C appeared in the relative trace. The corresponding weight losses were 22.1 %, 34.2 %, 4.2 % and the residue recovered at 800°C was 27 %.

In the DM-RS sample the shoulder was around at 190°C and it was associated with a weight loss of 17.6 %. It was present only one degradation weight loss step in the temperature range of 200°C-400°C, corresponding to 38.2 % of weight loss and a second effect smaller than the first one in the temperature range 420°C-490°C with a weight loss of 4.6 %. The residue recovered at 800°C was 29.5 %.

Table 3.17. Thermogravimetric Data for RS Based Materials Under Nitrogen Atmosphere.

Sample	T_{on} (°C)	T_{p1} (°C)	T_{p2} (°C)	T_{p3} (°C)	T_{p4} (°C)	T_{p5} (°C)	R_{800} (%)
DC-RS	277	-	182	313	341	462	27.0
M-RS	259	-	325	466	568	-	32.2
DM-RS	272	-	124	324	468	-	29.5
C-RS	258	194	306	325	465	-	31.8

Table 3.17 shows the onset temperatures for the RS based materials.

RS before and after milling (C-RS and M-RS) processes had the same

onset temperature, while this value increased of ca. 18°C for the sample after extraction (DC-RS). So, also for RS, the extractive composition influenced the thermal stability: the presence of wax, sugars, phenols made the material less stable respect to the same one after the extraction process.

The TGA (a) and DTGA (b) traces for the RS based materials under air atmosphere are reported in Figure 3.21 and the relative data are presented in Table 3.18.

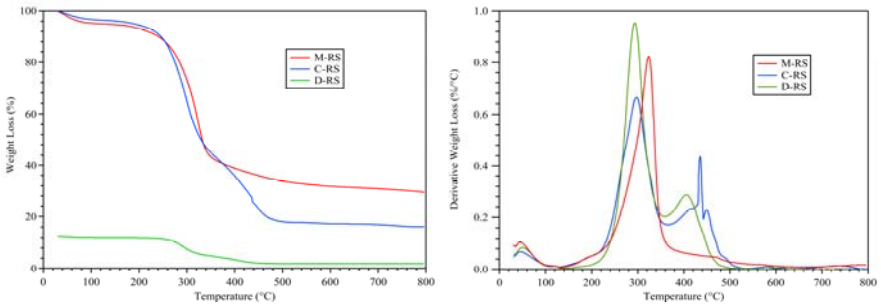

(a) (b)

Figure 3.21 TGA (a) and DTGA (b) Traces for RS Based Materials Under Air Atmosphere.

Under air atmosphere, the weight loss steps observed in the samples C-RS and M-RS (Fig. 3.21) were at least four, where two of them were overlapped as shown DTGA traces (Fig. 3.21b).

The first step (25°C-120°C) of all samples corresponded to the moisture and volatiles elimination and the relative weight losses were 3.3 %, 4.7 %, 3.9 % in the C-RS, M-RS, DM-RS, respectively.

The second step was a shoulder and it occurred in the temperature range of 120°C-240°C with a weight losses of 22.6 % for C-RS, 25.4 % for M-RS and 16.7 % for DM-RS. The third weight loss step occurred in the temperature range of 240°C-365°C and principally it represented the cellulose degradation.

This material was associated with some sugars that started to degrade at lower temperature respect to the same ones for the pure cellulose[160].

The weight losses were 29 % for C-RS, 25 % for M-RS and 41.3 % for DM-RS.

The fourth step for C-RS felt down in the temperature range of 365°C-500°C, corresponding to a weight loss of 24.6 %; the same material after milling presented a degradation weight loss step of 8.8 %.

The residues recovered at 800°C were 15.9 % for C-RS and 28.9 % for M-RS, respectively.

The DM-RS sample, under air atmosphere was degraded in four steps. The first step with a weight loss of about 3.9 % that it occurred in the temperature range of 25-100°C, represented the evolution of the moisture.

The shoulder with a weight loss of 16.7 % in the temperature range of 100-240°C, represented the extractives start decomposition of rice straw.

The third step with a weight loss of 41.3 %, represented mainly the decomposition of cellulose. The fourth step, associated a weight loss of 22.5 %, principally represented the decomposition of hemicellulose and lignin.

The residue recovered at 800°C was 13.7 %.

Table 3.18. Thermogravimetric Data for RS Based Materials Under Air Atmosphere.

Sample	T_{on} (°C)	T_{p1} (°C)	T_{p2} (°C)	T_{p3} (°C)	T_{p4} (°C)	T_{p5} (°C)	T_{p6} (°C)	T_{p7} (°C)	T_{p8} (°C)	R_{800} (%)
M-RS	264	193	323	468	-	-	-	-	-	28.9
DM-RS	258	293	405	609	-	-	-	-	-	13.7
C-RS	248	195	298	413	437	450	488	583	737	15.9

Figure 3.22 shows the TGA (a) and DTGA (b) traces also for WSFR and for the cellulose, while the relative data are in Table 3.19.

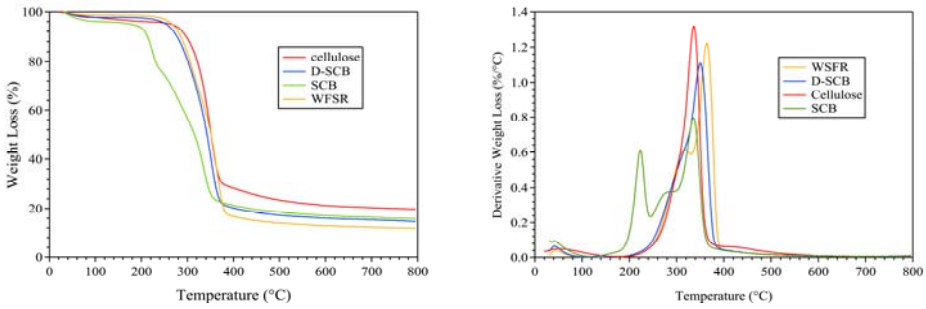

(a) (b)

Figure 3.22 TGA (a) and DTGA (b) Traces of SCB, DSCB, WSFR, and Cellulose Under Nitrogen Atmosphere.

WSFR (Fig.3.22) was degraded in four steps. The first step with a weight loss of about 1.2 % in the temperature range of 25-100°C represented the evolution of the moisture, while the second step with a weight loss of 37.8 % in the temperature range of 100-320°C represented probably the fraction of hemicellulose after extraction of water soluble carbohydrates.

The third step with a weight loss of 41.2 % occurred in the temperature range of 340-400°C and it represented mainly the decomposition of cellulose.

The fourth step with a weight loss of 4.2 % felt down in the temperature range of 400-800°C, and it principally represented the decomposition of cellulose and lignin. The residue recovered at 800°C was 11.4 %.

This material under air atmosphere, started to degrade at ca. 271°C with a maximum weight loss step of 39.3 % in the temperature range 250-370°C.

The cellulose was less thermal stable because it was accompanied by some sugars (pentosans) that degraded at lower temperature respect to the pristine cellulose. The residue recovered at 800°C was 3.2 %.

From the TGA trace of cellulose (Fig. 3.22a), a slow weight loss from room temperature up to 230°C was observed. This effect was attributed to the

desorption of physically adsorbed water. Cellulose began to decompose at 298°C with a weight loss step of 66 %. The residue recovered at 800°C was 19.9 %.

Table 3.19. Thermogravimetric Data for Cellulose, D-SCB, SCB and WSFR Under Nitrogen Atmosphere.

Sample	T_{on} (°C)	T_{p1} (°C)	T_{p2} (°C)	T_{p3} (°C)	T_{p4} (°C)	T_{p5} (°C)	R_{800} (%)
Cellulose	302	-	346	438	-	-	19.9
D-SCB	277	-	317	351	-	-	4.4
SCB	221	148	220	281	327	447	18.1
WSFR	277	-	315	366	-	-	11.4

Figure 3.23 shows the TGA (a) and DTGA (b) trend for cellulose and cellulose acetate (CA) under nitrogen atmosphere and the relative thermogravimetric data are in Table 3.20..

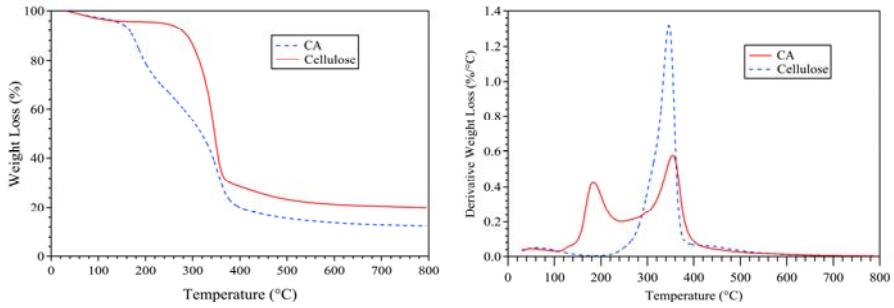

(a) (b)

Figure 3.23 TGA (a) and DTGA (b) Traces of Cellulose, and Cellulose Acetate (CA) Under Nitrogen Atmosphere**.**

The cellulose acetate (CA) degraded in five steps. The first step corresponded to the evaporation of the residual absorbed water and it occurred in the temperature range of 25°C-120°C. The weight losses were 3.1 % for the cellulose and 2.8 % for the cellulose acetate (CA), respectively.

The second step presented a shoulder between 120°C-140°C, it corresponded to the main thermal degradation of these materials and it occurred in the temperature range of 140°C-240°C. The weight losses were 2 % for the shoulder and 27.1 % for the peak, respectively.

The third peak represented the totally decomposition of the materials and the carbonization of the products to ash, that gave a weight loss step of ca. 66 % and it occurred in the temperature range of 240°C-420°C for cellulose acetate.

The fourth step with a weight loss of ca. 48.5 % felt down in the temperature range of 420°C-640°C and the residue recovered at 800°C was 11.4 %.

As we can observe from the same value for the onset temperatures in Table 3.20, the two materials hadn't the same thermal stability: the acetylation process created important difference in the structure of these materials.

Table 3.20. Thermogravimetric Data for Cellulose and Cellulose Acetate (CA) Under Nitrogen Atmosphere.

Sample	T_{on} (°C)	T_{p1} (°C)	T_{p2} (°C)	T_{p3} (°C)	R_{800} (%)
Cellulose	298	-	345	442	19.6
CA	145	128[a]	184	355	11.4

a: shoulder

Figure 3.24 shows the TGA (a) and DTGA (b) trend for cellulose and cellulose acetate (CA) under air atmosphere, while Table 3.21 reports the thermogravimetric data.

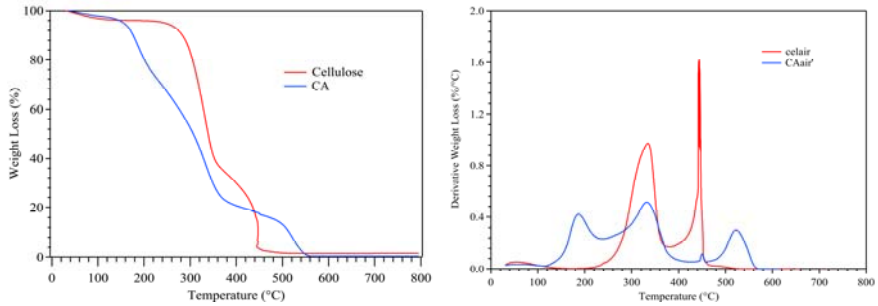

(a) (b)

Figure 3.24 TGA (a) and DTGA (b) Traces for Cellulose and Cellulose Acetate (CA) Under Air Atmosphere**.**

The TGA trend (Fig. 3.24a) showed at least four degradation weight loss steps for the cellulose and cellulose acetate. The first weight loss step corresponded to the moisture and volatiles decomposition occurred in the temperature range of 25°C-140°C. The weight losses were 3.1 % for cellulose and 2.3 % for cellulose acetate, respectively.

The onset temperatures, as it has been shown in Table 3.21, were 300°C for the cellulose and 160°C for the cellulose acetate: the acetylation process made the cellulose derivative less thermal stable than the pristine material.

The second peak presented a shoulder that it occurred in the temperature range of 220°C-240°C for cellulose and 120°C-140°C for cellulose acetate.

The shoulder corresponded to a weight loss of 67.4 % for cellulose and 27.9 % for cellulose acetate, respectively. For this latter material the second peak corresponded to the thermal decomposition of hemicellulose and the glycosidic links of cellulose[161].

The third weight loss step occurred in the temperature range of 240°C-

390°C and it corresponded to weight losses of ca. 49.3 % for cellulose acetate and 66 % for cellulose. It represented the thermal decomposition of α-cellulose. The fourth step occurred in the temperature range of 460°C-520°C for cellulose and 440°C-600°C for cellulose acetate, respectively.

The weight losses were 6.6 % for cellulose and 19 % for cellulose acetate and they were associated principally with the lignin decomposition.

The residues recovered at 800°C were 19.9 % for cellulose and 0.35 % for cellulose acetate respectively.

Table 3.21. Thermogravimetric Data for Cellulose and Cellulose Acetate (CA) Under Air Atmosphere.

Sample	T_{on} (°C)	T_{p1} (°C)	T_{p2} (°C)	T_{p3} (°C)	T_{p4} (°C)	R_{800} (%)
Cellulose	298	-	345	442	-	19.9
CA	161	188	331	450	522	0.35

The TGA (a) and DTGA (b) trend for alkaline-peroxide-soluble hemicellulose (APSH) under nitrogen and air atmosphere are reported in Figure 3.25, while the thermogravimetric data are in Table 3.22.

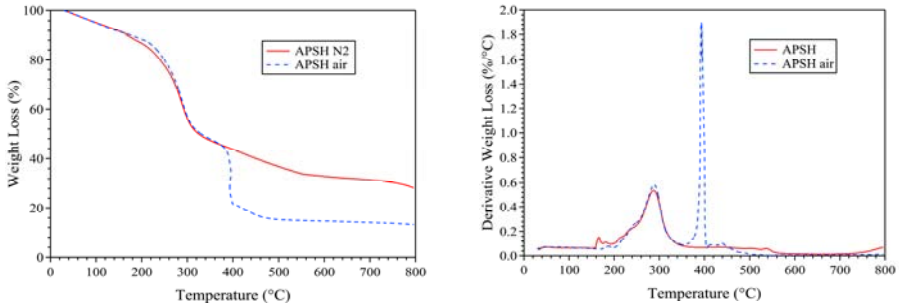

(a) (b)

Figure 3.25 TGA (a) and DTGA (b) Traces of Alkaline Peroxide Soluble Hemicellulose (APSH) Under Nitrogen and Air Atmosphere.

The first overlapped peak for the experiment conducted under nitrogen and air corresponded to the moisture evolved in the temperature range of 25°C-160°C. The relative weight losses were 4.8 % in nitrogen and 4.9 % in air, respectively.

The second DTGA peak (Fig. 3.35b) presented a shoulder for both samples independently from the experiment atmosphere. This shoulder felt down in the temperature range of 160°C-350°C and it corresponded to a weight loss of ca. 45.9 % when the material was analyzed in nitrogen atmosphere and 22.9 % when the same sample was analyzed in air atmosphere.

The third peak occurred in the temperature range of 350°C-550°C for the same sample in different conditions and it corresponded to a weight loss of ca. 24.1 % for the APSH in nitrogen atmosphere and 33.9 % for APSH in air atmosphere. The residues recovered at 800°C were 27.9 % and 12.9 % for APSH under nitrogen and under air atmosphere, respectively.

Table 3.22. Thermogravimetric Data for Alkaline Peroxide Soluble Hemicellulose (APSH) Under Nitrogen and Air Atmosphere.

Sample	T_{on} (°C)	T_{p1} (°C)	T_{p2} (°C)	T_{p3} (°C)	T_{p4} (°C)	T_{p5} (°C)	R_{800} (%)
$APSH_{N2}$	222	165[a]	235[a]	288	444	537	27.9
$APSH_{air}$	253	244	287	394	438	-	12.9

Table 3.22 reports the onset temperatures for the APSH under nitrogen and air atmosphere. This value was around at 250°C for the APSH under air atmosphere and it decreased of about 30 °C for the APSH under nitrogen one.

Figure 3.26 shows the TGA (a) and DTGA (b) traces for the alkaline-peroxide-soluble lignin (ASL) under nitrogen and air atmosphere, while the thermogravimetric data are in Table 3.23.

The ASL sample presented at least five weight loss steps in nitrogen atmosphere and six ones in air atmosphere. The first step corresponding to the moisture occurred in the temperature range of ca. 25°C-100°C and the relative weight losses were 2.1 % under nitrogen and 3.8 % under air atmosphere.

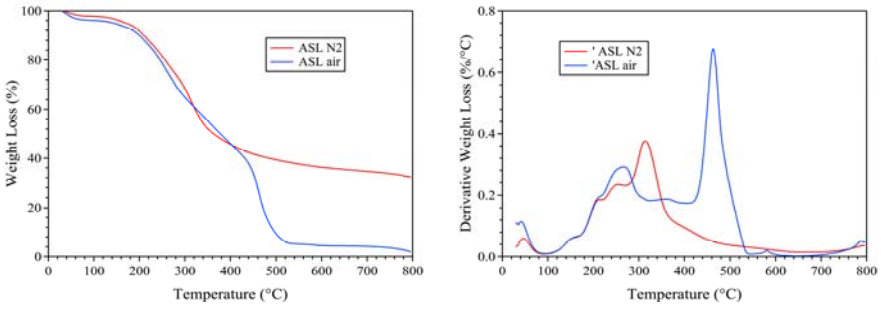

(a) (b)

Figure 3.26 TGA (a) and DTGA (b) Traces of Alkaline Soluble Lignin (ASL) Under Nitrogen and Air Atmosphere.

The shoulders of the main degradation peak occurred between 120°C and 290°C and they associated a weight loss of ca. 58.1 % for the TGA under nitrogen atmosphere. For the same experiment under air atmosphere this shoulder was comprised between 120°C and 220°C and the relative weight loss was 32.5 %.

The main degradation peak was shifted for the ASL under air atmosphere and it occurred in the temperature range of ca. 300°C-400°C in nitrogen atmosphere, that became 300°C-550°C when the experiment conditions were modified. The weight losses were 8.1 % for the first experiment and 55.1 % for the second one. The fourth step occurred in the temperature range of ca. 550°C-600°C for both samples, corresponding to a weight losses of 6.8 % for ASL under nitrogen and 3.1 % for ASL under air atmosphere.

Table 3.23. Thermogravimetric Data for Alkaline Soluble Lignin (ASL) Under Nitrogen and Air Atmosphere.

Sample	T_{on} (°C)	T_{p1} (°C)	T_{p2} (°C)	T_{p3} (°C)	T_{p4} (°C)	T_{p5} (°C)	T_{p6} (°C)	R_{800} (%)
ASL_{N2}	189	151	210	284	313	406	545	30.8
ASL_{air}	177	151	208	264	360	462	580	1.9

The onset temperature didn't change with the experiment conditions (Table 3.23).

3.4.3.2 Differential Scanning Calorimetry (DSC)

As shown by TGA analysis, the cellulose acetate (CA) started to degrade around at 312°C so for the DSC measurements, the temperature range 25-200°C was selected.

As we can see in the Figure 3.27, no peaks of fusion were evident in the traces. In the DSC traces, the exothermic transitions were represented upward following the International Confederation for Thermal Analysis (ICTA) convenction. At the end to visualize the traces in the best manner the relative offset were shifted from the zero point.

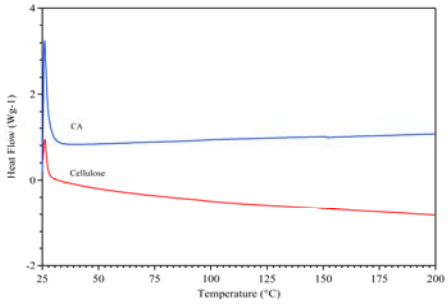

Figure 3.27 DSC Traces of Cellulose and Cellulose Acetate (CA) (Second Heating).

Cerqueira et al.[55], gave a correlation between the enthalpy of fusion and the cristallinity of the cellulose acetate (CA). The material started to degrade around 300°C, so the process that they considered as a fusion is a degradative process. Figure 3.28 shows the calorimetric traces for the SCB based materials while Figure 3.29 shows the calorimetric traces for the RS ones.

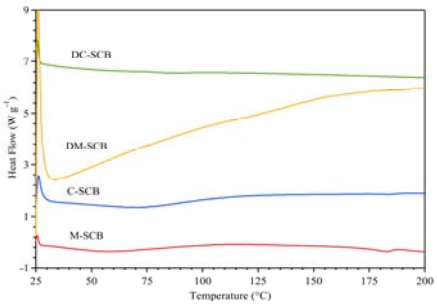

Figure 3.28 DSC Traces of M-SCB, C-SCB, DM-SCB, and DC-SCB (Second Heating).

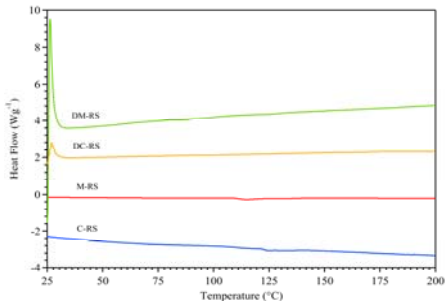

Figure 3.29 DSC Traces of M-RS, C-RS, DM-RS, and DC-RS (Second Heating).

As shown in these Figures, in the temperature range 25-200°C no glass transition temperatures are evident.

3.4.4 Infrared Spectroscopy (FTIR)

The FTIR spectra of M-SCB, DM-SCB, C-SCB, and DC-SCB are reported in Figure 3.30[40;43;44;45,53]. The FTIR spectrum of M-SCB (Fig. 3.30) showed a strong band around 3379 cm^{-1} due to the stretching of the O-H group, a weak band at 2924 cm^{-1} which attributed to the C-H stretching, band at 1727 cm^{-1} which attributed to the stretching of the carbonyl group, bands at 1630 cm^{-1}, 1603 cm^{-1}, and 1430 cm^{-1} which attributed to the stretching of

the benzene ring, bands at 1551-1510 cm^{-1} which attributed to the stretching of the carbonyl group and keto group, band at 1372 cm^{-1} which attributed to the $-CH_2-$ bending, a band at 1325 cm^{-1}, and 1053 cm^{-1} which attributed to the stretching of O-H, C-C, and C-O, and a band at 1246 cm^{-1} which attributed to the stretching of the C-O-C of the pyranose skeletal.

The FTIR spectrum of DM-SCB showed a strong band around 3365 cm^{-1} due to the stretching of the O-H group, a weak band at 2897 cm^{-1} which attributed to the C-H stretching, band at 1731 cm^{-1} which attributed to the stretching of the carbonyl group, bands at 1632 cm^{-1}, 1603 cm^{-1} , and 1426 cm^{-1} which attributed to the stretching of the benzene ring, bands at 1512 cm^{-1} which attributed to the stretching of the carbonyl group and keto group, band at 1374 cm^{-1} which attributed to the $-CH_2-$ bending, a band at 1327 cm^{-1}, and 1049 cm^{-1} which attributed to the stretching of O-H, C-C, and C-O, and a band at 1246 cm^{-1} which attributed to the stretching of the C-O-C of the pyranose skeletal.

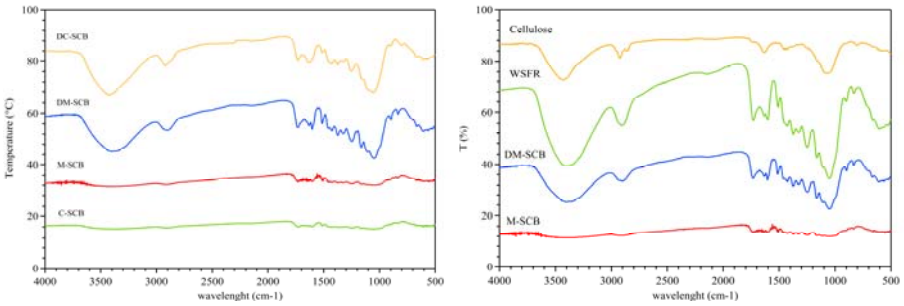

(a) (b)

Figure 3.30 FTIR Spectra of M-SCB, C-SCB, DM-SCB, and DM-SCB (a) and FTIR Spectra of SCB Before and After Dewaxing, Cellulose, WFSR (b).

The FTIR spectrum of C-SCB (Fig. 3.30) showed a strong band around 3401 cm^{-1} due to the stretching of the O-H group, a weak band at 2920 cm^{-1}

which attributed to the C-H stretching, band at 1734 cm^{-1} which attributed to the stretching of the carbonyl group, bands at 1637 cm^{-1}, and 1490 cm^{-1} which attributed to the stretching of the benzene ring, bands at 1509 cm^{-1} which attributed to the stretching of the carbonyl group and keto group, band at 1376 cm^{-1} which attributed to the $-CH_2-$ bending, a band at 1052 cm^{-1} which attributed to the stretching of O-H, C-C, and C-O, and a band at 1245 cm^{-1} which attributed to the stretching of the C-O-C of the pyranose skeletal.

The FTIR spectrum of DC-SCB showed a strong band around 3423 cm^{-1} due to the stretching of the O-H group, a weak band at 2920 cm^{-1} which attributed to the C-H stretching, band at 1730 cm^{-1} which attributed to the stretching of the carbonyl group, bands at 1635 cm^{-1}, and 1429 cm^{-1} which attributed to the stretching of the benzene ring, bands at 1509 cm^{-1} which attributed to the stretching of the carbonyl group and keto group, band at 1374 cm^{-1} which attributed to the $-CH_2-$ bending, a band at 1055 cm^{-1} which attributed to the stretching of O-H, C-C, and C-O, and a band at 1253 cm^{-1} which attributed to the stretching of the C-O-C of the pyranose skeletal.

The FTIR spectrum of WSFR showed a strong band around 3403 cm^{-1} due to the stretching of the O-H group, a weak band at 2904 cm^{-1} which attributed to the C-H stretching, band at 1729 cm^{-1} which attributed to the stretching of the carbonyl group, bands at 1601 cm^{-1}, and 1428 cm^{-1} which attributed to the stretching of the benzene ring, bands at 1509 cm^{-1} which attributed to the stretching of the carbonyl group and keto group, band at 1373 cm^{-1} which attributed to the $-CH_2-$ bending, a band at 1324 cm^{-1}, and 1050 cm^{-1} which attributed to the stretching of O-H, C-C, and C-O, and a band at 1248 cm^{-1} which attributed to the stretching of the C-O-C of the pyranose skeletal.

The FTIR spectrum of cellulose showed a strong band around 3429 cm^{-1} due to the stretching of the O-H group, a weak band at 2923 cm^{-1} which attributed to the C-H stretching, band at 1629 cm^{-1} which attributed to the adsorbed water molecules, a band at 1429 cm^{-1} which attributed to the of the

-CH_2- bending, and a strong band at 1073 cm^{-1} which attributed to the stretching of the C-O-C of the pyranose skeletal.

Figure 3.31 shows the FTIR spectra M-RS, DM-RS, C-RS, and DC-RS,[40;43;44;45]. The FTIR spectrum of M-RS showed a strong band around 3386 cm^{-1} due to the stretching of the O-H group, a weak band at 2924 cm^{-1} which attributed to the C-H stretching, bands at 1638 cm^{-1}, and 1419 cm^{-1} which attributed to the stretching of the benzene ring, a band at 1057 cm^{-1} which attributed to the stretching of O-H, C-C, and C-O, and a band at 1205 cm^{-1} which attributed to the stretching of the C-O-C of the pyranose skeletal.

The FTIR spectrum of D-milled-RS showed a strong band around 3407 cm^{-1} due to the stretching of the O-H group, a weak band at 2925 cm^{-1} which attributed to the C-H stretching, band at 1638 cm^{-1} which attributed to the stretching of the benzene ring, band at 1510 cm^{-1} which attributed to the stretching of the carbonyl group and keto group, band at 1374 cm^{-1} which attributed to the -CH_2- bending, a band at 1058 cm^{-1} which attributed to the stretching of O-H, C-C, and C-O, and a band at 1321 cm^{-1} which attributed to the stretching of the C-O-C of the pyranose skeletal.

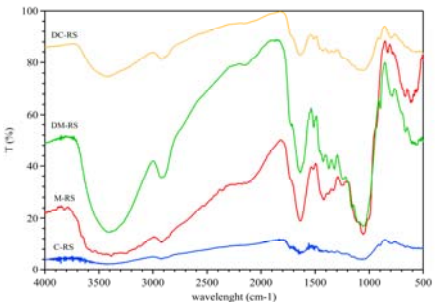

Figure 3.31 FTIR Spectra of M-RS, C-RS, DM-RS, and DC-RS.

The FTIR spectrum of C-RS showed a strong band around 3401 cm^{-1} due to the stretching of the O-H group, a weak band at 2920 cm^{-1} which attributed to the C-H stretching, band at 1734 cm^{-1} which attributed to the stretching of the carbonyl group, bands at 1637 cm^{-1}, and 1490 cm^{-1} which attributed to the

stretching of the benzene ring, bands at 1509 cm^{-1} which attributed to the stretching of the carbonyl group and keto group, band at 1376 cm^{-1} which attributed to the $-CH_2-$ bending, a band at 1052 cm^{-1} which attributed to the stretching of O-H, C-C, and C-O, and a band at 1245 cm^{-1} which attributed to the stretching of the C-O-C of the pyranose skeletal. The FTIR spectrum of DC-RS showed a strong band around 3400 cm^{-1} due to the stretching of the O-H group, a weak band at 2922 cm^{-1} which attributed to the C-H stretching, band at 1645 cm^{-1} which attributed to the stretching of the carbonyl group, a band at 1463 cm^{-1} which attributed to the stretching of the benzene ring, a band at 1028 cm^{-1} which attributed to the stretching of O-H, C-C, and C-O.

The FTIR spectra of the cellulose, and cellulose acetate (CA) are reported in Figure 3.32.

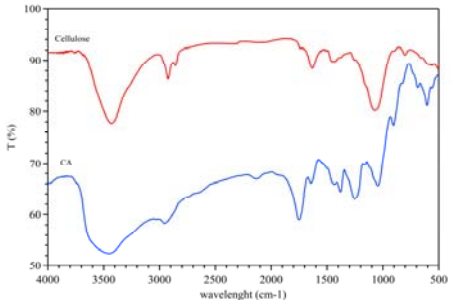

Figure 3.32 FTIR Spectra of Cellulose and Cellulose Acetate (CA).

The FTIR spectrum of CA showed a broad band around 3477 cm^{-1} due to the stretching of the O-H group which decreased with cellulose acetate as a result of esterification, compared to cellulose. Moreover for the cellulose acetate, there were a new three bands at 1752 cm^{-1} which was assigned to the C=O stretching vibration mode of the acetyl group, at 1378 cm^{-1} which was assigned to the CH_3 asymmetric bending vibration mode of the acetyl group, and at 1237 cm^{-1} which was assigned to the C-O stretching vibration mode of the acetyl group[46,47,53,54].

The FTIR technique made the *DS* determination easier and faster than the chemical titration method. The other problem with the titration method was the fact that below a certain DP the method broke down and gave incorrect results. Two peaks were of interest; the carbonyl group at 1751 cm^{-1} and the hydroxyl group at 3464 cm^{-1}. With the FTIR technique, the *DS* of any CA polymer could be determined with the aid of the calibration curve.

The DS can be determined as the ratio of the hydroxyl peak height to the carbonyl peak area in absorbance units[46,48,49].

Based on the ratio of hydroxyl peak height (0.094) to the carbonyl peak area (36.413) with respect the calibration curve did by Samios *et al.*[48], it was found that the degree of substitution (DS) to be 2.5.

Figure 3.33 shows the IR spectra for alkaline peroxide soluble hemicellulose (APSH) (a) and alkaline peroxide soluble lignin (ASL) (b).

FTIR absorption frequencies of functional groups in the alkaline-peroxide-soluble hemicellulose (APSH) and the FTIR absorption frequencies of functional groups in the alkaline-peroxide-soluble lignin (ASL) are in Tables 3.24 and 3.25.

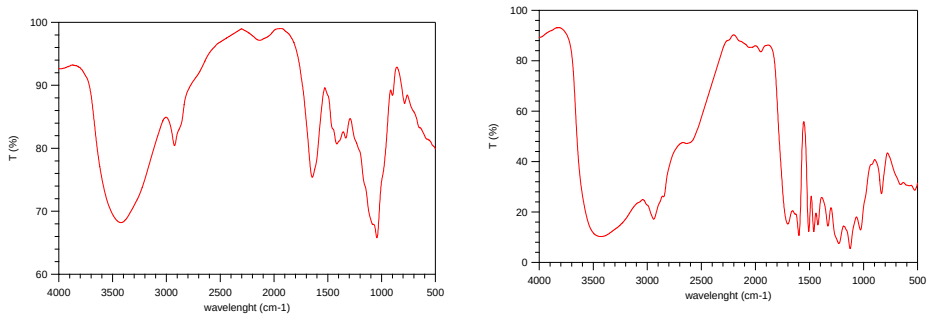

(a) (b)

Figure 3.33 FTIR Spectra of Alkaline Peroxide Soluble Hemicellulose (APSH) (a) and Alkaline Peroxide Soluble Lignin (ASL) (b).

Table 3.24. FTIR Absorption Frequencies of Functional Groups in the Alkaline-Peroxide-Soluble Hemicellulose (APSH).

Functional Groups	Wavenumbers (cm^{-1})
O-H stretching (Acid, Ethanol)	3426
C-H stretching (Alkyl, aliphatic)	2925
Absorbed water	1644
C-H bending	1416
O-H, C-C, C-O stretching	1332
C-O-C stretching (Pyranose ring skeletal)	1044
C-C stretching	785-466

Table 3.25 FTIR Absorption Frequencies of Functional Groups in the Alkaline-Peroxide-Soluble Lignin (ASL).

Functional Groups	Wavenumbers (cm^{-1})
O-H stretching (Acid, Ethanol)	3428
C-H stretching (Alkyl, aliphatic)	2940
C=O stretching (Carbonyl)	1700
C=C stretching (Aromatic skeletal mode)	1597
C=O stretching (Ketone and carbonyl)	1507
C=C stretching (Aromatic skeletal mode)	1422
C=C stretching (Aromatic skeletal vibrations)	1429
O-H, C-C, C-O stretching	1329
C-O-C stretching (Pyranose ring skeletal)	1228
Aromatic in plane deformation	1124
C-O stretching, C-O deformations (Ethanol)	1027
C-C stretching	834-526

3.5 Conclusions

The ligno-cellulosic materials (SCB, RS) dewaxing process gave better results for the milled sugar cane bagasse when compared with the cutted material, depending on the strong increase of the superficial area due to the milling process. The same process for rice straw did not produce the same effect but only a saving time.

TGA experiments showed that the dewaxed material has an higher thermal stability when compared with raw material.

This property was connected to the waxes amount, infact T_{on} showed an increase from 206°C up to 275°C for the M-SCB and from 221°C up to 277°C for C-SCB in going from the pristine sample to the dewaxed one.

This reflects also a drastic residue decreasing (from 18 % up to 4.4 %) for C-SCB before and after dewaxing.

The same trend for T_{on} and the residue was also confirmed for the SCB analyses conducted under air atmosphere. The only exception was the slight residue increase (from 2.3 % up to 2.9 %) for the DC-SCB. TGA analyses for RS samples conducted under nitrogen and air atmosphere gave the same informations.

Each component of both types of ligno-cellulosic materials was isolated by some chemical methodologies and thermally characterized by TGA and DSC experiments. Also the hemicellulose and lignin fractions soluble in alkaline solutions showed an higher T_{on} when compared to that recovered by TGA analysis performed under nitrogen atmosphere. The materials started to degrade when some oxidative processes were just verified during their weight loss steps.

The investigations on the chemical composition and structural features, performed by Fiber Analyzer and SEM instruments, allowed for the

determination of the percentage of each ligno-cellulosic component and for confirmation of the agglomerated distribution of the cellulose fibers and their acetylated products.

The FT-IR technique confirmed the structure of all SCB and RS samples, the structure of each isolated fraction and permitted the determination of the substitution degree for cellulose acetate considering the ratio of hydroxyl peak height (0.09) to the carbonyl peak area (36.4) according to the calibration curve.

3.6 Blends Based on Biodegradable Polymers of Natural and Synthetic Origin

Poly(lactic acid) is a condensation polymer of lactic acid, where lactic acid is produced via fermentation from renewable resources. It is a biodegradable polymer. PLA films were characterized for their tensile, thermal, gas permeation (carbon dioxide, oxygen) and vapour barrier properties[57]. The choice of plasticizers varied depending on the intended application.

For example, in food packaging, considerations such as toxicity, migration rates and miscibility are important determinations for creating a PLA blend[58].

Many packaging examples are cited in the literature such as a biaxially oriented surface-modified multilayered biodegradable polylactic acid film prepared by co-extruding PLA with methylsilsesquioxanes as a core material with a skin layer which is suitable for food packaging[59].

PLA films have better UV light barrier properties than polyethylene (PE) but they are worse than those of cellophane, polystyrene (PS) and poly(ethylenterephtalate) (PET). The vapour permeability coefficients of PLA are lower than those of PS and higher than those of PET[60].

Nature Works PLA is suitable for food packaging applications and it can be recycled back to monomers and polymers. It is fully compostable and it breaks down like other biobased materials (Cargill Dow LLC. 04). Efforts to recycle PLA would certainly provide an opportunity for its lower costs, particularly in fresh food applications[61].

The effect of moisture sorption on the stability of PLA films under variable humidity and temperature conditions was investigated by examining the decrease in the number average molecular weight (Mn) and the loss of their tensile strength in films. Generally, PLA is mechanically stable over a

wide range of humidity (dry to moist) and temperature (chilled to ambient temperature)[62].

The mechanical behaviour of various types of biodegradable materials depends, mainly, on their chemical composition, as well as application and storage conditions[164].

Various additives are incorporated in PLA formulations to improve functionality of bio-blends. Sometimes these additives in formulations could ever reach the levels of the conventional plastics.

It is well known that the environmental conditions during production, storage, and usage of these materials influence their mechanical properties.

Ageing during the useful lifetime also causes great losses in the elongation.

Briassoulis et al.[164] analyzed the overall mechanical behaviour of biodegradable films based on starch, PHB, PLA and PCL-starch, that may be considered suitable for agricultural applications, but also of partially biodegradable films.

Selected critical mechanical properties of films prior to their exposure to biodegradation were investigated and compared against those of conventional agricultural films.

Three major commercially available biobased degradable polymers groups were utilized to produce biodegradable films. These included, starch, polyhydroxybutyrate (PHB) and polylactides (PLA).

The non biobased biodegradable polymers included polyesters derived from petrochemical feedstock. Commercial films were developed from bio-copolyesters (e.g., Eastar) or from starch-PCL blends[165].

Other biodegradable materials were also used for film production (e.g., blends of soy protein and biodegradable polyesters, etc.)[165].

Photo-biodegradable polyethylene (PBD-PE) films containing starch were developed and used in agriculture[189]. They were better able to raise

temperature, preserve moisture, and increase crop yields, compared to conventional polyethylene films. They also had advantage over their synthetic counterpart in that they are environmentally degradable after their useful life is over.

Because of their low production cost, good physical properties, and light weight, many useful products were developed from these plastic blends for use in many fields, including agriculture. Particularly, the polyethylene (PE) mulch films were in use for many years to improve crop yields. One drawback for the PE films is that they don't degrade in soil and accumulates thus, have to be removed after their use which adds to the overall cost for farmers.

The waste films if left uncovered, pollute the soil and impacts the growth of crops the following year. To overcome this problem, alternate films techniques were developed in recent years but most of them were either produced at a much higher cost or exhibited poor degradability in soil.. A good option appeared to be the photo biodegradable polyethylene (PBD-PE) film whose physical and mechanical properties were close to those of PE films and also biodegradable in soil. Such films are commercially available at very low cost and show good time-controlled environmental degradability.

There have been a lot of reports on preparation, properties, and applications of degradable polymeric materials, but only few reports are available with respect to their agricultural application.

Wang et al.[189] reported some preliminary results on the effects of the agricultural application and the environmental degradation of the PBD-PE film.

3.6.1 PLABn Blends

3.6.1.1 Thermal Properties

Thermal characterization of the two pristine polymeric materials and their blends provided informations on the degradation temperature and the processability[68,69]. Thermal properties of PLA, Bionolle (Bn) and PLABn blends were assessed by thermogravimetry (TGA) and differential scanning calorimetry (DSC).

3.6.1.1.1 Thermogravimetric Analysis (TGA)

Figure 3.34 shows the weight loss and the derivative weight loss traces of PLA before and after melt processing. Table 3.26 provides informations on the thermal properties for the PLABn blends. The onset temperature was comprised between 310°C and 350°C.

Table 3.26 Thermogravimetric Data for PLABn Blends Under Nitrogen Atmosphere[a].

Sample	T_{on} (°C)	T_{p1} (°C)	T_{p2} (°C)	R_{800} (%)
PLA	332	364	-	0.98
Bn	353	395	-	2.04
PLABn20	343	373	393	0.95
PLABn40	324	355	381	1.54
PLABn50	314	346	380	1.53
PLABn60	338	367	397	1.63
PLABn80	339	336	393	1.61

a) T_{on} is the starting degradation temperature, T_p is the main degradation peak, R_{800} is the residue at 800°C.

Both pristine and melt processing PLA exhibited similar thermal behaviour. The onset temperature of decomposition in N_2 atmosphere was ca. 302°C and the residue recovered at 600°C were ca. 1.47 %.

Figure 3.34 shows the weight loss (a) and the derivative weight loss (b) decomposition traces for PLABn blends compared to pristine PLA and Bn.

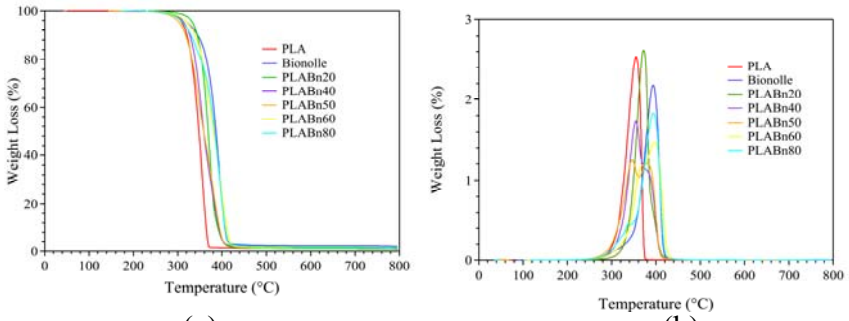

(a) (b)

Figure 3.34 TGA (a) and DTGA (b) Traces for PLABn Blends.

All the blends started to degrade in the temperature range of 25°C–310°C corresponding to the moisture volatilization and the weight loss steps of 0.36 %, 0.45 %, 0.56 %, 0.61 %, 0.48 %, for blends with Bionolle percentage increasing from 20 % to 80 %, respectively.

The first decomposition DTGA peak appeared when the Bionolle percentage raised to 40 % and it diminished progressively in the temperature range of 350°C–390°C.

A shoulder was apparent at the first weight loss in PLABn blends with compositions 40/60 and 20/80 which were mainly from the PLA decomposition. The relative weight losses were 87.2 % for PLABn20, 24.9 % for PLABn40, 56.4 % for PLABn60 and 17.3 % for PLABn80, respectively.

In the compositions 80/20 and 60/40, the main peaks in the temperature range of 360°C-400°C exhibited a shoulder at high temperature, ca 392°C.

The relative weight loss steps were 10.7 % for PLABn20 and 41.9 % for PLABn40. On the other hand, the shoulder appeared on the low temperature

side of the peak in the temperature range of 300°C-360°C for the composition 40/60 and 20/80. The relative weight loss steps were 41.1 % for PLABn60 and 17.3 % for PLABn80. In the temperature range of 340°C-440°C both blends showed a principal peak with a weight loss steps of 56.4 % and 79.7 % for PLABn60 and PLABn80, respectively.

The residue recovered at 800°C was 1.5 % but increased with increasing amount of Bn in the blend.

The derivative TGA traces (Fig. 3.34b) showed an overlapped peaks for the formulation PLABn50 and the relative weight loss steps in the temperature range of 280°C-430°C were 51.6 % and 44.1 %.

With 50 % Bionolle present in blends, the thermal stability decreased for pristine PLA (T_{on}=332°C) to the blend PLABn20 (T_{on}=314°C), whereas for the percentages higher than 50 % for Bionolle, the thermal stability increased up to 340°C in PLABn80.

The Bionolle appeared to be a poor plasticizing agent for the pristine PLA.

Infact, the blends with an high Bionolle contents had the same onset temperature as the pristine PLA.

3.6.1.1.2 Differential Scanning Calorimetry (DSC)

Figure 3.35 shows the DSC traces for the PLABn blends while Table 3.27 shows the relative thermodynamic properties.

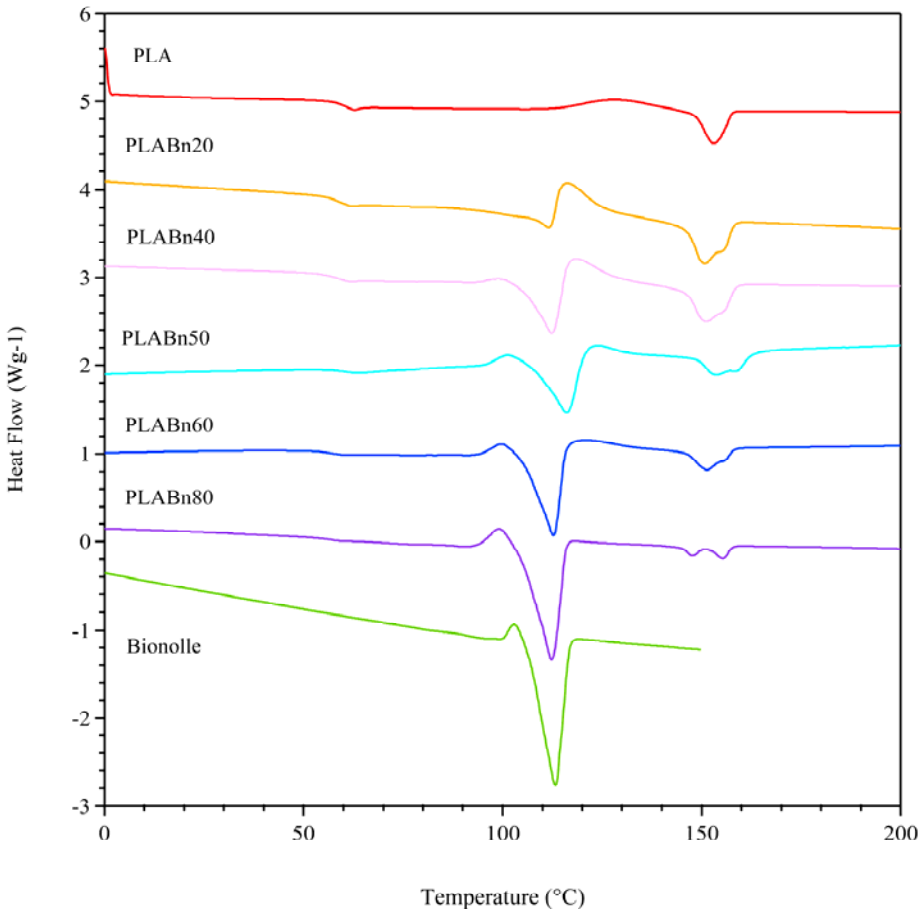

Figure 3.35 DSC Traces for PLABn Blends (2nd Heating).

Table 3.27 Thermodynamic Properties for PLABn Blends[a] (2nd Heating).

Sample	Tg (°C)	T_{cc1} (°C)	T_{m1} (°C)	ΔH_{m1} (J/g)	T_{cc2} (°C)	T_{m2} (°C)	ΔH_{m2} (J/g)	T_{m3} (°C)	ΔH_{m3} (J/g)
PLA	61	-	-	-	±130	153	13.58	-	-
Bionolle	-21	±105	113	61.63	115	-	-		-
PLABn20	59	-	111	7.19	118	150	22.15	154	6.07
PLABn40	59	±100	112	20.91	120	151	19.34	154	6.04
PLABn50	61	±100	116	24.43	115	154	10.82	159	5.48
PLABn60	57	±100	113	34.13	-	152	9.77	155	1.9
PLABn80	56	±100	112	50.28	-	148	3.12	155	3.49

a) Tg = glass transition temperature, Tcc = cold crystallization temperature, Tm = melting temperature, ΔH_m = melting heating.

The DSC traces of the blends showed a serie of peaks that correlated well the cold crystallization and melting processes.

The PLABn blends showed the melting peaks where the low and high transitions corresponded to Bionolle and PLA, respectively.

The high mobility of Bionolle chains plasticized only slightly the chains in PLA, decreasing the glass transition temperature (T_g) from 61°C to 56°C for the blend PLABn80 that contained the highest fraction of Bionolle (T_g=25°C).

The 50/50 blend of PLA and Bionolle had the same T_g as neat PLA.

All blends exhibited cold crystallization temperature (T_{cc}) for both polymer phases, which was followed by the corresponding melt transition.

It occurred around 128°C for the pure PLA and with an enthalpy value of ca. 13 Jg^{-1}.

The melting temperature ranged between 150°C-160°C respective of the weight ratio of PLABn in the blends.

The melting temperatures for Bionolle and PLA were 113°C and 153°C, respectively. The T_m of Bionolle decreased for all compositions containing less than 50 % PLA no change was observed with higher amounts of Bionolle present in the blend. On the other hand, the melting transition of PLA in the blends indicated two peaks. The first peak decreased from 150°C to 148°C with increased amount of Bionolle; exception was observed in blends containing only 50 % Bionolle.

The second melting peak of PLA in the blend was roughly 2°C higher than that of the pristine polymer and was irrespective the amount of PLA present in the formulation.

The peak intensity depended very much on the amount of the two polymeric materials present in the blend. Infact, increased Bionolle contents led to increase the cold crystallization peak that showed a decrease for PLA.

3.6.1.2 Mechanical Properties

The mechanical properties of PLABn blends are presented in Figure 3.36.

Substantially, significant changes were observed in blends with respect to their Young modulus (YM) and the elongation at break (EL).

YM value for neat PLA and unblended Bionolle are 225.6 MPa and 622 MPa, respectively.

The YM of the blends increased progressively with an increasing amount of Bn in the blend up to around 50 % approximately YM of 135 MPa.

Thereafter, any further increase in Bn content adversely impacted the YM of the blend.

The elongation at break, never decreased generally with increase in Bn content the only exception was a single peak at 20 % Bn content.

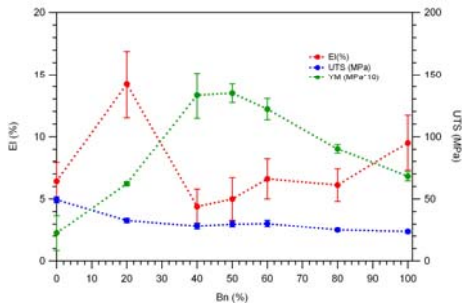

Figure 3.36 Graphic of the Mechanical Properties of PLABn Blends.

Wool[238] analyzed the preparation methods of triglycerides with acrylate functionality from various oils and model triglycerides.

The triglyceride-acrylates were homopolymerized and copolymerized with styrene. Although the model predictions overestimated the cross-link density, the trends in the cross-link density predictions matched the experimental results. In both cases, the cross-link density was found to increase gradually at low levels of acrylation and then linearly at higher levels of acrylation.

The deviation in the experimental results and model predictions were obtained from intramolecular cross-linking. Approximately 0.5 and 0.8 acrylates per triglyceride were lost to intramolecular cyclization for homopolymerized triglyceride-acrylates and triglycerides copolymerized with styrene, respectively.

Their tensile strength and modulus increased exponentially at low levels of acrylate functionality, but increased linearly at higher levels of acrylate functionality, as predicted by vector percolation theory.

The cross-link density is a function of the number of functional groups so the mechanical properties of triglyceride-based polymers were strong functions of the number of acrylates per triglyceride. As this property increased, the polymer chains became more tightly bound to each other, which increased this properties. This was indicative of a percolation phenomenon[239,240], that is a theory where the polymer properties are

correlated to the connectivity of the polymer network. So the crack in the polymer can travel through regions of much lower cross-link density and stiffness than the average across the whole polymer.

Something similar happens for the PLA/Bn blends containing a Bn amount up to 20 %: until this percent weight ratio, the obtained blends appear to be good for the mechanical properties, because there are strong interactions between the two biodegradable polymers such as hydrogen bounding or between carboxylic groups.

3.6.2 PHB/Cellulose Acetate (CA)

3.6.2.1 Morphology

SEM photomicrographs for CA/PHB blends are shown in Figure 3.37.

The selected percentages for cellulose acetate were 20 %, 40 %, 50 %, 60 %. The blends CA/PHB (20/80) (Fig. 3.36a) and CA/PHB (40/60) (Fig. 3.37b) showed two phases where the particles of cellulose acetate (CA) were dispersed in the PHB matrix. It can be observed that some spherical cellulose acetate particles were pull out probably due to the low adhesion between PHB and CA.

The adhesion between CA and PHB appeared to improve when the cellulose acetate contents were increased as shown in blends CA/PHB (50/50) (Fig. 3.37c) and CA/PHB (60/40) (Fig. 3.37d). Micrographs (c) and (d) showed an homogeneous blend.

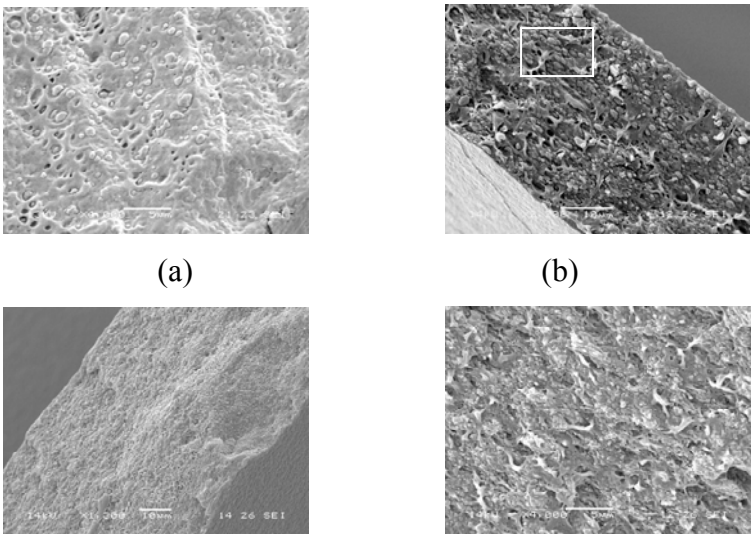

(a) (b)

(c) (d)

Figure 3.37 SEM Photomicrographs for CA/PHB (20/80)-4000X (a), CA/PHB (40/60)-2200X (b), CA/PHB (50/50)-1300X (c), CA/PHB (60/40)-4000X (d).
Subset: high magnification 1000X

3.6.2.2 Thermal Properties

Thermal characterization of neat PHB and CA components and their blends was performed to obtain informations about degradation, processing temperatures and the components compatibility[46,53,55].

Attemps were also made to study the thermal properties of PHB, cellulose acetate (CA) and CA/PHB blends were assessed by thermogravimetry (TGA) and differential scanning calorimetry (DSC).

3.6.1.1.1 Thermogravimetric Analysis (TGA)

Figure 3.38 shows the weight loss (a) and the derivative weight loss (b) traces of CA/PHB blends and the neat polymers. After initial moisture volatilization between 25°C-120°C, the blends started to degrade in the temperature range of 200°C–280°C.

The weight losses due to the humidity elimination, were 2.4 %, 4.4 %, 4.5 %, 7.7 % for CA/PHB (20/80), CA/PHB (40/60), CA/PHB (50/50), CA/PHB (60/40), respectively.

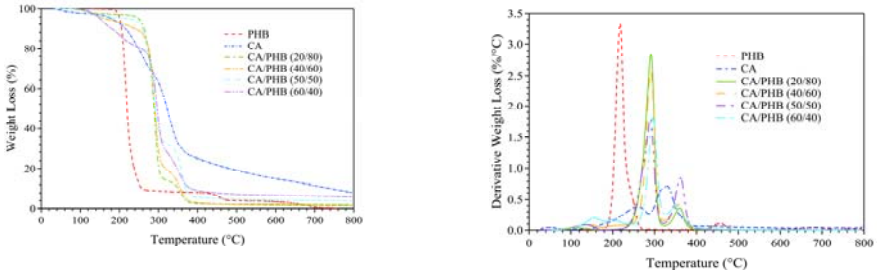

(a) (b)

Figure 3.38 TGA (a) and DTGA (b) Traces for CA/PHB Blends Under Nitrogen Atmosphere**.**

At least four degradation weight loss steps were apparent in the DTGA traces shown in Fig. 3.38b. The first step corresponded to weight losses of 11.7 % for CA/PHB (20/80), 18 % for CA/PHB (40/60), 26.3 % for CA/PHB (50/50) and 10.7 % for CA/PHB (40/60). The second steps corresponded to weight losses of 83.1 % for CA/PHB (20/80), 74.3 % for CA/PHB (40/60), 63.4 % for CA/PHB (50/50) and 54 % for CA/PHB (60/40).

In the third step, decomposition peak as were observed in the temperature range of 400°C–500°C associated with weight losses of 0.6 % for CA/PHB (20/80), 1.2 % for CA/PHB (40/60), 1.7 % for CA/PHB (50/50)

and 17.7 % for CA/PHB (60/40). The residue recovered at 800 °C was around 1-3 % for all selected blends.

PHB started to degrade at 202°C and the residue recovered at 800°C was 0.73 %.

The cellulose acetate (CA) started to degrade at 160°C and the residue recovered at 800°C was roughly about 8.3 %.

There were four overlapped steps involved in the pyrolysis of cellulose acetate[53]. The first one was connected with the moisture volatilization, it showed a relative weight loss of ca. 7.6 % and it occurred in the temperature range of 25°C-130°C.

The second step was in the temperature range of 130°C-210°C with relative weight loss of 25 %, while the third step was in the range of 210°C-290°C where the total decomposition of the cellulose structure took place indicating a weight loss of 38.7 %. The fourth step was comprised in the temperature range of 290°C-410°C, attributed to the remnant carbon[53] with relative weight loss of 9.5 %.

The blending of PHB with the cellulose acetate led to increase thermal stability in the polymeric materials. Infact all the blends had the onset temperature higher than the PHB which was around 231°C.

The blend CA/PHB (50/50) had a similar thermal behaviour to that of pristine PHB. Infact its onset temperature was around at 256°C, the closest value to the PHB onset temperature.

Table 3.28 provides data on the thermal properties for the blends and the pure polymers.

Table 3.28 Thermal Properties for CA/PHB Blends and the Pristine Materials Under Nitrogen Atmosphere[a].

Sample	T_{on} (°C)	T_{p1} (°C)	T_{p2} (°C)	T_{p3} (°C)	T_{p4} (°C)	R_{800} (%)
PHB	202	-	217	248[a]	457	0.73
CA	231	133	174	257	329	8.3
CA/PHB(20/80)	264	108	291	358	-	1.9
CA/PHB(40/60)	271	135	290	355	-	1.6
CA/PHB(50/50)	256	137	289	362	-	1.7
CA/PHB(60/40)	279	154	200	295	352	2.9

a) T_{on} is the starting degradation temperature, T_p is the main degradation peak, R_{800} is the residue at 800°C.

3.6.1.1.2 Differential Scanning Calorimetry (DSC)

The Figure 3.39 shows the DSC traces for the pristine PHB, cellulose acetate (CA) and their blends while the Table 3.29 records the relative thermodynamic properties.

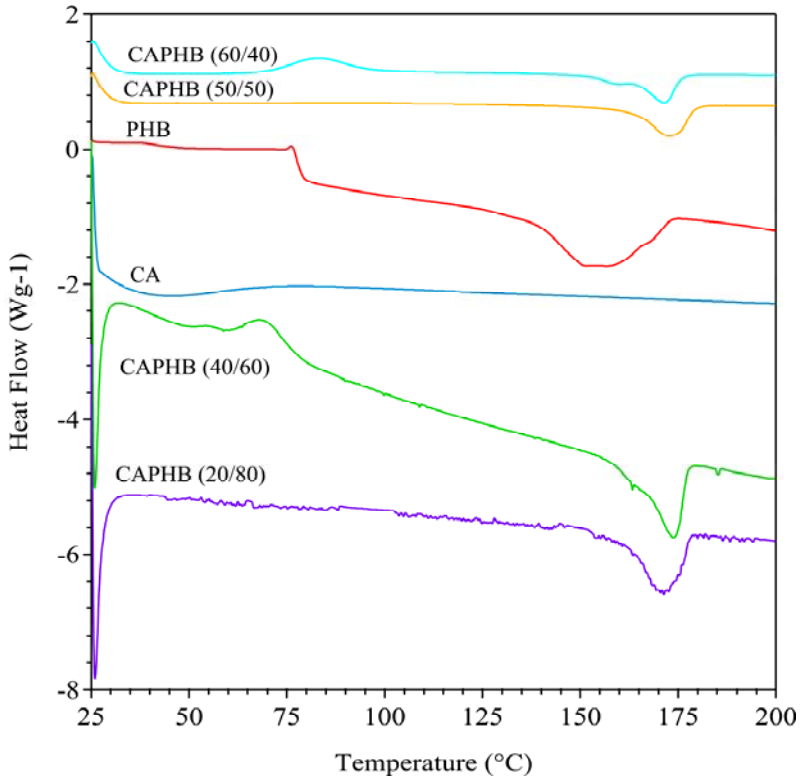

Figure 3.39 DSC Traces for PHB, CA and CA/PHB Blends.

Table 3.29 Thermodynamic Properties for PHB, Cellulose Acetate (CA) and their Blends[a].

Sample	Tg (°C)	T_{m1} (°C)	ΔH_{m1} (J/g)	T_{m2} (°C)	ΔH_{m2} (J/g)	T_{m3} (°C)	ΔH_{m3} (J/g)
PHB	77.49	136	6.93	166	101.41	166	10.64
CA	-	42.48	44.12	-	-	-	-
CA/PHB(20/80)	-	164	11.69	174	53.15	-	-
CA/PHB(40/60)	41	69	24.24	173	70.03	-	-
CA/PHB(50/50)	102	-	-	173	34.58	-	-
CA/PHB(60/40)	-	83	24.21	160	8.31	171	20.52

a) Tg = glass transition temperature, Tm = melting temperature, ΔH_m = melting heating.

The DSC traces for CA/PHB blends showed a glass transition temperature for only CA/PHB (50/50) and CA/PHB (60/40) blends. The values were ca. 41°C for the first sample and ca. 102°C for the second, and the glass transition temperature for the PHB was around 77°C.

Data indicated that CA made the blends more rigid compared to pure PHB expecially when the CA percentage was increased up to 50 %.

The two overlapped melting peaks showed enthalpy values of ca. 11.69 Jg^{-1} and 53.15 Jg^{-1} for the CA/PHB (20/80) blend.

The corresponding temperatures were 164°C for the first peak and 174°C for the second. The melting enthalpy decreased with the increased CA amount (Table 3.29) but not the temperatures. Also the peaks intensity increased when the CA content was increased.

The blends CA/PHB (40/60) and CA/PHB (60/40) also showed peaks at 69°C and 83°C corresponding to the moisture volatilization in these two blends, respectively.

3.6.2.3 Wide Angle X-ray Diffraction (WAXS)

WAXD patterns were performed on CA/PHB blends, where the CA percentage varied from 20 to 60.

Figure 3.40 shows the WAXD diffraction patterns of pure samples and their binary blends.

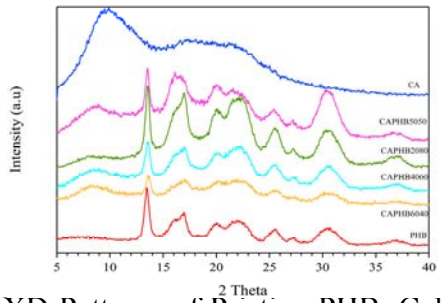

Figure 3.40 WAXD Patterns of Pristine PHB, Cellulose Acetate (CA) and their Blends**.**

The x-ray diffraction pattern of PHB is shown in the Figure 3.40.

The pattern of diffraction peaks appeared to be typical of a semi-crystalline material. Interestingly, the positions and intensities of these diffraction peaks remained unchanged when PHB was blended with cellulose acetate indicating that the addition of cellulose acetate didn't impact in the semi-crystalline structure of PHB.

3.7 Conclusions

PLABn blends, obtained by compression moulding, were investigated for their thermal and mechanical properties. The TGA experiments confirmed the poor plasticizing nature of Bionolle towards the neat PLA, as shown by the same values for the onset temperature of the two polymers.

The 50/50 blend composition showed the same T_g as neat PLA, probably due to a partial miscibility of the two polymeric materials in this formulation.

YM increased with increasing Bn content, while UTS and EL decreased: thus the addition of Bn to PLA mixtures is positive for processing and for composite flexibility.

Also CA/PHB blends, obtained by film casting, were analysed for their morphological, structural and thermal characteristics.

SEM analysis confirmed an higher adhesion between CA and PHB when the cellulose acetate contents were increased from 20 to 60 %, while the TGA analysis pointed out that the blending of PHB with CA improved the thermal stability of the polymer, as confirmed by the higher value of T_{on} of the blends with respect to the pristine PHB.

The 50/50 blend composition showed a T_{on} value similar to that of PHB sample, probably due to a miscibility of the two polymeric phases in the blend.

3.8 Composites Based on Biodegradable Materials and Natural Organic Fillers

Algae, a low value raw material from renewable resource of marine origin were proposed for the production of eco-compatible composites.

Fibers derived from the green alga *Ulva armoricana*, common to French, Spanish and Italian costs, were evaluated for the production of hybrid films in combination with polymers, such as poly(hydroxybutirate) (PHB) and polycaprolacton (PCL)[68,71].

PHB, PCL and Ulva were utilized for the production of hybrid composites via compression moulding. Results obtained were quite encouraging for composites showing excellent forming properties and mechanical characteristics, indicating the suitability of Ulva in plastic formulations due mostly to significant amounts of crystalline cellulose present as a structural component of the cell walls[68].

PCL was used to develop composite materials suitable as scaffolds for bone engineering[69]. Scaffolds based on PCL reinforced with long glass fibres were prepared by using continuous melt impregnation (extrusion/calendering) and film stacking[70].

Poly(hydroxybutirate) (PHB), is a microbially-derived biodegradable polyester that has shown a good promise as an alternative to petroleum-based polymers and for preparing blends incorporating other natural materials.

Because PHB has physical properties quite similar to polypropylene, this polymer has attracted much attention as a PE substitute for a wide range of agricultural, marine and medical applications. However, due to its high cost, currently its use is mainly restricted to medical applications[5].

Injection-molded composites based on PHB or PCL and natural materials, especially algae, were developed and considered for commercialization in

single use consumer items[6-19]. Agriculture (mulch films), packaging, construction and biomedicine are the sectors where these materials are expected to final useful applications.

Eco-compatible and biodegradable composites were also produced using rice which is available in large quantities in Italy. Rice is easily processable in a twin screw extruder for use in various food and non-food applications.

Biological materials provide a good example of nature's capacity to develop functionality in polymers utilizing a variety of approaches[166] that can be adapted in engineered materials.

For example, self-assembly, self-cleaning and self repair are some common properties found in natural materials. These functionalities were simulated in engineered products such as commercially available nano-particles, sol-gel coatings and dendrite polymers for many useful applications.

Another approach is to use bio-based materials in a broad range of products that are biodegradable, lightweight and they have high strength and antimicrobial activities. Particularly, successful development of diagnostic products would require broader understanding and creating novel surfaces with bio-active molecules.

The hybrid materials, where bio-active polymers are combined with structural polymers is an important area of polymer science. Much focus is being diverted in developing smart surfaces and intelligent machines using embedded sensors in materials.

Embedded sensors would allow to monitor the structural health application of surface coatings and quality of product in response to any change in the ambient environment.

Beside embedded sensors, could be useful tool in developing functionalized hybrid materials.

The use of produced hybrid materials was demonstrated in controlling

mechanical vibrations in response to functionalizations in magnetic and electric fields, as well as in temperature.

The usefulness of such materials in automotive and consumer electronics is already being recognized, but there is a growing realization that medical applications will become an increasingly promising area, particularly for piezoelectric and sensor-suited materials.

Many biodegradable polymers were used in developing products to replace petrochemicals[167], but most of the research was focused on their biodegradability aspects.

Now, more themselves, there is a need to establish the safety of these materials and their by-products when they breakdown in the environment.

To verify their non toxicity, the biodegradation must be carried out in accelerated laboratory tests where metabolites and residues can be recovered.

To reproduce the natural conditions (compost, field) as closely as possible, degradation experiments must be run on solid-state substrates. In this regard, Grima et al.[167] reviewed aerobic degradation in solid-state substrates, focusing in particular on the environmental, physical, and chemical parameters, such as substrate nature, moisture, temperature, C/N ratio, and pH which influence biodegradation kinetics. This study also aimed at finding the solid substrate most suitable for residues and metabolites recovery.

The most significant parameters would appear to be the substrate type, moisture content, and temperature. Inert substrates such as vermiculite were found to be well suited for the residue extraction.

This review also opened the field to new research aimed at optimizing conditions for aerobic solid-state biodegradation and at recovering the metabolites and residues, generated during the degradation process.

In this report, the external parameters that influence biodegradation kinetics were presented. These included the material concentration in the solid medium, the environmental conditions (temperature, pH, moisture,

oxygen availability, composition and concentration of inorganic nutrients of the solid medium), the microbial population (concentration, nature, and interactions), the presence or absence of other degradable substances, and the conditions and properties of the test system (volume and shape of the vessels).

Also the measurement procedures currently used in laboratory for solid-state fermentation were examined in detail and issues related to residue recovery were addressed.

Today's consumer plastics are designed with little consideration for their ultimate disposability or the impact of feedstock used in making them[187], which led to unintended environmental consequences.

This created a need to design and engineer products using biodegradable polymers that had the performance characteristics of today's materials but biodegrade upon disposal in soil into humic substances.

Many farm derived and bio-derived polymers such as starch, cellulose and protein oils are excellent raw material for obtaining chemicals, pharmaceuticals and nutraceuticals as well as for manufacturing plastic composites.

In this regard, soy proteins were compounded with synthetic biodegradable plastics such as polycaprolacton or poly (lactic acid) to make molded products, edible films and or shopping bags indicating a promising future for such materials in bringing real environmental benefits.

3.8.1 Organic Fillers

3.8.1.1 Ulva Fibres

3.8.1.1.1 Morphology

Fiber size, along with their morphology, surface characteristics, dispersion in the polymer matrix and its compatibility with other adjuvants are all important determinants in dictating the overall quality of the composites.

For this purpose, efforts were made to investigate the size distribution of fibers in ulva preparation.

Results are presented in Table 3.30 which shows the dimensional distribution of micronized ulva obtained using standard sieves asper ASTM.

More than 60 % of ulva fibers were found to be above 0.212 mm in length.

Table 3.30 Micronized Ulva Fibres Distribution.

Mesh	(mm)	U (%)
40	$\phi > 0.425$	0.2
40-50	$0.300 < \phi < 0.425$	0.2
50-70	$0.212 < \phi < 0.300$	3.4
70-100	$0.150 < \phi < 0.212$	13.2
100-140	$0.100 < \phi < 0.150$	30.9
140-270	$0.053 < \phi < 0.100$	19.0
270	$\phi < 0.053$	33.1

Fibers granulometry for ulva used as a filler could be an important tool for composites production.

Figure 3.41 shows the micrometric dimension of ulva particles that create aggregates in the material. The ulva fiber appeared as an homogenous material.

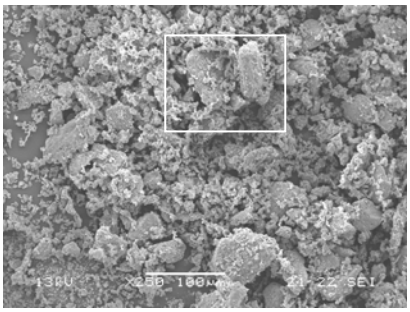

Figure 3.41 SEM Photomicrograph for Micronized Ulva-250X.

3.8.1.1.2 Thermal Properties

For a successful melt processing, it is critically important the information on its thermal stability is available. Therefore, ulva fibers were processed and evaluated to obtain information on their degradation temperature for material processing.

Figure 3.42 shows TGA and DTGA traces for the micronized ulva.

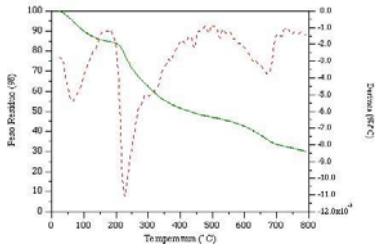

Figure 3.42 TGA and DTGA Traces for Ulva Fibres.

After an initial loss of 6.1 % at temperature ranging between 25°C-144°C, attributed mostly to humidity and volatiles, micronized ulva fibers started to decompose at a temperature around at 221°C.

Two decomposition peaks were evident; the first at 237°C and the second peak at 693°C. The first peak was in the temperature range of 200°C-500°C while the second one was in the temperature range of 650°C-730°C and the weight losses associated with them were 22.1 % and 8.8 %, respectively. The first peak showed two overlapped shoulders that were in the temperature range of 300°C-430°C and 430°C-500°C and with corresponding weight losses of 15.2 % and 2.9 %, respectively.

The residue recovered at 800 °C was about 41 % which was due to the high amount of inorganic salts and siliceous materials present in algal sample.

3.8.1.1.3 Infrared Spectroscopy

Algal samples were further characterized using infrared spectroscopy.

Figure 3.43 shows the IR spectrum of micronized ulva and Table 3.31 reports the principal wavenumbers for this material.

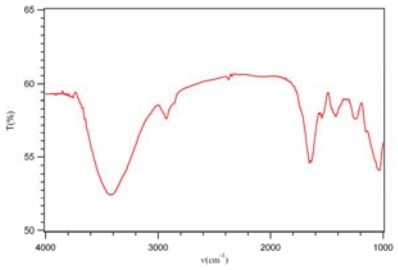

Figure 3.43 Ulva IR Spectrum.

Table 3.31 FTIR Absorption Frequencies of Functional Groups in the Micronized Ulva.

Functional Groups	Wavenumbers (cm^{-1})
O-H stretching	3420
C-H stretching	2920-2850
C=O stretching	1655
CH_2 bending	1420
C-O stretching	1256-1030
C-H bending	840

Spectrum appeared to be quite typical of a plant material with a strong absorption in the OH region indicative of hydroxyl containing entities in the sample such as cellulose and the polysaccharides.

3.8.1.2 Ground Rice, Chaff and Farinaccio

3.8.1.2.1 ***Morphology***

Table 3.32 shows the size distribution of ground rice obtained using standard ASTM protocols.

Table 3.32 Ground Rice Granules Distribution.

Mesh	(mm)	U (%)
40	$\phi > 0.425$	0.1
40-50	$0.300 < \phi < 0.425$	0.2
50-70	$0.212 < \phi < 0.300$	0.8
70-100	$0.150 < \phi < 0.212$	35.1
100-140	$0.100 < \phi < 0.150$	36.1
140-270	$0.053 < \phi < 0.100$	25.9
270	$\phi < 0.053$	1.7

The size distribution analyses of ground rice granules indicated that over 95 % the granules were within the size range of 0.06-0.212 mm.

Figure 3.44 shows the SEM photomicrograph for the ground rice granules.

The picture presented zones with aggregates of big dimensions, confirming the homogenous nature of this material.

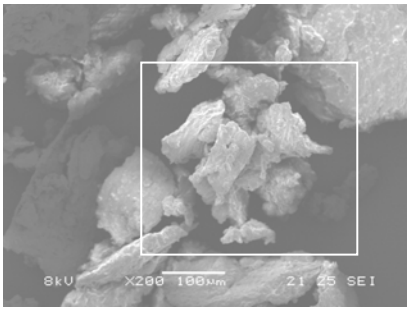

Figure 3.44 SEM Photomicrograph for Ground Rice-200X.

Table 3.33 shows the size distribution of chaff granules.

Table 3.33 Chaff Granules Distribution.

Mesh	(mm)	P (%)
30	$\phi > 0.06$	26.38
30-40	$0.425 < \phi < 0.06$	14.01
50-70	$0.212 < \phi < 0.300$	40.32
70-100	$0.150 <$ < 0.212	14.92
100-140	$0.100 < \phi < 0.150$	4.06
140-270	$0.053 < \phi < 0.100$	1.5
270	$\phi < 0.053$	0

The size distribution analyses of chaff granules indicated that over 95 % the granules were within the size range of 0.06-0.212 mm which was quite distinct compared to the micronized ulva and ground rice samples.

SEM analysis of chaff confirmed the presence of large aggregates compared to the other fillers. Chaff appeared to be a suitable heterogeneous material for use as fillers in making composites.

Figure 3.45 shows the SEM photomicrograph for the chaff.

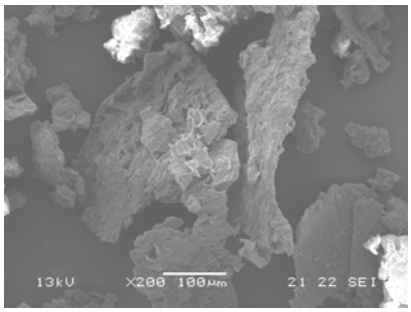

Figure 3.45 SEM Photomicrograph for Chaff-200X.

Table 3.34 shows the dimensional distribution of farinaccio obtained by standard sieving procedures.

Table 3.34 Farinaccio Granules Distribution.

Mesh	(mm)	Fc (%)
30	$\phi > 0.06$	15.94
30-40	$0.425 < \phi < 0.06$	12.14
40-50	$0.300 < \phi < 0.425$	20.66
50-70	$0.212 < \phi < 0.300$	16.64
70-100	$0.150 < \phi < 0.212$	22.57
100-140	$0.100 < \phi < 0.150$	8.99
140-270	$0.053 < \phi < 0.100$	3.05
270	$\phi < 0.053$	0

Figure 3.46 shows the SEM photomicrograph for rice farinaccio.

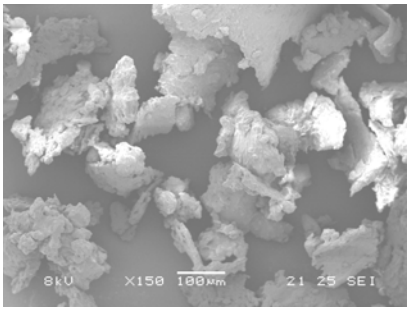

Figure 3.46 SEM Photomicrograph for Farinaccio-150X.

SEM photomicrograph of farinaccio showed mostly huge aggregates compared to the chaff. The aggregates had medium size dimensions and the material appeared only as an homogeneous phase.

Probably the grinding process of the material created some superficial zones of gelatinization or proteins and polysaccharides intercalation. Also this raw material is suitable as filler in making bio-composites.

3.8.1.2.2 Thermal Properties

Figure 3.47 shows TGA and DTGA trace for the ground rice.

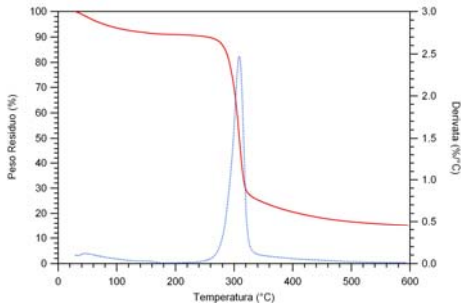

Figure 3.47 TGA and DTGA Trace for Ground Rice.

Initial weight loss attributed to the loss of humidity and other volatile compounds was 11.2 %. The decomposition temperature of ground rice was around at 280°C and only one decomposition peak was observed which was correlated with the decomposition of amidaceous substances. The relative weight loss at this step was 82.3 %.

The residues recovered at 800 °C were about 15 %. The high amount of residues are indicative of an high fiber content in the samples.

Figure 3.48 shows TGA and DTGA chaff (a) and farinaccio (b) traces.

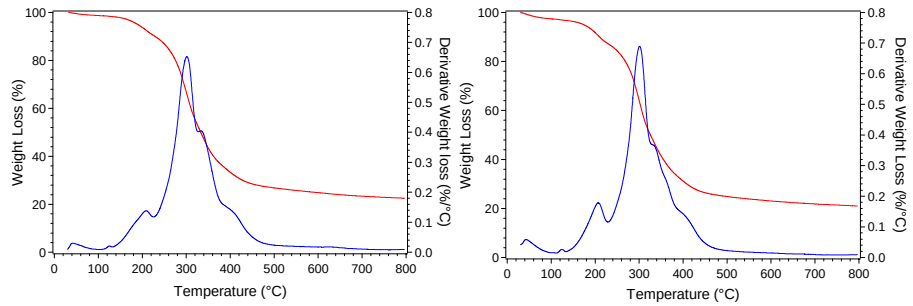

(a) (b)

Figure 3.48 TGA and DTGA Traces for Chaff (a) and Farinaccio (b).

After initial weight losses, both chaff and farinaccio samples degraded at much lower temperatures when compared to ulva and ground rice. This pointed to the creating evident challenges of processing complex organic matter with polymers.

There were three overlapped decomposition peaks for chaff and four ones for farinaccio, that ranged between 170°C-300°C.

The weight losses were 7.8 %, 37.7 % for the chaff and 15.4 % for the farinaccio.

The residues recovered at 800 °C were around 22.4 % for chaff and 20 % for farinaccio due to high fibrous component in the samples.

Table 3.35 records the thermal properties for the fibers under nitrogen atmosphere.

Table 3.35 Thermal Properties for the Fibres Under Nitrogen Atmosphere.

Sample	T_{on} (°C)	T_{p1} (°C)	T_{p2} (°C)	T_{p3} (°C)	R_{800} (%)
Ulva	221	62	228	671	41
Ground Rice	280	309	-	-	15
Chaff	169	208	301	335	22.4
Farinaccio	179	207	301	331	20

The onset temperature for these fibres was comprised between 170°C and 280°C. Both chaff and farinaccio are ground rice by-products and they indicated a much lower thermal stability compared to the ground rice itself.

Ulva fibre exhibited an intermediate behaviour with an higher T_{on} than rice by-products but a much lower T_{on} compared to rice. This behaviour and significantly higher residues recovered at 800°C were indicative of siliceous components present in the material.

3.8.1.2.3 Infrared Spectroscopy (FTIR)

Figure 3.49 shows the IR spectrum of the ground rice and Table 3.36 reports the principal wavenumbers for this material.

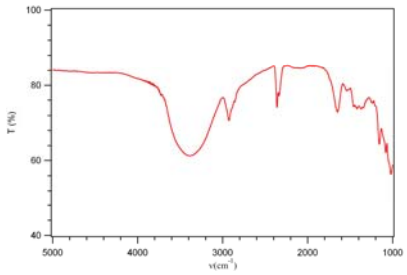

Figure 3.49 Ground Rice IR Spectrum.

Table 3.36 FTIR Absorption Frequencies of Functional Groups in the Ground Rice.

Functional Groups	Wavenumbers (cm^{-1})
O-H stretching	3380
C-H stretching	2920-2850
C=O stretching	1650
C-O stretching	1150-1020
C-H bending	570

Spectrum presented a strong absorption in the OH region indicative of hydroxyl containing entities in the sample such as starch and amilopectin.

Also the C=O and C-H stretching were evident in the spectrum.

Figure 3.50 shows the IR spectrum of the chaff and Table 3.37 reports the principal wavenumbers for this sample.

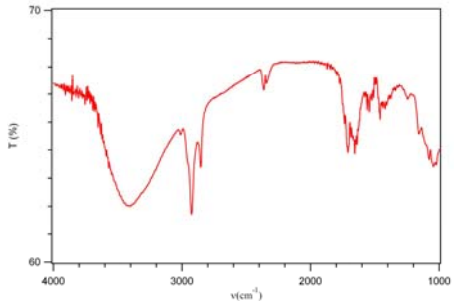

Figure 3.50 Chaff IR Spectrum.

Table 3.37 FTIR Absorption Frequencies of Functional Groups in the Chaff.

Functional Groups	Wavenumbers (cm^{-1})
O-H stretching	3400
C-H stretching	2920-2850
C=O stretching	1710
C-O stretching	1150-1040
CH_2 bending	1650-1460
C-H bending	710

Figure 3.51 shows the IR spectrum of the farinaccio and Table 3.38 reports the principal wavenumbers for this material.

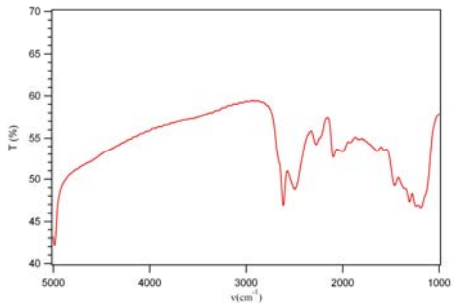

Figure 3.51 Farinaccio IR Spectrum.

Table 3.38 FTIR Absorption Frequencies of Functional Groups in the Farinaccio.

Functional Groups	Wavenumbers (cm^{-1})
O-H stretching	3390-3100
C-H stretching	2920-2850
C=O stretching	1650
C-O stretching	1050
CH_2 bending	1540

Both chaff and farinaccio showed the typical absorptions of hydroxyl and carboxylic groups present in the materials. Also the stretching and bending of C-H and CH_2 were visible and in good agreement with the spectrum graph.

3.8.1.3 Polymeric Materials

3.8.1.3.1 Thermal Properties

When we have to make blends and composites, it is important to evaluate the polymer thermal stability and degradation temperature for obtaining useful informations on the melt processing conditions.

So the thermogravimetric analysis led us to improve the knowledgement on hydrolene (LFT) (a) and polyvinyl alcohol (PVA 18/88) (b) which TGA and DTGA traces are reported in Figure 3.52.

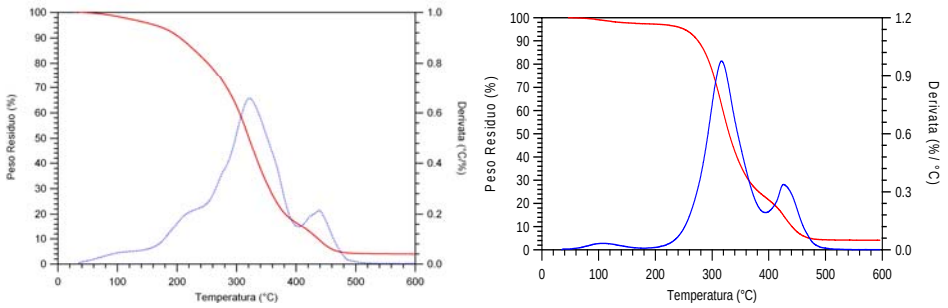

(a) (b)

Figure 3.52 TGA and DTGA Traces of Hydrolene (LFT) (a) and Polyvinylalcohol (PVA 18/88) (b).

Initial weight loss in LFT, which was a mixture of PVA by-products and inks, was 3.8 % in the temperature range of 25°C-142°C. Two main decomposition peaks were observed in hydrolene samples at 322°C and 439°C. The corresponding weight losses at these temperatures were 51.6 % and 12 %, respectively.

For the first peak, the trace showed two shoulders at the temperature around at 214°C and 278°C with associated weight losses of 15.2 % and 13 %, respectively. The residue recovered at 600 °C was 3.7 % and it was higher than many other polymeric materials.

PVA samples showed an initial weight loss around at 2.55 % between 25°C-178°C. The decomposition trace showed two PVA decomposition peaks around at 318°C and 428°C. The corresponding weight losses were 74.6 % and 18.4 % and the residue recovered at 600 °C was 4.1 %.

The presence of additives, in the hydrolene, made this material thermally less stable than PVA. Infact its T_{on} was 234°C, compared to PVA which was around 271°C.

Figure 3.53 shows TGA and DTGA traces for PHB (a) and PCL 6500 (b).

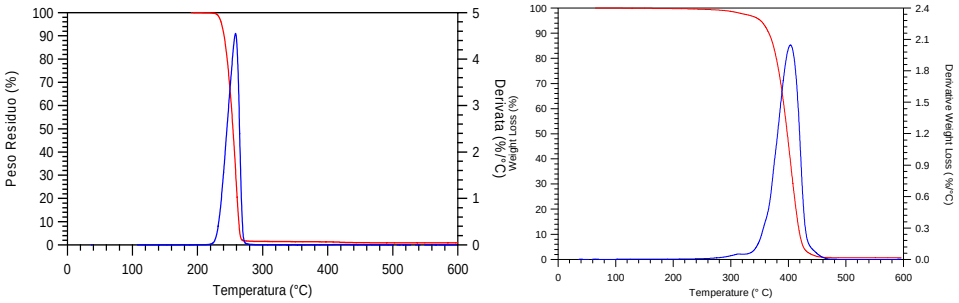

(a) (b)

Figure 3.53 TGA and DTGA Traces of PHB (a) and PCL 6500 (b).

The thermal properties of these leading biodegradable polymers such as PHB, PCL (PCL 6500) and PLA were also carried out for comparative pourpouses. PHB and PCL showed initial weight losses of 0.03 % and 0.24 %, respectively. Poly(hydroxybutirate) (PHB) started to decompose around at 239°C and a single decomposition peak was observed around at 260°C.

The weight loss associated with this peak was 98 %. The total residue recovered at 800°C was 0.48 %.

PCL, on the other hand, started to decompose around at 362°C with a single decomposition peak at 404°C. The associated weight loss was 25.3 %.

The residue recovered at 800°C was 0.16 %.

Figure 3.54 shows TGA and DTGA traces for poly-lactic acid (PLA).

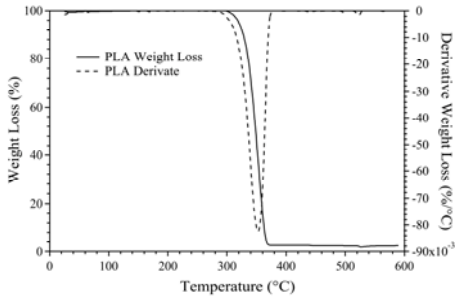

Figure 3.54 TGA and DTGA Traces for PLA.

PLA had a some what higher initial weight loss compared to PHB and PCL. The weight loss in PLA was 0.31 % in the temperature range of 25°C-256°C. PLA started to decompose around at 320°C and a single degradation peak was observed. The residues obtained at 800°C was roughly 1.01 %.

Table 3.39 records the thermal properties for the polymeric material under nitrogen atmosphere while Table 3.40 reports the thermodynamic parameters for the selected polymeric materials.

Table 3.39 Thermal Properties for the Polymeric Materials Under Nitrogen Atmosphere.

Sample	T_{on} (°C)	T_{p1} (°C)	T_{p2} (°C)	R_{800} (%)
Bionolle 1020	350	412	-	1.4
Bionolle 1050	348	412	-	0.7
PLA	326	364	-	0.4
PLA[c]	302	354	-	0.1
PHB	281	302	-	3.0
PHB[d]	239	258	-	0.5
PCL 6500[d]	320	403	-	0.2
PCL 6500[e]	362	404	-	0.7
LFT rig Verde[d]	188	439	322	3.7
PVA 18/88	264	316	426	4.1

PLA [c] = PLA after Brabender processing, [d] = samples analyzed at 800°C, [e] = PCL 6500 after Brabender processing.

For the biodegradable polymers, the T_{on} values (Table 3.39) were higher for PHB and PLA processed at Braebender in comparison to the pure materials. The only exception was PCL 6500, for which the Braebender processing improved the thermal stability.

The only material that presented an high residue recovered at 800°C, was hydrolene (LFT), due to the additives introduction in the material.

This was the same reason for which all materials had only one decomposition peak except LFT polymer.

Table 3.40 Thermodynamic Properties for Polymeric Materials.

Sample	Tg (°C)	T_c (°C)	ΔH_c (J/g)	T_{m2} (°C)	ΔH_{m2} (J/g)
Bionolle 1020	-33.1	-	113.5	103.7	27.9
Bionolle 1050	-32.4	-	113.5	100.9	14.3
PLA	63.9	-	-	154.7	28.6
PHB	0.9	56.5	53.3	173.1	82.5
PCL 6500	-	22.2	93.1	55.9	78.8
LFT	55.3	125.9	21.4	173.4	16.0

The glass transition temperature (T_g) presented an high positive value only for PLA, confirming the rigidity of the material and the need to plasticize it in making composites.

The cold crystallization enthalpy was quite high for Bionolle and PCL 6500, while the melting enthalpy was high for PHB and PCL 6500. These two polymers also had high melting enthalpy values (82.5 J/g for PHB and 78.8 J/g for PCL 6500) compared to the other polymers.

3.8.1.4 Composites based on PCL/ulva

3.8.1.4.1 Morphology

Fibers were well dispersed throughout the matrix and exhibited considerable cohesion with the polymer. At the macroscopic level, film was

smooth, flexible and strong, but a microscopic examination revealed the presence of regions with exposed fibers or fibers aggregates.

These inconsistencies might have resulted from the imprecise control of the film thickness from compression moulding.

Figure 3.55 shows the SEM photomicrographs for the PCL 6500 (a) and a PCL blend containing 30 % of ulva as a biological filler (b).

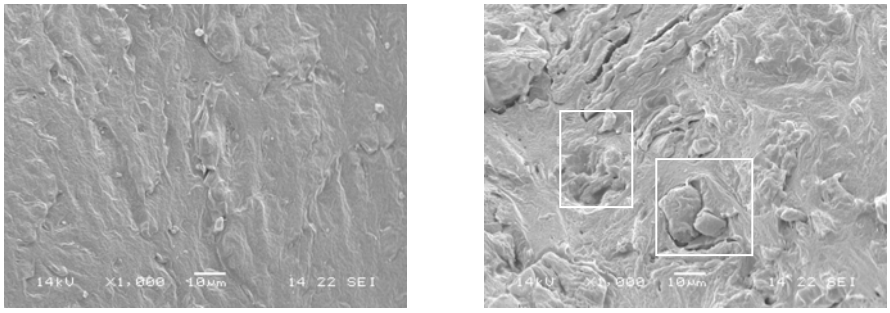

(a) (b)

Figure 3.55 SEM Photomicrographs for PCL 6500-1000X (a) and PCLU30-1000X (b).

A good compatibility appeared to be at the interface between PCL and ulva. However some inconsistencies were noted throught the matrix.

Both, PCL 6500 and the blend PCLU30 showed a smooth surface where the fibers were quite well dispersed in the polymer matrix making the film stronger when the filler agent was present.

3.8.1.4.2 Thermogravimetric Analysis (TGA)

Figure 3.56 shows the TGA (a) and DTGA (b) traces for the selected compositions of PCL/Ulva (70/30, 50/50, 30/70) composites and for the pristine materials.

The first step corresponded to the humidity and volatiles elimination and it

occurred in the temperature range of 25°C-100°C. The weight losses were 1.2 % for PCLU30, 2.7 % for PCLU50 and 2.3 % for PCLU70.

The T_{on} was between 350°C and 365°C for all PCLU composites. With increased fiber content, a decrease in the thermal stability was observed in composite.

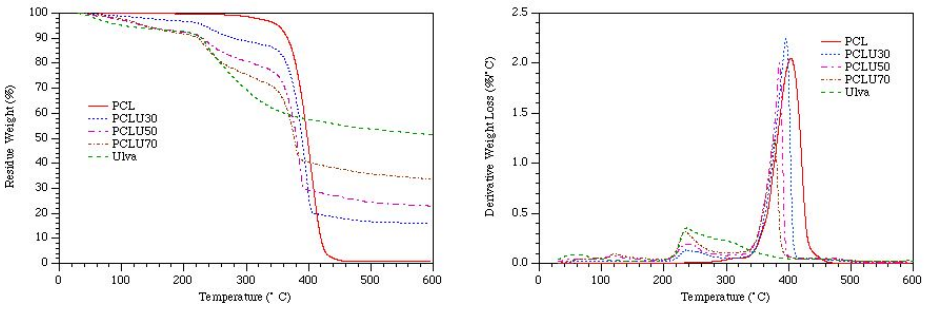

(a) (b)

Figure 3.56 TGA (a) and DTGA (b) Traces for PCL/Ulva Composites.

PCLU30 blend showed two degradation peaks that fall down around at 235°C and 396°C with associated weight losses of 10.7 % and 70 %, respectively.

PCLU50 trace also showed two peaks at 237°C and 384°C. The weight losses corresponding to these steps were 13.5 % and 50 % respectively.

For PCLU70 samples, peaks were observed at 234°C and 378°C, with their relative weight losses of 18.3 % and 33.7 %, respectively.

The residue recovered at 600 °C increased proportionally with increased ulva content which was doing to the high quantity of siliceous material in algal cell mass. The values were 16 % (PCLU30), 23 % (PCLU50) and 33.5 % (PCLU70) respectively.

Table 3.41 records the thermal properties for the selected composites.

Table 3.41 Thermal Properties for the PCL/Ulva Composites.

Sample	T_{on} (°C)	T_{p1} (°C)	T_{p2} (°C)	T_{p3} (°C)	R_{600} (%)
PCLU30	365	235	396	-	16.0
PCLU50	359	119	237	384	23.0
PCLU70	350	120	234	378	33.5

T_{on} was found to be between 350°C-370°C and the loss of thermal stability was proportional to the amount of fibers in the samples.

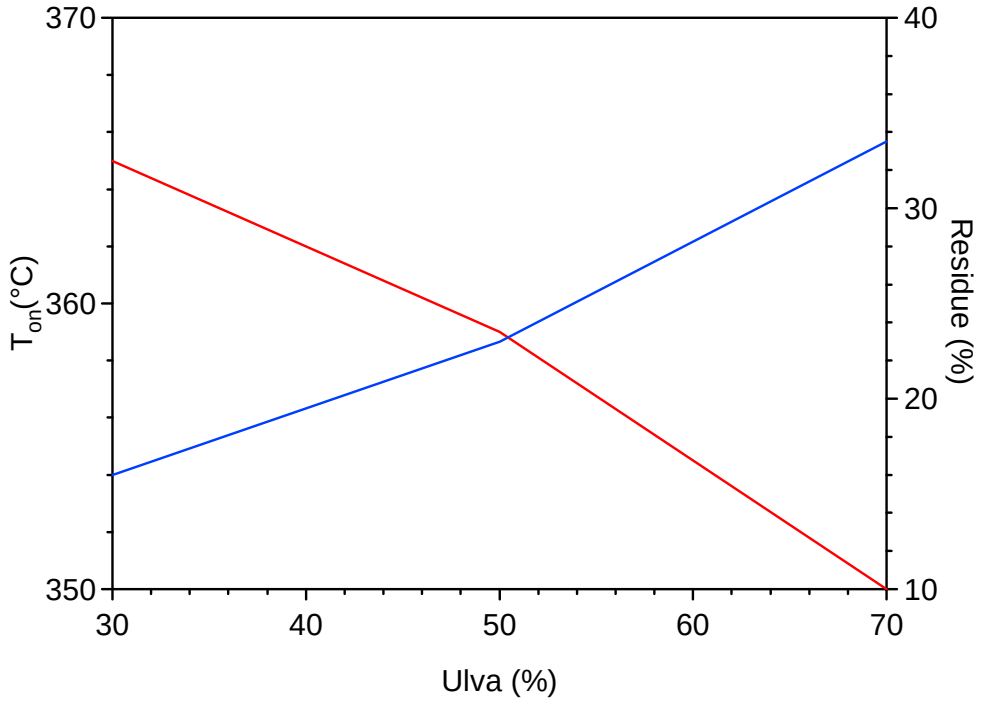

Figure 3.57 T_{on} and Residue Trend for PCL/Ulva Composites.

The T_{on} and residue trend for PCL/Ulva composites is shown in Figure 3.57.

There was an inverse proportionality between the two parameters: the increase in the percent of ulva reduced the composite thermal stability connected with an increased siliceous material amount, which did not pyrolize at 600°C.

The 50 % algal content seemed to be a critical concentration: from this point the thermal stability started to be strongly affected to the presence of an high recovered residue.

3.8.1.4.3 Differential Scanning Calorimetry (DSC)

The DSC traces for the composites based on PCL/Ulva and the pristine materials are provided in Figure 3.58.

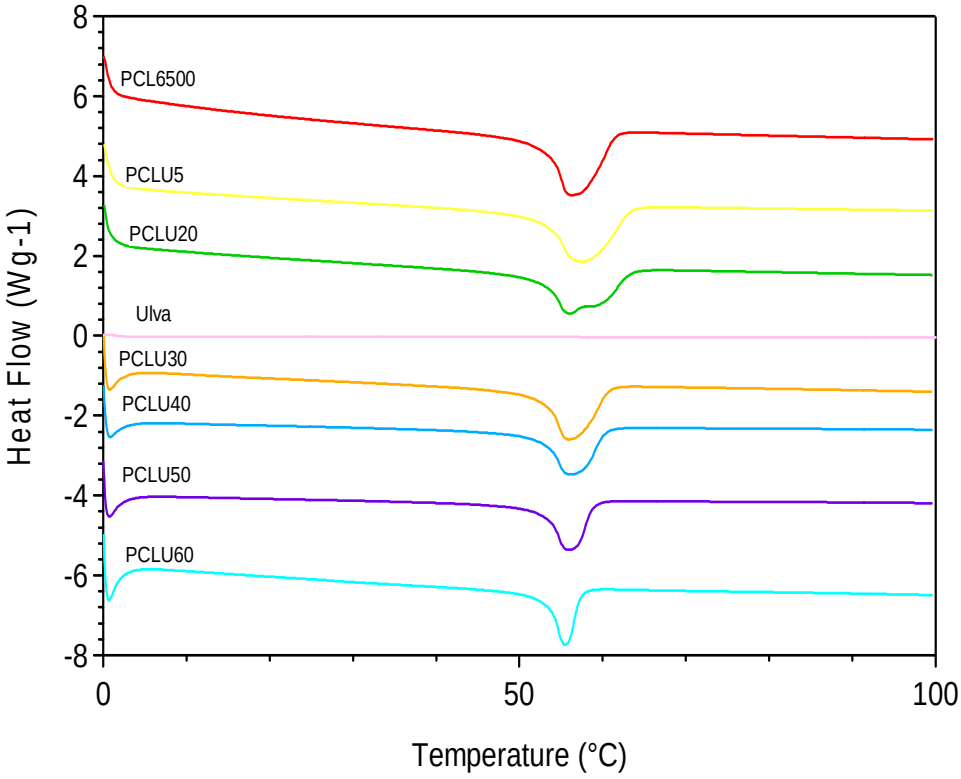

Figure 3.58 DSC Traces for PCL/Ulva Composites.

The DSC traces showed single melting peak for all PCL/Ulva formulations. The only exception was the composite PCLU20 which showed a double melting peak, connected with the algal components, for this particular formulation.

Table 3.42 records the thermodynamic parameters for the PCL/Ulva composites.

Table 3.42 Thermodynamic Properties for PCL/Ulva Composites.

Sample	T_c (°C)	ΔH_c (J/g)	T_{m1} (°C)	ΔH_{m1} (J/g)	T_{m2} (°C)	ΔH_{m2} (J/g)
PCL	29.39	-78.7	56.14	66.75	-	-
PCLU5	31.49	-80.46	57.45	65.9	-	-
PCLU10	31.37	-67.62	55.88	56.04	-	-
PCLU20	31.25	-68.03	56.02	35.14	57.8	20.77
PCLU30	31.81	-59.82	55.93	48.93	-	-
PCLU40	31.59	-51.49	56.29	41.94	-	-
PCLU50	33.59	-41.98	55.97	35.75	-	-
PCLU60	33.62	-33.64	55.52	29.02	-	-

The data presented in Table 3.42 showed a progressive decreasing in melting heat (ΔH_m) with increased algal content. The organic fillers probably contributed towards the mobility of the polymeric chains, thus decreasing the demand for the energy required for the melting of the polymeric material.

Also a decrease in the crystallization heat was observed, because of the composites lost some of their crystallinity due to the presence of the organic fillers, that acted as a nucleating agent for the crystallization of polymer chains[87,91]. The filler did not appear to have any impact on the glass transition temperature (T_g) of PCL that was observed at -60°C for all samples tested.

The melting temperature in most composites was in close proximity to that of neat PCL[89,90]. The decrease in blend's crystallinity was due to the presence of algal biomass, probably interfered with the movements of polymer chain, thus impacting its morphology and amorphous behaviour.

3.8.1.4.4 Mechanical Properties

The specimens in the shape of dog-bones were stamped out and tested for their mechanical properties. Before testing, specimens were preconditioned at 50 % relative humidity. The results from the Instron test are provided in Table 3.43

Table 3.43 Mechanical Properties for the PCL/Ulva Composites.

Sample	El (%)	StDv	UTS (MPa)	StDv	YM (MPa)	StDv
PCL	813	87	26.8	3.7	374	7
PCLU30	75	18	7.5	0.8	472	28
PCLU40	33	17	8.2	0.9	652	35
PCLU50	6	1.5	6.6	0.7	779	0.15
PCLU60	3	0.7	6.1	0.8	789	82
PCLU70	1	0.3	3.2	0.8	465	101

El = Elongation at Break, UTS = Ultimate Tensile Strength, YM = Young Modulus, StDv = Standard Deviation.

PCL is a thermoplastic and ductile polymer[89] and the laminates produced from it had an high elongation at break (> 800 %). The addition of ulva improved the Young Modulus (YM) of the blends with a loss of both El and UTS that showed a concomitant decrease. Thus, ulva was only suitable as filler and it was not recommended as a reinforcement in blends.

Particularly, when the ulva content was greater than 40 %, the elongation at break (EL) was drastically impacted the UTS showing only a modest change when Ulva content ranged between 30 and 60 percent. The blend with 70 % Ulva content (PCLU70) was very fragile.

3.8.1.5 Composites based on PHB/Ulva

3.8.1.5.1 Morphology

The SEM photomicrographs for the PHB composites containing 30 % (a) and 50 % (b) of ulva are shown in Figure 3.59.

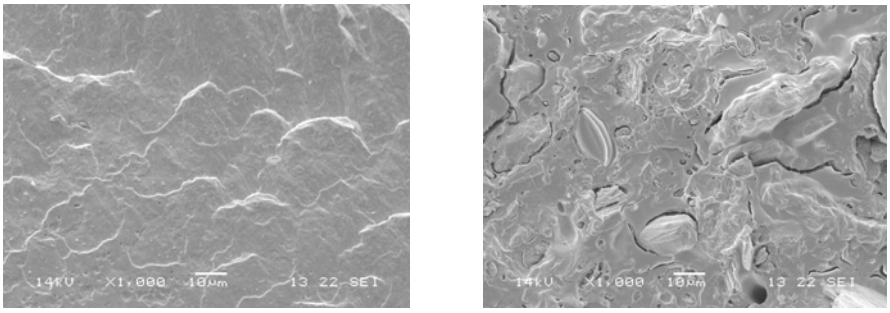

(a) (b)

Figure 3.59 SEM Photomicrographs for PHBU30-1000X (a) and PHBU50-1000X (b).

When examined visibly, composites showed a rather smooth surface.

However, few SEM inconsistencies were obvious. Some cracks were visible at the interface between the polymer matrix and algal material.

The cracks were an indication of a poor compatibility between these two materials. In the formulation with 50 % algal content (PHBU50), the ulva fibre formed large aggregates dispersed throughout the polymeric matrix.

3.8.1.5.2 Thermogravimetric Analysis (TGA)

The TGA (a) and DTGA (b) traces for the selected PHB/Ulva compositions (70/30 and 50/50) and pristine materials are presented in Figure 3.60.

Both composites showed an humidity and volatiles elimination in the temperature range of 25°C-100°C and their corresponding weight losses were 1.1 % (PHBU30) and 1.4 % (PHBU50).

Both PHBU30 and PHBU50 started to decompose at a temperature around at 266°C.

The main decomposition peak occurred between 240°C-300°C and the weight losses were 74.05 % for PHBU30 and 57.9 % for PHBU50.

It represented the total pyrolysis of the polymeric material. This peak showed a shoulder in both DTGA traces (Fig. 3.59b) that felt down in the temperature range of ca. 190°C-240°C corresponding to a weight losses of 4.3 % for PHBU30 and 6.9 % for PHBU50.

The residue recovered at 600 °C increased with the alga content confirming that the ulva contains an high quantity of siliceous materials. The values were 14.2 % for PHBU30 and 22.5 % for PHBU50.

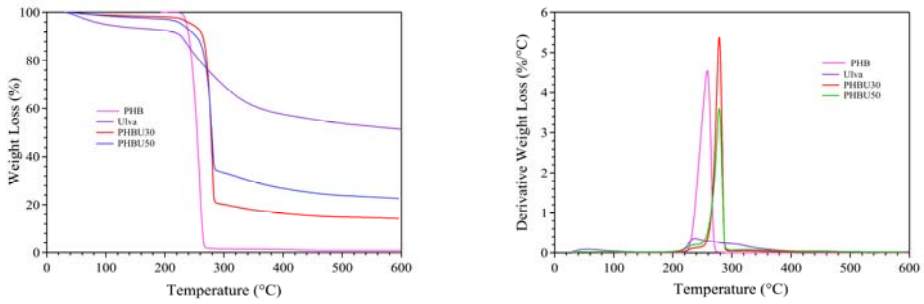

(a) (b)

Figure 3.60 TGA (a) and DTGA (b) Traces for PHB/Ulva Composites.

The DTGA trace (Fig. 3.60b) showed that the two peaks of the pure components were shifted towards intermediate values indicating that the thermal stability depended on the presence of Ulva that was present in the composites.

Table 3.44 records the thermal properties for PHB/Ulva composites.

Table 3.44 Thermal Properties for the PHB/Ulva Composites.

Sample	T_{on} (°C)	T_{p1} (°C)	T_{p2} (°C)	T_{p3} (°C)	R_{600} (%)
PHBU30	268	234[a]	279	-	14.2
PHBU50	265	232[a]	279	-	22.5

a: shoulder

Both formulations PHBU30 and PHBU50 showed the same thermal stability as indicated by the similar T_{on} values. Also the degradation effects were the same in both formulations confirming that the algal biomass acted only as a filler agent.

3.8.1.5.3 *Differential Scanning Calorimetry (DSC)*

Figure 3.61 shows the DSC traces for the composites based on PHB/Ulva and the pristine materials.

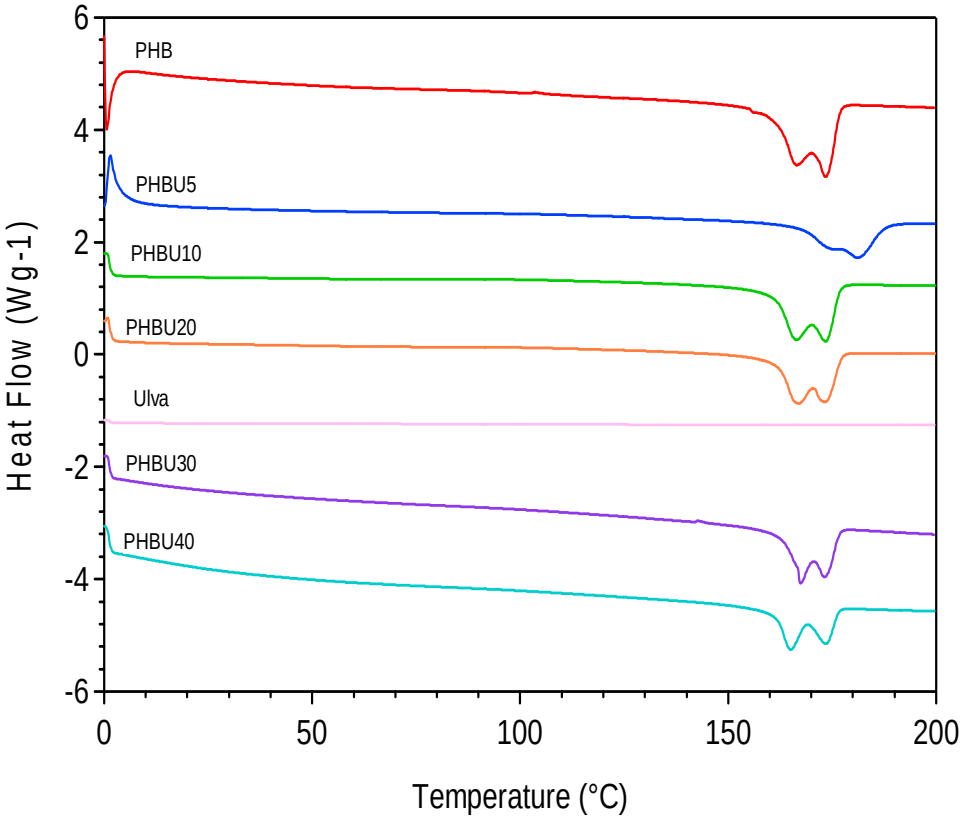

Figure 3.61 DSC Traces for the PHB/Ulva Composites.

Composites blended with variable amount of Ulva fibers was processed in a Braebender and analyzed along with PHB controls. DSC traces for all samples indicated a double fusion peak similar in the shape and temperature value.

Table 3.45 records the thermodynamic properties for the PHB/Ulva composites.

Table 3.45 Thermodynamic Properties for the PHB/Ulva Composites.

Sample	T_c (°C)	ΔH_c (J/g)	T_{m1} (°C)	ΔH_{m1} (J/g)	T_{m2} (°C)	ΔH_{m2} (J/g)
PHB	90.38	-94.37	167	55.04	173	35.48
PHBU5	85.55	-48.61	176	26.72	181	28.68
PHBU10	91.82	-69.55	166	49.98	173	28.55
PHBU20	91.09	-62.71	167	42.78	173	25.86
PHBU30	91.04	-54.76	168	32.71	173	23.5
PHBU40	92.02	-44.84	165	28.31	173	19.24

Addition of only 5 % algal content resulted in a melting temperature increase[22] of about 10°C in blends. Interestingly, only half as much heat (ΔH_m), was required to meet PHB blended with algae compared to neat PHB.

This indicated that the algal biomass had an impact on the melting heat (ΔH_m) of the PHB polymer in the blend.

3.8.1.5.4 Mechanical Properties

After conditioning at 50 % relative humidity, the PHBU20 and PHBU30 dog bone specimens were analyzed for their mechanical properties as reported in Table3.46.

Table 3.46 Mechanical Properties for the Composites PHBU20 and PHBU30.

Sample	El (%)	StDv	UTS (MPa)	StDv	YM (MPa)	StDv
PHBU20	1.2	0.1	19.1	2.9	2209.6	163.7
PHBU30	1.1	0.1	15.3	2.0	2280.6	282.6

El = Elongation at break, UTS = Ultimate tensile strength, YM = Young Modulus, StDv = Standard deviation.

Samples had a low elongation at break due to the inconsistencies present in the laminates containing ulva fibres. The Young Modulus (YM) increased gradually with the uniform increment of ulva fibre loading in the composite[93].

3.8.1.6 Composites based on PHB/PCL

3.8.1.6.1 Thermogravimetric Analysis (TGA)

Figure 3.62 shows the TGA (a) and DTGA (b) traces for several selected PHB/PCL compositions (10/90, 20/80, 30/70, 90/10, 80/20, 70/30).

For all composites, the humidity and volatiles elimination occurred at temperature between 25°C-100°C and the weight losses at this step were 0.02 % for PHB10PCL90, 0.003 % for PHB20PCL80, 0.07 % for PHB30PCL70,

0.13 % for PHB70PCL30, 0.18 % for PHB80PCL20 and 0.012 % for PHB90PCL10.

Composites with high percentage of PCL started to degrade in a temperature range comprised between 370°C and 385°C. Whereas, composites with high percentage of PHB started to degrade between 230°C-280°C..

The data indicated that composites with high amount of PCL were much more thermally stable than PHB composites.

Two decomposition peaks were evident for all composites and their intensity varied depending on the polymer (PHB or PCL) amount present in the composite, recovered from pyrolysis during the TGA experiments.

In the first step, the temperature felt down in the range of 200°C-340°C and the corresponding weight losses were 10.7 % for PHB10PCL90, 20 % for PHB20PCL80, 30.4 % for PHB30PCL70, 68 % for PHB70PCL30, 72.4 % for PHB80PCL20 and 88 % for PHB90PCL10.

Interestingly, the weight loss steps showed an increase in their values when the amount of PHB was increased.

The second step occurred in the temperature range of ca. 280°C-500°C and the corresponding weight losses were 88.3 % for PHB10PCL90, 79.5 % for PHB20PCL80, 69.1 % for PHB30PCL70, 24 % for PHB70PCL30, 21 % for PHB80PCL20 and 11.6 % for PHB90PCL10.

The second DTGA peak also showed two shoulders for the composite PHB70PCL30 in the temperature range of 350°C-390°C, which were attributed to the pyrolysis effects of some impurities present in the pristine PCL. This was completely opposite to what was observed in the first DTGA peak.

The residue recovered at 800°C included some partially pyrolyzed part of the polymeric material estimated to be around 0.64 % for PHB10PCL90, 0.43

% for PHB20PCL80, 0.55 % for PHB30PCL70, 0.03 % for PHB70PCL30, 1.01 % for PHB80PCL20 and 0.46 % for PHB90PCL10.

Table 3.47 records the thermal properties for the PHB/PCL composites.

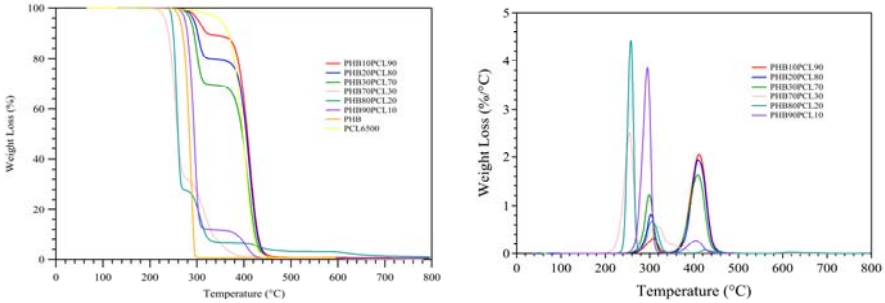

(a) (b)

Figure 3.62 TGA (a) and DTGA (b) Traces for PHBPCL Composites.

Table 3.47 Thermal Properties for the PHBPCL Composites.

Sample	T_{on} (°C)	T_{p1} (°C)	T_{p2} (°C)	T_{p3} (°C)	R_{800} (%)
PHB10PCL90	290	308	411	-	0.64
PHB20PCL80	289	302	409	-	0.43
PHB30PCL70	285	300	408	-	0.55
PHB90PCL10	274	294	403	-	0.46
PHB80PCL20	246	258	304	425	0.99
PHB70PCL30	236	255	315	380	0.00

The thermal stability of PHB and PCL blends was directly proportional to the amount of PCL present in the composites (Table 3.47). The blend PCLU30 seemed to be less thermally stable compared to the other formulations, which had higher T_{on}, decreasing or increasing the algal content in the blend.

3.8.1.6.2 Differential Scanning Calorimetry (DSC)

Figure 3.63 shows the DSC traces for the PHBPCL composites.

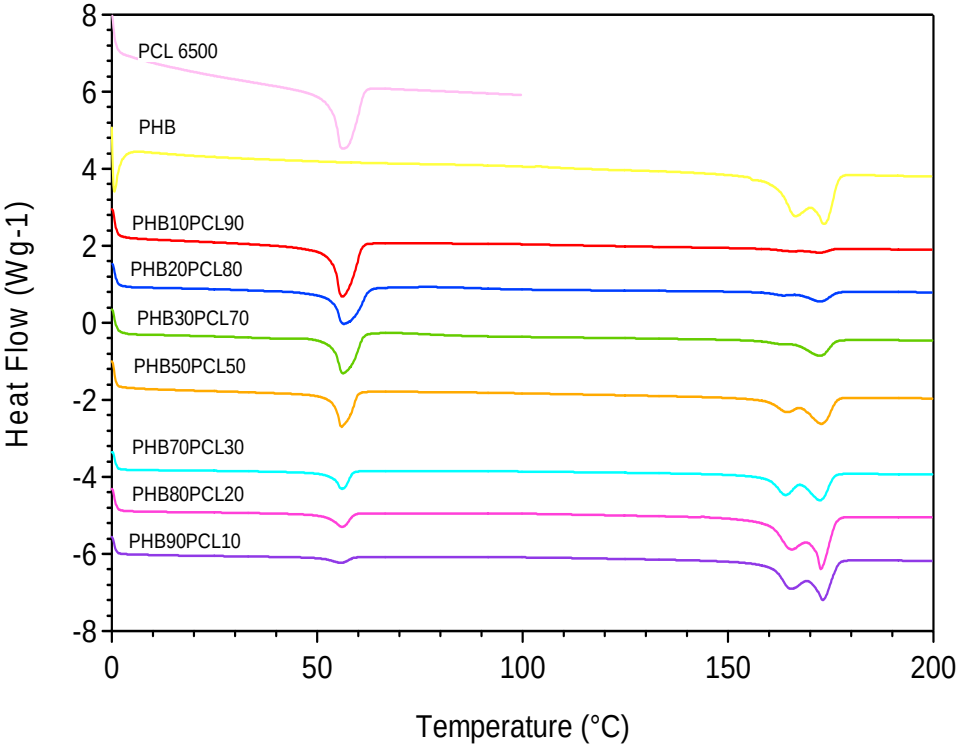

Figure 3.63 DSC Traces for the PHBPCL Composites.

All the DSC traces showed the PCL melting peak near 60°C. The peak intensities decreased considerably as the amount of PCL polymer decreased in the blends.

A second PHB melting peak was also apparent at 170°C in all formulations. The peak intensity increased with increased PHB content in the blend.

The decrease in the heat flow for PHB composites was noted increased PHB content. The heat flow of 6 J/g was observed in composites with 90 %

PHB content. The heat flow of PCL showed an increase, depending on the PHB content in composites.

Table 3.48 records the thermodynamic properties for the composites based on PHB and PCL.

The melting enthalpy showed a trend similar to that of melting temperature indicating a decrease in melting enthalpy with a decrease in PCL percentage and an increase in melting enthalpy with an increase in PHB content.

Table 3.48 Thermodynamic Properties for the PHBPCL Composites.

Sample	T_{m1} (°C)	ΔH_{m1} (J/g)	T_{m2} (°C)	ΔH_{m2} (J/g)	T_{m3} (°C)	ΔH_{m3} (J/g)
PHB10PCL90	56.17	51.14	165.65	2.17	172.3	3.49
PHB20PCL80	56.59	41.64	163.58	3.40	172.49	10.10
PHB30PCL70	56.39	36.11	165.01	3.62	172.38	16.45
PHB50PCL50	55.97	26.87	164.45	15.23	172.70	24.61
PHB70PCL30	56.16	12.49	163.87	12.94	172.28	30.95
PHB80PCL20	56.14	10.90	165.45	40.00	172.55	36.04
PHB90PCL10	55.87	4.93	165.47	21.78	173.15	46.02

3.8.1.6.3 Mechanical Properties

After conditioning (50 % RH), selected PHBPCL specimens were analyzed for their mechanical properties. Data are presented in Table 3.49.

Table 3.49 Mechanical Properties for the PHBPCL Composites.

Sample	El (%)	StDv	UTS (%)	StDv	YM (MPa)	StDv
PHB10PCL90	631	63	20.1	1.8	436	8
PHB20PCL80	590	22	16	1.3	470	35
PHB30PCL70	532	18	11.9	0.9	501	42
PHB50PCL50	2.5	0.2	9.8	1.8	676	103
PHB70PCL30	4.0	0.4	22.5	1.9	1427	135
PHB80PCL20	6.4	1.1	26.9	5.2	1297	72
PHB90PCL10	7.81	0.8	30.6	3.8	1604	89

Figure 3.64 shows the mechanical properties of PHBPCL composites.

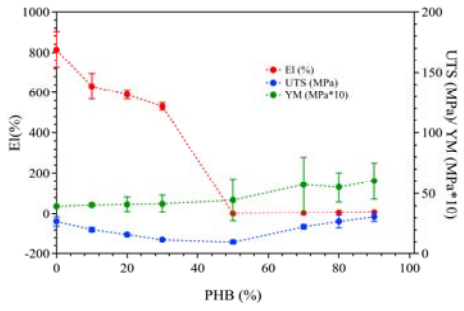

Figure 3.64 Elongation at Break, Ultimate Tensile Strength and Young Modulus for the PHBPCL Composites.

PCL is a thermoplastic polymer and as expected showed an excellent elongation at break (EL) without any additives. The laminates based on PCL with added PHB polymer had a negative impact on its elongation.

Addition of a small quantity of PHB polymer resulted in a decrease in elongation at break.

In a 50/50 PHBPCL blend, EL decreased from 800 % to almost zero percent yielding a fragile material. The effect on UTS was only evident when PHB content increased over 50 % in the blend. Young Modulus (YM) stayed small through out and any variations in PHB or PCL did not have any impact on the YM of the composite.

3.8.1.7 Composites based on PHBPCL/Ulva

3.8.1.7.1 Thermogravimetric Analysis (TGA)

Figures 3.65 and 3.66 show the TGA (a) and DTGA (b) traces for selected PHB/PCL composites containing 10 %, 20 % and 30 % of ulva..

Weight losses due to humidity and volatiles elimination, that occurred in the temperature range of 25°C-100 were 0.04 % for (PHB80PCL20)90U10, 0.13 % for (PHB80PCL20)80U20, 1.5 % for (PHB80PCL20)70U30, 0.5 % for (PHB70PCL30)90U10, 0.18 % for (PHB70PCL30)80U20 and 0.34 % for (PHB70PCL30)70U30.

The DTGA traces (Fig. 3.65b and 3.66b) showed two weight loss steps, typical of pyrolyzed polymeric materials occurred in the temperature range of 200°C-360°C and 200°C-300°C. The weight losses associated with the first and the second step were 71.75 % and 14.42 % for (PHB80PCL20)90U10, 66.4 % and 3.04 % for (PHB80PCL20)80U20, 63.7 % and 16.7 % for (PHB80PCL20)70U30, 63.8 % and 23.8 % for (PHB70PCL30)90U10, 60.05 % and 26.9 % for (PHB70PCL30)80U20, 51.35 % and 25.6 % for (PHB70PCL30)70U30.

In PHB/PCL (80/20) blends containing 10 and 20 % of ulva, the second peak showed a shoulder, that felt down in the temperature range of ca. 300°C-360°C. The weight losses were 5.7 % for (PHB80PCL20)90U10 and 18.02 % for (PHB80PCL20)80U20.

The residue recovered at 800°C increased with an increase in the algal content, as this material had a large quantity of siliceous material, which was only partially pyrolyzed at 800 °C.

The weights obtained were 3.1 % for (PHB80PCL20)90U10, 7.9 % for (PHB80PCL20)80U20, 11.3 % for (PHB80PCL20)70U30, 3.0 % for (PHB70PCL30)90U10, 7.2 % for (PHB70PCL30)80U20 and 11.8 % for (PHB70PCL30)70U30.

The DTGA traces (Fig.3.66b) showed sharp but narrowly spaced degradation peaks for PHB/PCL and Ulva blends. Table 3.50 records the thermal properties for the PHBPCL/Ulva composites.

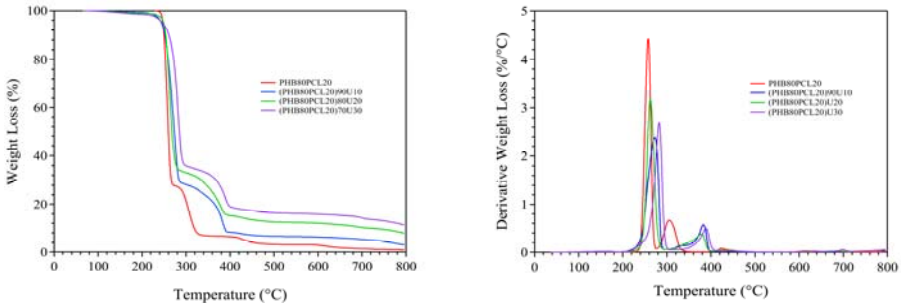

(a) (b)

Figure 3.65 TGA (a) and DTGA (b) Traces for the (PHB80PCL20)Ulva Composite.

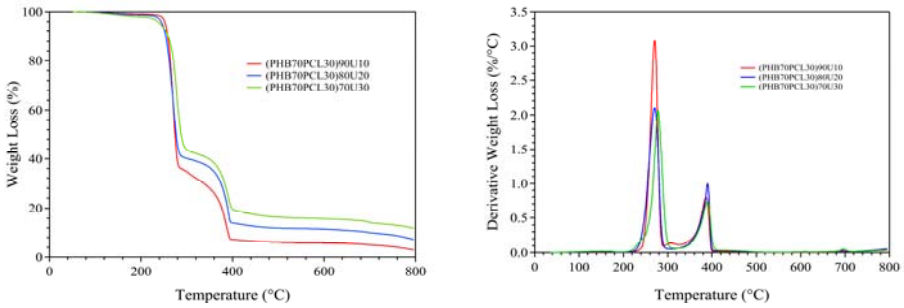

(a) (b)

Figure 3.66 TGA (a) and DTGA (b) Traces for the (PHB70PCL30)Ulva Composite.

Table 3.50 Thermal Properties for the PHBPCL/Ulva Composites.

Sample	T_{on} (°C)	T_{p1} (°C)	T_{p2} (°C)	T_{p3} (°C)	Tp_4 (°C)	R_{800} (%)
PHB80PCL20	247	257	303	424	-	1.01
(PHB80PCL20)90U10	246	273	327[a]	382	420	3.07
(PHB80PCL20)80U20	249	263	335	379	428	7.9
(PHB80PCL20)70U30	258	233[a]	282	389	696	11.3
PHB70PCL30	235	255	315	356	380	0.0
(PHB70PCL30)90U10	254	272	306	387	-	3.0
(PHB70PCL30)80U20	249	271	392	691	-	7.2
(PHB70PCL30)70U30	265	239[a]	279	391	696	11.8

The T_{on} showed an increase of about 10°C with increased ulva content for both formulations.

3.8.1.7.2 Differential Scanning Calorimetry (DSC)

Figure 3.67 shows the DSC traces for the PHBPCL/Ulva composites.

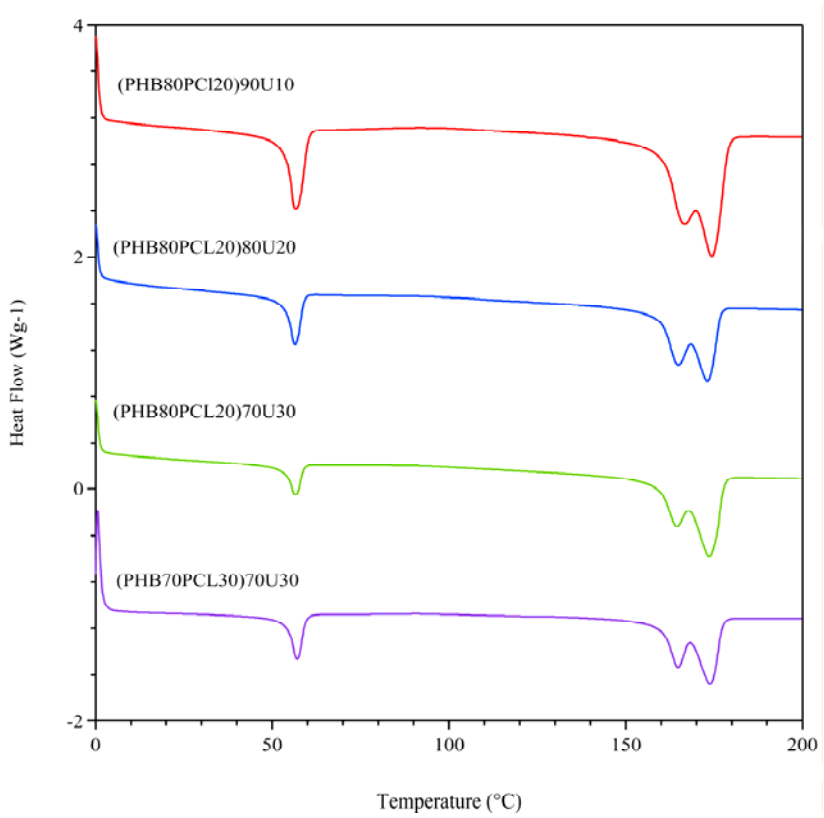

Figure 3.67 DSC Traces for the PHBPCL/Ulva. Composites.

The melting peak of PCL material was around 60°C which showed a decrease in its intensity when PHB/PCL ratio was modified.

Sharp double melting peaks, typical of PHB material, were present around at 170°C in blend (PHB80PCL20)90U10.

Table 3.51 shows the thermodynamic properties for the PHBPCL/Ulva composites.

Table 3.51 Thermodynamic Properties of the PHBPCL/Ulva Composites.

Sample	T_{m1} (°C)	ΔH_{m1} (J/g)	T_{m2} (°C)	ΔH_{m2} (J/g)	T_{m3} (°C)	ΔH_{m3} (J/g)
PHBPCL(80/20)90U10	56.43	21.21	166.26	-37.04	173.83	41.42
PHBPCL(80/20)70U30	56.30	7.02	164.03	18.93	173.04	27.72
PHBPCL(70/30)80U20	56.32	11.62	164.48	21.70	172.75	21.74
PHBPCL(70/30)70U30	56.91	10.14	164.68	16.08	173.63	20.45

Increasing the ulva amount, the PCL melting temperature remained constant for all compositions, while the melting henthalpies decrease with the ulva content werease. The ulva fibers make polymeric chains less movable respect to the pristine polymers, so it is necessary a minor quantity of energy to melt the composite materials.

3.8.1.7.3 Mechanical Properties

After conditioning (50 % RH), selected PHBPCL/Ulva specimens were analyzed for their mechanical properties.

Data are reported in Table 3.52, while Figure 3.68 shows the trend of these properties for the formulations containing a weight ratio 80/20 and 70/30 for the polymers PHB and PCL and an ulva content from 10 to 30 percent.

Table 3.52 Mechanical Properties for the PHBPCL/Ulva Composites.

Sample	El (%)	StDv	UTS (%)	StDv	YM (MPa)	StDv
PHBPCL(80/20)90U10	3.4	0.3	22.8	0.8	1795.1	129
PHBPCL(80/20)80U20	2.8	0.3	13.0	2.2	1589.8	120
PHBPCL(80/20)70U30	1.6	0.4	12.8	2.8	1496.9	178
PHBPCL(70/30)90U10	4.1	0.4	17.9	1.7	1343.8	93
PHBPCL(70/30)80U20	3.5	0.4	17.4	2.1	1527.5	119
PHBPCL(70/30)70U30	2.7	0.3	16.2	1.1	1482.3	97

Formulations containing PHBPCL weight ratio 80/20 and 70/30 loaded with ulva, showed small values for the elongation at break (EL) which showed a decrease with increased algal content (Table 3.52).

So the produced composites resulted more fragile compared to the PHBPCL ones characterized by the same weight ratio between the two polymeric materials.

Young Modulus (YM) and the Ultimate Tensile Strength (UTS) with decreased values showed that they were higher than that obtained for the formulations PHBPCL without ulva.

So a variations in algal content had an impact on the YM of the composite.

The effect on UTS was evident for all formulations as indicated from the high values in Table 3.52.

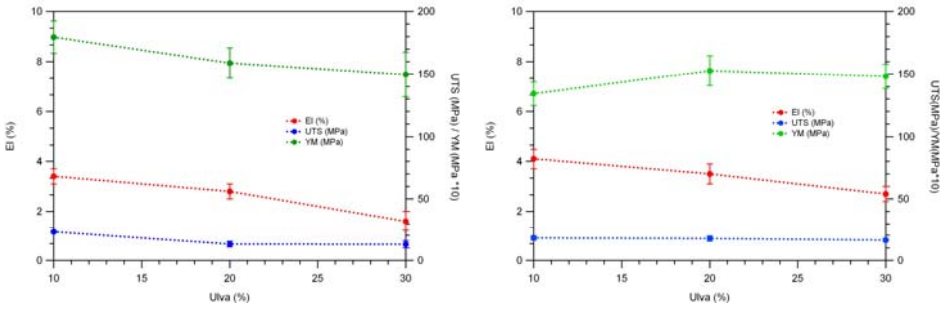

(a) (b)

Figure 3.68 Young Modulus, Elongation at Break, Ultimate Tensile Strength for the PHB/PCL (a) and PHBPCL/Ulva (b) Composites.

3.8.1.8 Composites based on Hydrolene/Ground Rice

3.6.1.8.1 Morphology

The SEM photomicrographs for the hydrolene (LFT) blends containing 30 % (a) and 50 % (b) of ground rice (FR) as natural filler, are shown in Figure 3.69.

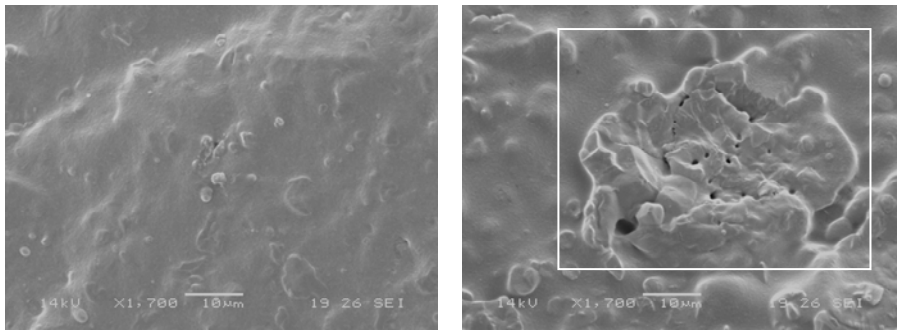

(a) (b)

Figure 3.69 SEM Photomicrographs of LFTFR30-1700X (a), and LFTFR50-1700X (b) Composites.

Fibers were well distributed throughout the matrix and exhibited considerable cohesion with the polymer. The smooth, flexible, strong blends showed the presence of regions with fiber aggregates, that partially filled the ground rice inconsistencies: infact some of them were still evident in the matrix.

3.6.1.8.2 Thermogravimetric Analysis (TGA)

Figure 3.70 shows the TGA (a) and DTGA (b) traces for the selected compositions of LFTFR 90/10, 70/30, 60/40, 50/50, 40/60 composites and for the pristine materials.

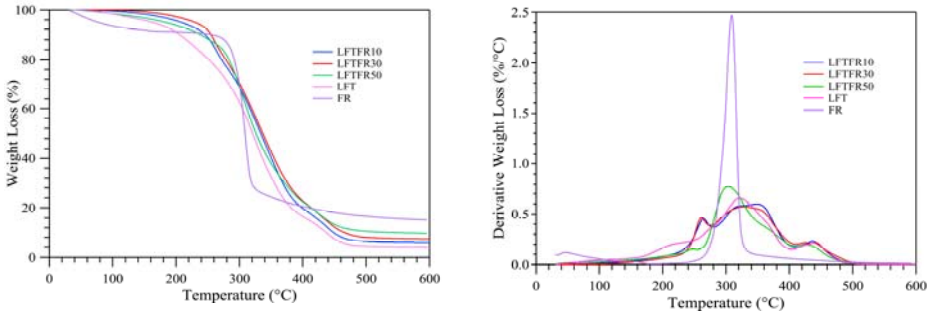

(a) (b)

Figure 3.70 TGA (a) and DTGA (b) Traces of the LFTFR Composites.

LFTFR composites showed at least five weight loss steps. The first one corresponded to the humidity loss and it was connected with the increasing of the ground rice amount, as this material retains a fairly high quantity of water even after prolonged drying. It occurred in the temperature range of 25°C-100°C with corresponding weight losses of 0.5 % for LFTFR10, 0.13 % for LFTFR30, 0.3 % for LFTFR40, 1.5 % for LFTFR50 and 0.8 % for LFTFR60.

The second step was in the temperature range of 100°C-270°C and it represented the pyrolysis of some additives (1.24 %) contained in the Hydrolene.

The weight losses were 22.7 % for LFTFR10, 19 % for LFTFR30, 10.4 % for LFTFR40, 11.2 % for LFTFR50 and 8.5 % for LFTFR60.

All compositions, except LFTFR10, showed a shoulder at the beginning of the second peak, that felt down in the temperature range of 100°C-260°C.

The third and the fourth overlapped peaks represented the main degradation effect and they occurred in the temperature range of 270°C-410°C. The weight losses were 58.1 % for LFTFR10, 60.4 % for LFTFR30, 49.4 % for LFTFR40, 48.7 % for LFTFR50 and 55.5 % for LFTFR60.

The maximum degradation peak assumed a constant value for an high organic material (content higher than 40 %) amount in the composite.

The fifth peak occurred in the temperature range of 410°C-490°C and the corresponding weight losses were 12.5 % for LFTFR10, 7.7 % for LFTFR30, 15.0 % for LFTFR40, 11.4 % for LFTFR50 and 11.7 % for LFTFR60.

The residue recovered at 600°C presented high values connected with the additives amount contained in LFT polymer, that didn't decompose at the experiment temperature. The values were 4.9 % for LFTFR10, 6.9 % for LFTFR30, 10.3 % for LFTFR40, 9.7 % for LFTFR50 and 12.3 % for LFTFR60.

The DTGA trend (Fig.3.68b) is more clearer when the ground rice amount is higher than 50 % respect to the same type of composites where the ground rice was present in the quantity of 10-30 %.

Table 3.53 reports the thermal properties of the LFTFR composites.

Table 3.53 Thermal Properties of the LFTFR Composites.

Sample	T_{on} (°C)	T_{p1} (°C)	T_{p2} (°C)	T_{p3} (°C)	T_{p4} (°C)	T_{p5} (°C)	T_{p6} (°C)	R_{600} (%)
LFTFR10	234	280	349	436	-	-	-	4.90
LFTFR30	236	208	329	426	441	-	-	6.85
LFTFR40	282	256	307	376	433	454	468	10.3
LFTFR50	277	245	304	362	426	-	-	9.65
LFTFR60	278	244	307	372	424	-	-	12.30

The onset temperature increased about 30°C with the ground rice percentage, so the presence of the filler inside the composite made higher the thermal stability of the material.

3.6.1.8.3 Differential Scanning Calorimetry (DSC)

Figure 3.71 shows the DSC traces for the composites based on hydrolene and ground rice while Table 3.54 shows the thermodynamic parameters.

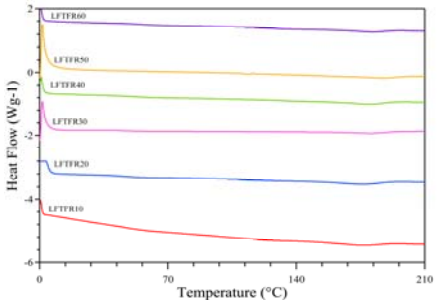

Figure 3.71 DSC Traces of the LFTFR Composites.

Table 3.54 Thermodynamic Parameters of the LFTFR Composites.

Sample	T_g (°C)	T_m (°C)	ΔH_m (J/g)
LFTFR10	55.8	175.2	11.17
LFTFR20	51.05	175.6	13.41
LFTFR30	51.5	180.54	7.48
LFTFR40	56.9	180.1	9.49
LFTFR50	47.8	187.49	4.24
LFTFR60	65.3	181.44	5.79

Melting heat (ΔH_m) showed small values for high percentages of ground rice (50-60 %).

The glass transition temperature (T_g) was around to the value of the pristine LFT. The ground rice addition decreased the amorphous behaviour of the polymeric matrix: LFT chains became more movable so the material was more easily processable.

3.6.1.9 Composites based on LFT/FR/$CaCO_3$

3.6.1.9.1 Morphology

Figure 3.72 shows the SEM photomicrographs for the composite LFTFR40 containing $CaCO_3$.in the weight ratio 5 % (a) and 25 % (b).

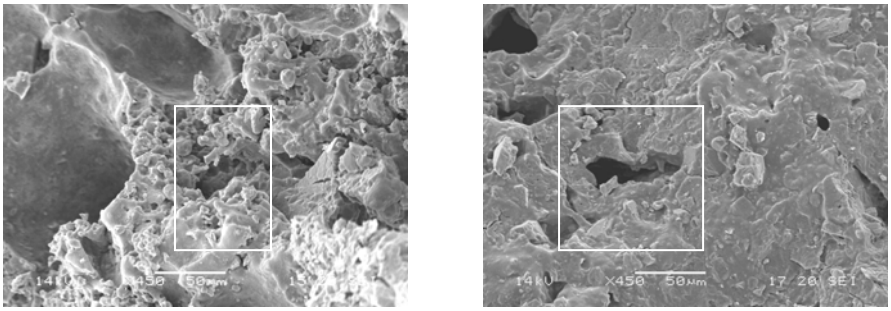

(a) (b)

Figure 3.72 SEM Photomicrographs for LFTFR40$CaCO_3$5-450X (a), and LFTFR40$CaCO_3$25-450X (b) Composites.

Calcium carbonate addition promotes a good adhesion between the polymeric matrix (LFT) and the ground rice (FR).

The composite containing $CaCO_3$ in the weight ratio 5 % presents dominions characterized by different dimensions of the ground rice granules.

As in the hydrolene polymeric matrix, some holes are evident.

3.6.1.9.2 Thermogravimetric Analysis (TGA)

Figure 3.73 shows the TGA (a) and DTGA (b) traces comprised in the temperature range 30°C-600°C for the composites containing LFT/FR/$CaCO_3$ in the weight ratio 50/40/10, 35/40/25, 25/40/35.

Increasing the $CaCO_3$ amount, these composites start to decompose at higher temperature compared to the pristine materials and the formulation LFTFR40.

Six decomposition peaks are evident, between which, the maximum thermal degradation one is in the temperature range of 258°C-341°C for LFTFR40C10, 251°C-340°C for LFTFR40C25 and 196°C-400°C for LFTFR40C35 with a corresponding weight losses of 38 % for the first, 36.5 % for the second and 44.6 % for the third one. It doesn't change in intensity by adding inert material.

This is the third effect while the first peak, connected with the moisture and volatiles elimination and the second connected with the pyrolysis of some material components, felt down in the temperature range of 25°C-100°C and 100°C-196°C. The relative weight losses were 0.6 %, 0.74 %, 0.86 % in the first case and 11.6 %, 8.4 %, 2.1 % in the second one.

The third peak presents a shoulder that decreases in intensity and comprises between 340°C-400°C for LFTFR40C10, 340°C-396°C for LFTFR40C25 and 340°C-423°C for LFTFR40C35, with weight losses of 19.6 %, 14.9 % and 5.41 %.

The weight loss steps at temperature superior at 400°C were connected with the degradation of some inert material components. The percentages were 5.2 % for LFTFR40C10, 6.5 % for LFTFR40C25, 6.4 % for LFTFR40C35.

The residue recovered at 600°C shows increased values with $CaCO_3$ amount increase, as this material doesn't decompose at the thermogravimetric experiment temperature. The relative weight losses were 19.7 % for LFTFR40C10, 20.2 % for LFTFR40C25, 26.6 % for LFTFR40C35.

The DTGA trend (Fig. 3.72b) showed traces overlapping in a temperature ranges of 100°C-300°C and 350°C–450°C. Calcium carbonate refrains decomposition of the composite containing 40 % of ground rice as seen from

T_{on} formulations (Table 3.55). The degradation process appears to be controlled by the interactions between $CaCO_3$, the polymeric matrix and the ground rice, that were very strong.

In Table 3.55 are collected the thermal parameters for the LFT/FR/$CaCO_3$ composites.

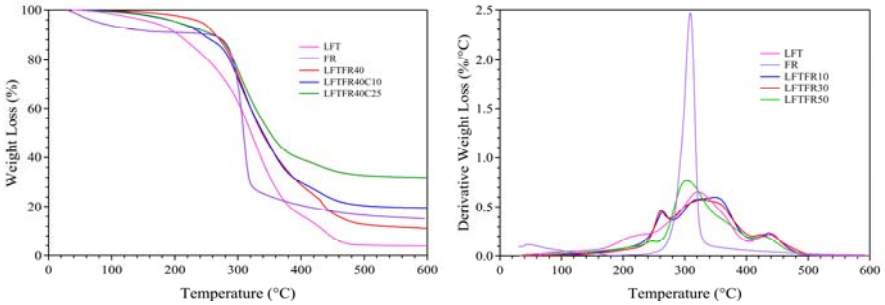

(a) (b)

Figure 3.73 TGA (a) and DTGA (b) Traces of LFT/FR/$CaCO_3$ Composites and the Pristine Materials.

Table 3.55 Thermal Parameters of the LFT/FR/$CaCO_3$ Composites.

Sample	T_{on} (°C)	T_{p1} (°C)	T_{p2} (°C)	T_{p3} (°C)	T_{p4} (°C)	T_{p5} (°C)	R_{600} (%)
LFTFR40C10	243	245	302	353	429	691	14.2
LFTFR40C25	278	218	301	350	432	699	20.2
LFTFR40C35	275	304	422	545	699	778	26.8

3.6.1.9.3 Differential Scanning Calorimetry (DSC)

Figure 3.74 shows the DSC traces for the LFT/FR/$CaCO_3$ composites, while in Table 3.56 are collected the relative thermodynamic parameters.

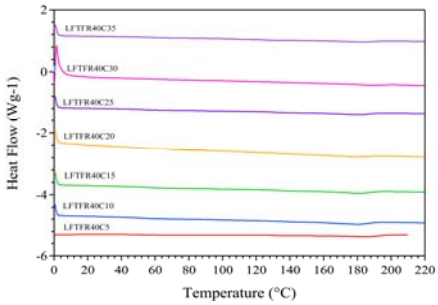

Figure 3.74 DSC Traces of the LFT/FR/$CaCO_3$ Composites.

Table 3.56 Thermodynamic Parameters of the LFT/FR/$CaCO_3$ Composites.

Sample	T_g (°C)	T_m (°C)	ΔH_m (J/g)
LFTFR40C5	54.8	180.33	8.69
LFTFR40C10	55.2	179.95	7.18
LFTFR40C15	58.1	180.85	6.75
LFTFR40C20	41.13	179.81	5.37
LFTFR40C25	39.71	180.15	5.50
LFTFR40C30	-	188.12	2.65
LFTFR40C35	61.21	183.34	3.97

The amorphous part of the polymeric matrix is increased when a 20-25 % of $CaCO_3$ was added in the formulation and the relevant glass transition temperature (T_g) drops down to minimum values.

The melting temperature (T_m) shows values similar to that of composites based on PHB and useful to produce them by compression moulding.

3.6.1.10 Composites based on LFT/FR/$CaCO_3$/$CaSO_4$

3.6.1.10.1 Morphology

Figure 3.75 shows the SEM photomicrograph for the composite LFTFR40$CaCO_3$ containing 5 % of $CaSO_4$.

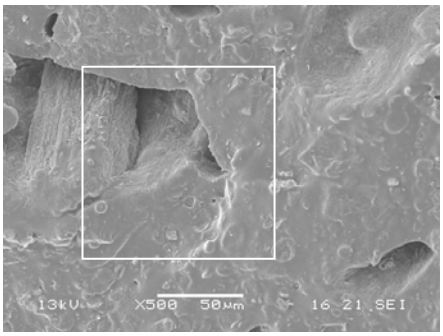

Figure 3.75 SEM Photomicrograph of the LFTFR40$CaCO_3$_$CaSO_4$5-500X Composite.

Also the $CaSO_4$ addition improved the adhesion between the polymer LFT and the filler FR, creating a drastic decrease in the number of inconsistencies.

The laminates surface appeared to be smooth and rigid.

3.6.1.10.2 Thermogravimetric Analysis (TGA)

Figure 3.76 shows the TGA (a) and DTGA (b) traces for the composites containing LFT/FR/$CaCO_3$/$CaSO_4$ in the weight ratio 50/40/5/5, 40/40/10/10 and 30/40/15/15 in the temperature range between 30°C and 800°C.

The addition of $CaSO_4$ to the blend leads to an increase of the degradation temperature, the number of peaks and the residue recovered at 800°C for all formulations.

LFTFR40C10G10 and LFTFR30C15G15, after humidity loss, that occurs in the temperature range of 25°C-100°C, display the maximum degradation peak at 270°C-280°C temperature range. The corresponding weight losses were 1.3 % for the first formulation and 0.96 % for the second one.

Below 250°C, the DTGA traces show small thermal effects that were correlated with the calcium sulphate thermal decomposition.

The residue recovered at 600°C, had a drastic decrease (7.7 %) for the formulation containing 10 % weight ratio of $CaSO_4$, while the values were 19.8 % for LFTFR40C10G5 and 35.1 % for LFTFR40C10G15. The increased trend depends on the $CaSO_4$ amount increase which doesn't decompose at temperature at which the experiment is conducted.

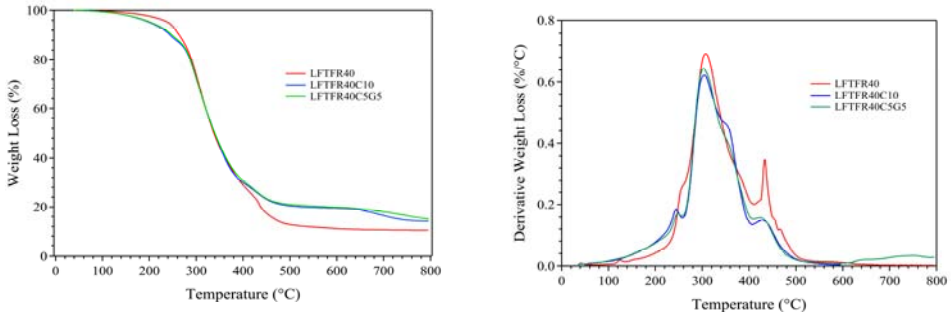

(a) (b)

Figure 3.76 TGA (a) and DTGA (b) Traces for LFT/FR/$CaCO_3$/$CaSO_4$ Composites.

In Table 3.57 are collected the thermal parameters of the LFT/FR/$CaCO_3$/$CaSO_4$ composites.

Table 3.57 Thermogravimetric Data of the LFT/FR/$CaCO_3$/$CaSO_4$ Composites.

Sample	T_{on} (°C)	T_{p1} (°C)	T_{p2} (°C)	T_{p3} (°C)	T_{p4} (°C)	T_{p5} (°C)	R_{600} (%)
AC5G5	266	248	303	354	427	-	19.8
AC10G10	275	227	303	354	427	687	7.7
AC15G15	274	223	305	345	429	689	35.1

A = Serie Basata su LFT/FR40.

The thermal stability remains constant for all formulations, as seen from the T_{on} data in Table 3.57, while the formulation containing both 10 % of $CaSO_4$ and $CaCO_3$ appears to be more thermally stable (T_{on}= 275°C) compared to the same formulation without calcium sulphate (T_{on}= 243°C).

3.6.1.11 Composites based on LFT/PHB/PFc/$CaCO_3$/$CaSO_4$

3.6.1.11.1 Morphology

Figure 3.77 shows the SEM photomicrographs for the composites containing $CaCO_3$ (30 % and 55 %), PHB (5 % and 30 %) and a constant weight ratio (10 %) of LFT and $CaSO_4$.

The holes in the polymeric matrix have small dimensions, when the calcium carbonate amount increases.

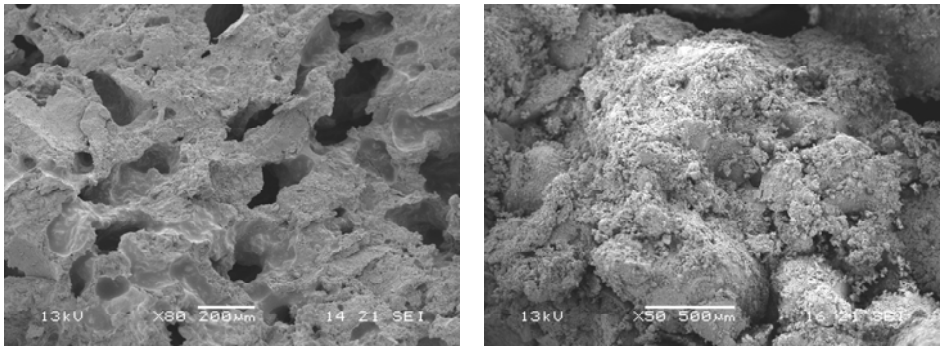

(a) (b)

Figure 3.77 SEM Photomicrographs of LFT10/PHB30/PFc20/C30/G10-80X (a) and LFT10/PHB5/PFc20/C55/G10-50X (b) Composites.

3.6.1.11.2 Thermogravimetric Analysis (TGA)

Figure 3.78 shows the TGA (a) and DTGA (b) traces of the composites containing LFT/PHB/PFc/$CaCO_3$/$CaSO_4$ in the weight ratio 5/20/20/45/10, 10/30/20/30/10 and 10/5/20/55/10 in a temperature range between 30°C and 800°C. PFc is a mixture consisting in chaff and farinaccio in the weight ratio 80/20.

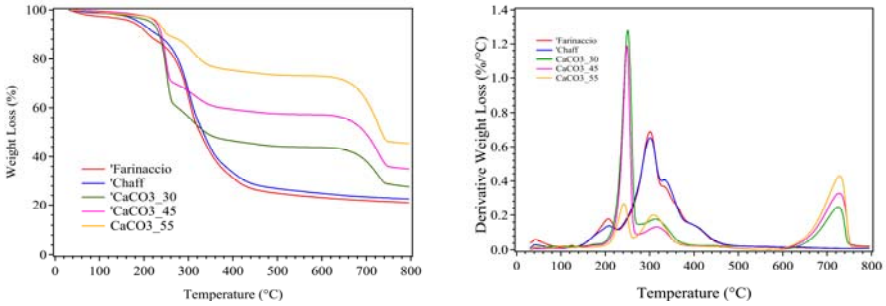

(a) (b)

Figure 3.78 TGA (a) and DTGA (b) Traces of the LFT/PHB/PFc/$CaCO_3$/$CaSO_4$ Blends.

After humidity and volatiles loss that occurred in the temperature range of 25°C-100°C, these samples started to degrade in a temperature range around at 220–230°C.

The DTGA traces (Fig. 3.78b) showed three decomposition peaks and the residue recovered at 800°C tend to increase with the increasing of the inorganic components content. The traces are overlapped between 0 and 300°C.

The decrease of inorganic components addition tends to decrease the natural material degradation. Higher temperatures are infact recorded for the chaff and flour in the composites with respect to the pristine organic compounds.

In Table 3.58 are collected the thermal parameters of the blends based on LFT/PHB/PFc/$CaCO_3$/$CaSO_4$.

Table 3.58 Thermal Parameters of the LFT/PHB/PFc/$CaCO_3$/$CaSO_4$ Blends.

Sample	T_{on} (°C)	T_{p1} (°C)	T_{p2} (°C)	T_{p3} (°C)	R_{600} (%)
LFT10PHB30PFc20C30G10	230	250	315	726	27.6
LFT5PHB20PFc20C45G10	230	248	318	727	34.8
LFT10PHB5PFc20C55G10	223	241	311	728	45.2

The increased amount of the two polymers and $CaCO_3$ hadn't impact on the T_{on} values, which remained constant for all formulations.

The recovered residue at 600°C were 27.6 % for LFT10PHB30PFc20C30G10, 34.8 % for LFT5PHB20PFc20C45G10, 45.2 % for LFT10PHB5PFc20C55G10, showing an increased trend with the increase of the inorganic part in the formulation.

3.9 Conclusions

The density and fragility for the produced composites were identified and natural biodegradable materials such as ground rices or algal biomasses were selected with the aim to improve the eco-compatibility of the final product.

Inert inorganic materials, such as $CaCO_3$ and $CaSO_4$, were used to confer an high density to the composites.

The selected polymeric matrix was Hydrolene (PVA) in form of granules and aqueous solution (30 % in weight) with good ligand properties, solubility and biodegradability in aqueous environment. PHB and PCL were utilized to improve the composite degradation.

The thermal characterization pointed out the possibility to process the blends at high temperatures, so the selected formulations were processed by means of a Braebender mixer in a first phase and the promising mixtures were processed in a double screw extruder in a second phase.

Exceptions were the formulations with an high inorganic material content, that were directly blended in a Turbo-Mixer followed by a compression moulding step.

The results appeared to be good, as the obtained laminates were consistent, fragile and they could reach the desired density.

4 THE FOAMING AGENTS

Chemical foaming agents (CFAs), also known as blowing agents, are used to produce foamed plastics in sheet or profile estrusion, injection and roto moulding for a wide variety of applications.

This market is dominated by Asia (China in particular) with large volumes going into low-end consumer goods and of the estimated 159 Ktons of them for thermoplastics sold in 2005: 46 % used in China, 23 % in other Asian countries, 17 % in Europe, 6 % in North America, 8 % in the rest of the world. Global supply of foaming agents is dominated by Asian companies and these products are predicted to grow 5.5 % AAGR through 2009. In particular a growth of 8 % is predicted for China and 2-4 % for the other regions.

A chemical foaming agent decomposes thermally into carbon dioxide and nitrogen, that are liquids under the process pressure and they can mix with the molten polymer. When a pressure drop occurs at the die or in the mould, these two gases expand into bubbles within the polymer matrix. The polymer cools and the bubbles freeze, creating a foamed plastic.

The CFAs have also a nucleation effect, that results in a reduced cell size, when they are used in combination with physical blowing agents such as pentanes or other hydrocarbons.

Resin technology plays an important role in foaming: amorphous resins with highly branched chains and high melt strength are easier to foam than crystalline, linear, low melt strength one.

The most widely used type of chemical foaming agent is azodicarbonamide (ADCA) that is an exothermic CFA and it decomposes into nitrogen. On the market, we can find also endothermic agents that are complicated formulations based on a variety of chemistries such as sodium bicarbonate/citric acid derivatives, that release carbon dioxide. About 88 % of global CFA volume is ADCA, with 5 % in the endothermic forms and 7 % in various other types, including 4,4-oxybis benzene sulphonylhydrazide

(OBSH).

The European Commission's Directive 2004/1/EC suspends the use of ADCA in food contact materials, because of this product was used in sealing gasket for the lids of glass jars and bottles, such as baby food, becouse of this product decomposes into toxic by-products.

The main applications are in the automotive sector, (low-density polypropylene foam), electronics (housings for televisions, computers, printers), packaging (new PLA biopolymer resins), building and construction (fencing, decking, window and door profiles, wood plastic composites), the nucleation in direct gas extrusion systems, that use gases such as nitrogen or isopentane to make foamed polystyrene and polyethylene. It is important also the new production of high-temperature resins such as Foamazol ^{TM} X0-230 formulated for the use in high temperature polycarbonate foaming applications such as structural foam moulding, injection moulding and extrusion. Another example is Hydrocerol XH designed for use with resins based on polycarbonate and nylons that require extra high processing temperatures over 500°C, roto-moulding that uses azodicarbonamide powders along with resins in powder form[(190)].

The main features of these products are the use in injection, rotational and structural foam moulding, the exceeded performance levels of currently available CFA's, the consistent results, the uniform cell structures, the wide range of activity levels and gas yields, the hybrid endo/exothermic grades in a single pellet and the elimination of sink marks.

The benefits are the uniform weight reductions, the fast degassing, the lower production costs and the lower raw material usage, the achieved superior surface characteristics, the enhanced physical properties and the increased "strength-to-weight" ratio[(193,194)].

For many years, some foaming agents such as thermoplastic micro-spheres (TMS), namely Expancel Micro-spheres, were successfully used providing a

consistent, tight, uniform cell structure in the polymer matrix that is necessary to maintain the achieved densities and the mechanical properties.

Wood Plastic Composites (WPC) consist of a mixture of wood flour bound into plastic matrices. Most commonly used thermoplastic resins in WPC include polypropylene (PP), polyethylene (PE), acrylonitrile butadiene styrene (ABS), styrene acrylonitrile (SAN), acrylonitrile styrene acrylonitrile (ASA), polyvinyl chloride (PVC) or polystyrene (PS). Foaming agents grades such as SAFTEC TFPE-504 are preferred for use with wood composites[(192)].

Thermoplastic Expancel® Micro-spheres are essentially hollow balloons consisting of a thermoplastic outer shell encapsulating hydrocarbons as a blowing agent. The particle size of the micro-spheres ranges from 10–32 microns diameter in their unexpanded form. On applying heat, the thermoplastic shell softens, the hydrocarbon gas pressure inside increases, and the micro-spheres will expand approximately four times in diameter compared to their original sizes[(191)].

The foaming agents and the additives are modifying their chemistries to support technologies involving both microcellular applications and foamed wood/plastic composite technology. This consists in a combination of a range of polymers, wood/cellulosic fibers and special additives to produce applications that include floor decking, pallets, roofing tiles and mouldings.

So many companies have developed their own technologies to produce microcellular foam structures.

For example Collins & Aikaman's Intellimond is a process control system that achieves Class A surface, decreases the part density and reduces the cycle times, while the Sulzer Chemtech process is a plastic processing mixers for foam applications utilizing an unique intersecting channel design.

This technology cross-mixes and homogenizes polymers and additives very efficiently. The latest technologies for microcellular foaming use a new compact gas counter pressure module[(192)]..

EPI is marketing patented endothermic (EPIcor), exothermic (EPIcell), and exo-endo (POLYcor) CFAs with special emphasis on its endothermic line of CFAs. These latter products are more versatile than the exothermic ones and they can be used in numerous new applications and products that currently do not use any type of CFAs[193].

Two-step synthesis for a new liquid foaming agent based on dodecanol phthalic anhydride anionic salt temperature resistant foam flooding, are used for the technical requirements of the process.

The foaming agents (lauryl alcohol and phathalic anhydride) are the starting raw materials and they are involved in the esterification and the synthesis. Rose-Mile with Waring Blender mixing and foaming agents on liquid foam system and its salt, anti-oil performance evaluation were studied showing that the foaming agent (SDS and ABS-keung) on the oil sands was not nearly adsorption.

A sulphate anionic surfactant can maintain its main chemical features at high temperatures sustaining a good foaming capacity and decomposition temperature above 300°C. In cyclic steam stimulation or steam flooding, the foam can be inhibited by adding gas channelling and regulating injection profile, improve the efficiency of gas injection to extend the cycle, and increase the oil production.

The foaming agent has a surfactant nature and it consists in a variety of chemical products that are mainly used for the tertiary oil recovery in the mining bubble displacement.

The foam components will be in proportion mixed with water (or other material), and the gas at the same time by a certain percentage or indirect injection into the can.

Foam used in oil recovery is a relatively new technology, and so it has a huge market potential, a displacement effect and a swept volume that is much larger than a simple injection of water and polymer.

Application of foam flooding has achieved good results. The products can be used alone giving better results and better performance of flooding to maximize the synergy effect[197].

The specialists of LLC Stroy-Beton present a new protein foaming agent for light weight cellular concrete (foamed concrete) GreenFroth.

This product contains natural surfactants that are mixed with organic raw materials, which work in synergy with them. GreenFroth shows an increased ratio and an higher resistance compared to the other imported foaming agents and synthetic ones.

Consequently it is possible to reduce the consumption of the foaming agent on each cubic meter of foam concrete approximately to 45 % that adds to the quality and the strength of the produced foam concrete. The flexible system of deliveries was carried out to have this foaming agent always in store and to dispatch customers without any delays[195].

GreenFroth allows to produce foam concrete of density ranging from 200 up to 1600 kg/m^3. In this case, the foaming agent is a protein that contains natural surfactants mixed with organic raw materials. For this reason it has a pleasant odour and its main qualities include a higher resistance of foam and better characteristics of the foaming process in comparison with other protein foaming agents.

GreenFroth is produced in a special developed foam generator Fomm-PGM. The foam is added into main cement mixture as an homogeneous dispersion, during the mixing process, in a mixer. Stabilising components contained in GreenFroth provide keeping pores of foam concrete for the whole period of its processing. The expected characteristics were the humidity resistance, the high strength and the ecological friendliness.

In comparison to the other protein foaming agents the required amount of GreenFroth is 45 % less on each cubic meter of foam concrete

GreenFroth is used for foam concrete production of normal and light

filters. Depending on the main formula it is possible to produce mixtures of density from 200 kg/m^3 to 1600 kg/m^3, while a density less than 600 kg/dm^3 requires special composition, production and usage.

The foaming agent is provided as a concentrate and it is needed to prepare 2,5 % water solution mixture for producing foam. After that the generator produces a foam of density 50 gr/l: this means that it is recommended to be applied on 20 % ratio of foaming, at 2,5 % initial water solution mixture. So a less foam amount is needed and a concrete foam of higher strength[195] is produced.

The foam generator allows for control of gypsum board void structure regulating the respective amounts of the two soap streams. The first is a standard board soap, such as alkyl chain length 8-12 carbon length and ethoxy group chain length of 1-4 units, while the second is an unethoxylated one with an alkyl chain length of 6-16 carbon units that can be branched or un-branched.

In addition to regulate the ratio of the two soaps, it can be used a predominant amount of the alkyl sulphate oligomer that is a foaming agent forming unstable foam voids in the gypsum slurry.

The first soap is represented by the formula: $CH_3\ (CH_2)_X\ CH_2\ (OCH_2\ CH_2)_Y\ OSO_3^-\text{-}Me^+$ where X ranges from 2 to 20, Y ranges from 0 to 10 with a major portion of Y being greater than 0 and M is a cation, while the second soap is represented by the formula: $R\ OSO_3^-\text{-}Me^+$ where R is an alkyl group containing 2 to 20 carbon atoms and M is a cation. More preferably X ranges from 4 to 16, Y ranges from 1 to 6 and R is an alkyl radical containing 4 to 16 carbon atoms. In the best mode, X ranges from 6 to 12, Y ranges from 2 to 4 and R is an alkyl radical containing 6 to 12 carbon atoms.

Either cation is selected from the group consisting of sodium, potassium, magnesium, ammonium, quaternary ammonium and their mixtures.

Preferably, each cation is either sodium or ammonium. The ratio by weight of the first foaming agent to the second foaming agent generally is less than 50/50. Typically, it ranges from 50/50 to 0/100, but the best ratio ranges from 40/60 to 10/90[196].

FascomTM Chemical Foaming Agents are a range of polymer additives of significant technical importance for providing production, economic, environmental and physical improvements when processing a wide range of polymers.

FA's are different than other classes of polymer additives and they are designed to decompose during normal processing of that polymer at elevated temperatures (>150ºC). They release an high volume of gas that can be trapped within the polymer melt creating a cellular or a foamed structure.

By forming a cellular structure the initial benefit created is a reduction in specific gravity which affords a number of potential properties including the easier handling, the reduced polymer requirement, the improved product dimensions, the improved insulation, the cushioning, the design aesthetics.

WSL have an extensive range of products and chemistries designed to cover numerous applications, processing methods and temperatures.

Typical applications include; uPVC foamed profile, pipe and sheet, PVC plastisols for flooring, wall covering, belting and artificial leather, polyolefines for extrusion, injection moulding and rotational moulding and rubber for extrusion and moulding operations[198].

OnCap™ has formulated CFA products that are available in concentrated powder or pellet form in carrier systems compatible with most application resins. CFA concentrates are usually used in very small amounts (0.1-1.0 %) even if some applications may require higher addition rates up to 6 % or 8 %.

They are easy to handle and feed using the conventional feeding equipment used in polymer processing.

CFAs find use across a wide range of market applications, including

packaging, transportation, medical devices, building and construction, wire and cable, toys and other consumer goods, industrial goods, and wood/plastic composites.

PolyOne offers a one-stop source of colour and additive concentrates, colour and additive systems, and associated technology and support services.

It has than 20 manufacturing locations in North America, Europe and Asia, with colour labs, design centers and sales offices located around the world[199].

Table 3.59 reports the main foaming agents produced by Alqemia Group[200], while Table 3.60 shows the relative product description.

Table 3.59 Main Foaming Agents by Alqemia Group[200].

Product	Reaction Type	Processing Temp (°C)	Active Conc (%)	Add. Level (%)
FM0N830LD	Exothermic	210-240	35	2-35
FM0N840LD	Exothermic	195-240	40	2-35
FM0N850LD	Exothermic	210-240	30	1-4
FM0N860LD	Exothermic	180-210	30	1-4
FM0N870LD	Exothermic	170-200	30	1-4
FM0N880LD	Endothermic	170-280	40	0.5-4
FM0D410LD	Endothermic	170-280	70	0.5-2
FM0D890LD	Endothermic	170-240	40	0.5-4
FM0N990LD	Exo/Endo	170-240	30	0.5-4

Table 3.60 Product Description[200].

Product	Product Description
FM0N830LD	ADCA suitable for PE including cross linked foams
FM0N840LD	ADCA affering accelerated foaming for PE including cross linked foams
FM0N850LD	ADCA designed for high output/high shear processing
FM0N860LD	ADCA with accelerated foaming designed for extrusion and injection moulding
FM0N870LD	ADCA with highly accelerated foaming designed for extrusion and injection moulding
FM0N880LD	Endothermic system with good nucleation for injection moulding of polyolefins
FM0D410LD	Endothermic system with good nucleation suitable for extrusion and injection moulding of polyolefins
FM0D890LD	Endothermic system with good nucleation suitable for extrusion and injection moulding
FM0N990LD	Combination system allowing good gas yield and broad process window

MILLIFOAM is a gypsum foaming agent that is optimized by selecting the chain length, the degree of ethoxylation and the cation. The selected foam stabilizers contribute to the formation of a strong low density gypsum board.

MILLIFOAM helps to stabilize gypsum plaste board by the following phenomena:

1. the repulsion of surfactant head groups retains the thickness of the lamellar and it reduces the bubble film drainage.
2. the rapid diffusion of the surfactant to the expanded surface reinforces the film thickness, preventing the natural deformation of the film.
3. the densely packed surfactant film can reduce the diffusion of the gas through the liquid interface and it can help prevent the bubble destruction.

The advantages are the greater consistency and the product quality, the small bubble size, the creation and the stabilization of the air bubbles within gypsum slurry, the regular foam structures, the avoiding areas of weakness and the reduced-strength board, the avoiding unsightly air voids at the edge of the sheets, the avoiding bubbles that cause paper bonding problems or blistering. The application dosage (0.01 and 0.05 % by weight of gypsum) depends on the sources and the manufacturing plant methods[201].

The product range is in Table 3.61.

Table 3.61 MILLIFOAM Product Range[201].

Products	Description Ion	Total Active Active Mater (%)	Cation	Foam Stabilizer
MILLIFOAM B	Alkyl ether Sulphate	32	Na^+	-
MILLIFOAM C	Alkyl ether Sulphate	31	Na^+	Yes
MILLIFOAM D	Alkyl ether Sulphate	75	NH_4^+	Yes

AQF-2™ foaming agent is used to stabilize the gas and liquid levels of foamed fracturing fluids. The temperatures are between 24°C and 93°C and the typical agent concentrations are 2 to 5 gal/Mgal of fracturing fluid.

At temperatures between 24°C and 149°C, typical agent concentrations are 6 to 10 gal/Mgal of fracturing fluid.

The oily surfaces act as defoaming agents in many foamed systems, and most foaming agents are oil-intolerant. However, AQF-2 foaming agent is less adversely affected by the presence of oil. In addition, this agent can slightly counteract the defoaming tendencies of some materials, such as SandWedge® treatment(202).

Counter grades for foaming agents are used in the production, such as Porofor ADC/M-C1 (Bayer); Porofor ADC/F-C2 (Bayer); Porofor ADC/L-C2 (Bayer); Porofor ADC/S-C2 (Bayer); Azobul F1 and Azobul B (Arkema); ADC-5 (China); Porofor CHZ-21.

Being the counter grades of the abovementioned brands Cellcom foaming agents have more advantages taking into consideration the quality and the price ratio(203).

The addition of about 3 % of a mixture containing 70 % DIACID 1550 dicarboxilic acid and 30 % Na-DDBS sulfonate soap to a typical pigmented size press solution produces a density reduction of from about 1.1 gm/cc to about 0.13 gm/cc using an Oakes foam generator. The methods currently being used to obtain low foam densities include an increase of the consumption of foaming agent or an utilize of a more active one, both of which tend to increase costs. The synergistic interaction of DIACID 1550 dicarboxylic acid, that is an emulsifying agent, with the sodium salt of an alkyl benzene sulfonate that is a detergent surfactant, produced a lower density foam than either component used individually.

The paper industry uses this mixture as a coating or surface size application, the textile industry uses it in the surface treatment of fabrics

while the plastics and carpeting industries use the mixture for producing voids in solid materials[204].

DIACID 1550 dicarboxylic acid is a product of Westvaco Corporation and it contains two major isomers (Fig 3.79):

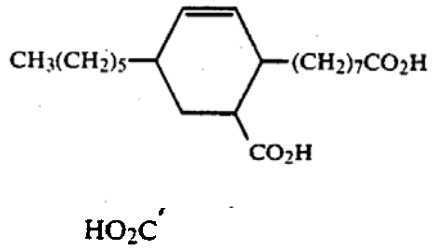

Figure 3.79 DIACID 1550 Dicarboxylic Acid Isomers.

Na-DDBS is the most typical and common alkylbenzene sulfonate, a detergent surfactant from the general class of alkylarylsulfonate soaps represented by the formula (Fig. 3.80):

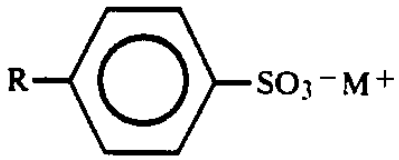

Figure 3.80 Alkylarylsulfonate Soap.

where M is sodium or potassium and R is dodecyl.

The trade name LithoFoam includes several foaming agents, that are protein based on enzymatic active components, developed especially for the building material industry. Diluted in water and processed in a foam generator with compressed air, they produce a very fine and stable high quality foam.

Standard protein based on foaming agents, are made with protein hydrolyzate from animal proteins out of horn, blood, bones of cows, pigs and other remainders of animal carcasses. This leads on the one hand to a very

intense stench of such foaming agents and on the other hand to a broad range of molecular weight of the proteins because the raw materials are always changing[205]. The new innovative foaming agent technology created by Dr. Lucà und Partner, however, is not based on the unattractive protein hydrolysis but on a biotechnological procedure. LithoFoam products have a neutral, technical odour and they are adjustable to every need. This goal was reached using right concentrations for the active enzymes and proteins (3-10 %). As less superfluous external material that could disturb the properties of the concrete mix can be inserted in the foam. The low ratio of active agents is made possible through a special process using nanotechnology, developed by Dr. Lucà und Partner. So LithoFoam foaming agents can be offered at prices far below those of competitors. The advantages are the products variety, the improved silicone oil and frost resistance, the anti bacterial properties (effective against mildew). The foam gross density adjustable to 20-180 kg/m³ and the high efficiency are important parameters for roofing, flooring, block production and casting in situ walls[205].

CELOGEN products are chemical foaming agents (CFAs) or chemical blowing agents (CBAs) that are used to impart a cellular structure to foam plastics, rubber, and thermoset resins by releasing nitrogen gas during the processing. They are available in a variety of particle sizes to optimize cell size, and they can be cured by using liquid cure media (LCM), hot air, fluid bed or microwaves. They are effective in natural, butyl, EDPM, neoprene, nitrile, silicone and SBR rubbers.

Acticell activator enhances Celogen® foaming agent performance over a wide range of temperatures. Manufacturers can use it to reduce the energy costs by processing at lower temperatures, or to improve the productivity at the temperatures they're using now. This product is economical, can be dispersed easily and it is compatible with NR, SBR, butyl, EPDM (Royalene®) and Neoprene rubber formulations[206].

5 EFFERVESCENT MATERIALS

The chemical reaction that creates the fizz in effervescent bath and shower products is quite simple and it consists in an acid neutralization with a carbonate salt with carbon dioxide gas realising, the salt of the acid and water production.

Figure 3.79 shows the scheme of the effervescent reaction:

Acid + Carbonate Salt_CO_2_ + Acid Salt + H_20

Ex: Citric Acid + 3$NaHCO_3$_3CO2_ + Na_3Citrate + 3H_20

Figure 3.79 Effervescent Reaction Scheme.

A small amount of water is needed to start the reaction, becouse of without water, neither the acid nor the carbonate can dissociate, but when the reaction is started, it generates more water.

All raw materials used in an effervescent product must be anhydrous and they must be stored in manufacturing environments where they must also be designed to maintain dryness.

Typically these facilities are dehumidified to less than 10 % RH. To protect them from the ambient humidity, the effervescent products are usually packaged in high barrier foil and/or polymer films or in heavy-wall jars that contain desiccant packs[207,209,210,211,231].

The raw materials for effervescent product are[209]:

1. Sodium Carbonate: available as an anhydrous form and as a monohydrate or a decahydrate. It adsorbs moisture and it is water-soluble.
2. Sodium bicarbonate is a white crystalline powder. It is available in five particle-size grades from fine powders to free flowing granules.

3. Citric acid: available abundantly, inexpensive, good solubility in water and alcohol. It is available as fine granular, free flowing powder forms of different particle sizes such as coarse, medium, fine.

4. Fumaric acid: available as a white granules or crystalline powder. The solubility in water is reached using the form of salt such as mono sodium or potassium fumarate.

The promotion of the effervescent reaction between citric acid and sodium bicarbonate[217] creates a fine connected porous structure in polymer membranes which were prepared by a novel microwave assisted effervescent disintegrable reaction.

Other raw materials used in the effervescent reaction are tartaric, ascorbic, malic, adipic, succinic and acetyl salycilic acids and their relative salts, potassium carbonate and bicarbonate, sodium sesquiscarbonate, sodium glycine, L-lysine, arginine, amorphous calcium carbonate[229].

Fragrances and essential oils (0.5 % and 3 %) are virtually always included in these products providing a technical assistance in designing perfumes for use in effervescent products.

The oil must be compatible with effervescent bases by avoiding materials such as glycol solvents that may cause instability to occur by allowing partial dissociation of the acid or carbonate[207].

Functional materials (1-2 %) such as freeze-dried aloe, chamomile extract in oil, and even dried flower buds and bulk herbs can be introduced in the formulation.

Also emollient materials such as squalane, vitamin E, almond oil and many cosmetic esters are frequently incorporated, again, generally from 0.1 % to 2 %. Surfactants are used both as fragrance emulsifiers and as foamers.

In the first case, surfactants prevent the perfume oil from floating on the water's surface. Typical emulsifiers are PEG-30 castor oil, Polysorbate 80 or 85 and Laureth 4. The precise choice will depend on the HLB of the perfume oil.

If surfactants are going to be used to create foam, special formulations are required to achieve consumer acceptable performance. Polyquaternium 10 and PEG (0.2-4 %) can also be added to help modify skin feel and the feel of the bath water. Binders such as sorbitol, lactose and maltodextrin (10-20 %) are almost always needed to make good, solid effervescent tablets.

These formulations can also contain materials such as fumed silica, calcium silicate, cornstarch, talc[(207)], that make more efficient the powders flow preventing the sticking on the production equipment[(211)].

The production process of an effervescent product is a conventional solid dosage form manufacturing[(222)] that considers its special characteristics.

To overcome the problem of the moisture is necessary that all machines must allow for proper venting with air of a sufficiently low moisture content.

The tablets are compressed by an high speed rotary tablet presses[(224)] using a dry method that consists in a direct compression or a roller compaction used in the solid dosage forms.

There are two granulates methods that consist in making of wet granulation using two separate granulation steps for the alkaline and the acid components with a subsequent dry blending step. This can be done in a high shear granulator, with subsequent drying, a single-pot or in a fluid bed spray granulator.

Thiokol Corporation uses several thermal setting urethane and epoxy slurry formulations in the production of rocket motors and pyrotechnic devices used as liners that contain solids with thixotropic characteristics, thermal resistance and inert behaviour.

Their application is accomplished by methods such as spraying or

atomizing with centrifugal force (sling lining). The solids loading causes an increase in the viscosity so that a diluent, such as ozone, toxic and/or flammables solvents, is required in order to spray them[212,213].

Effervescent tablets, based on sugar alcohols[219] such as sylitol, erythritol, mannitol, showed medicine and health care curative effect.

The patent number:200410021760.7. includes the effervescent tablets and the effervescent granules. The sugar alcohol is a natural and healthy sweetener, existing in some fruit or vegetable and it made from the sugar or plant. It has an extremely low heat, it can only be absorbed partly or utilized slowly in the body and it may cross through the cell membrane, offering nutrition supplement and auxiliary medicine for diabetes patient.

Moreover sugar alcohol promotes the growth of the beneficial bacterium in the body, maintaining the ecological balance of the intestines and it promotes the liver glycogen to synthetic, improve liver function.

In the Chinese market, effervescent tablets are a novel, fashionable form of a drug or health-care food that are raising bunches of light bubble in water constantly and they have good sense organ effects and well received by people, especially children. In addition effervescent tablets have a lot of excellent characteristics such as the speed dissolution in water that is very quick. When the tablets keep in touch with water, the sour and alkali happens to react, producing a lot of carbon dioxide, fully dissolved in a short period of time[217,219].

There is also a type of effervescent tablet based on pearl[214]. This product is a novel calcium supplement food, extracting from the natural concentrated liquid of pearl with a patent technology. The tablets contain active calcium, through a spray and a drying process to make powder and refined meticulously with a number of specific materials. It can generate an immediate gasification reaction as soon as it was meeting with water and a wonderful phenomenon of bubbling appeared in the drinks cup. Moreover,

the product is rich in active calcium and aminoacids that are dissolved rapidly and readily absorbed in the body.

The product causes no precipitation produced by the oxalic acid which influencing the absorption of calcium as compared with plant foods; it does not combine with phosphoric acid in the bone that is hard absorbable in the body as compared with animal osseous calcium. Moreover it is more stable than other effervescent product in which the only nutritive element is Vitamin C, being easily destroyed through oxidation.

It also contains traces of zinc, copper, iron, manganese and selenium, 18 kinds of amino acids and taurine in addition to calcium.

An example of tablets is constituted by the LiFizz Strawberry Flavored Effervescent Calcium Plus D tablets[(215)] that are used for acne, aging, healthy skin, hair, nails, wrinkles. These tablets are unwrapped and a desiccant protects the tablets from air and moisture, keeping them fresh.

For the same reason, a cap is designed with a spiral "shock absorber" to help the reduction product damage to the unwrapped tablets and the carton is designed with folded inner tabs to help secure the tube[(216)].

A new method of expanding plastic during moulding looks to change the way plastic goods are manufactured in the future. By infusing microscopic bubbles into the interior of plastic, MicroGREEN, an Arlington Washington based firm, has developed a solid-state microcellular technology that increases strength and more importantly, vastly reduces the use of plastic source materials.

MicroGREEN's patented technology, developed at the University of Washington, promises to increase output while lowering material costs by up 75 % or more. The process can be tailored to each specific application and it can be used with a variety of virgin and recycled plastics, such as PET and even bio-plastics like PLA. The process does not chemically alter the plastic so the end product can be recycled over and over again.

The process that creates a naturally smooth outer surface, is lighter weight, it has excellent insulating qualities and it requires less manufacturing[218].

DISINBIO[220] is a China s first instant-effervescent organic chlorine solid disinfectant, characterized by its performance stability, quantity precision, high efficiency broad-spectrum, minimizing corrosion while disinfecting without leaving harmful residues. The main ingredients are sodium dichloroisocyanurate, formally approved by the FDA and EPA for food, medical equipment and drinking water disinfection. Other components are sodium dichloroisocyanurate (DCCNa), potassium bromide (KBr), boric acid (H3B03), potassium chloride (KCl), sodium chloride (NaCl), synergists, decomposers, anti-interference agents, stabilizers. The formulation is available in tablet, granule and powder form.

The benefits are the efficiency in killing bacteria, candida albicans, fungi and bacterial spores, hepatitis virus, alternaria, bacillus subtilis, influenza virus, HIV and other pathogenic micro-organisms.

The main applications are the use in medical and health care, in the anti-epidemic (drinking water, tableware, fruits & vegetables, environment, public utensils, etc), in the public and domestic areas, foodstuff (beverages), livestock (fishery), aquaculture, in the industrial and agricultural production purposes and areas where disinfection is needed. The advantages are the germicidal effect, infact the instant effervescent in solid dosage forms allows for the accurate quantity in usage, the safety for the users and the environment, the stable performance with the resistance to the organic materials, acid, alkali and other chemical properties, the minimum corrosion, the versatility[220].

Calcium phosphate cements[221] (CPCs) are biocompatible and osteoconductive materials used in dental, craniofacial and orthopaedic applications. One of the most important advantages of these materials is their replacement with bone followed by re-sorption.

A mixture of $NaHCO_3$ and citric acid monohydrate was added to the apatite cement component as an effervescent additive for producing interconnected macro-pores into the cement matrix.

The obtained results showed that the addition of only 10 wt % of the effervescent additive (based on the cement powder) to the CPC components lead to producing about 20 V % macro-pores (with the size of 10 to 1000 mum) into the cement structure[221].

Effervescent creatine and creatine monohydrate are different chemical states of the same molecule. EC is a zwitterion, meaning it has both a positive and negative charge on it. Researchers claim that this form is absorbed faster into the bloodstream. Following that logic, manufacturers of EC claim that CM is not as well absorbed; therefore, EC is better than CM[223].

Chunthong et al[225] create a formulation composed of lactose, PVP K-30, and the effervescent base that can be applied by spraying on plant or by direct broadcasting to water to evaluate its physical and biological characteristics and to test the efficiency of a novel bacterial formulation in suppressing sheath blight disease development in greenhouse conditions.

The effect of regular intake of low doses of an effervescent multivitamin preparation on the free-radical-producing activity of murine peritoneal macrophages under conditions resembling a possible infection was studied in vitro. The multivitamin supplementation increased the number, and the reactive oxygen species-producing activity of macrophages and it lowered the steady-state free radical concentrations of liver and spleen as measured by electron paramagnetic resonance spectroscopy[226].

Tartary buckwheat[227], another type of biological effervescent tablets, mainly contains many kinds of active ingredients such as flavone, which is showed by the modem research and it can prevent and cure cerebrocardiovascular disease and diabetes and lower the blood fat.

For the time being, its processing technique is quite poor, producing a very

simple and non good dissolubility of the flavone extract.

These effervescent tablets contain both sodium bicarbonate and an organic acid, which in the water they can create a large amount of carbon dioxide so as to make the tablet fast to dissolve, nice to taste and easy to carry, making them especially suitable for children, elder and patients who have difficulty in swallowing. The main applications were the use in drugs and health-keeping food.

The TCMCR formulation was successfully prepared with sodium chloride, sodium hydrogen carbonate and hydroxypropylmethylcellulose (HPMC) as osmotic agents[228].

Typical drain cleaners can be in liquid or granular form and they contain sodium hydroxide, sodium nitrate and aluminum.

Sodium hydroxide is usually the largest component in these mixtures, it generates heat when it is dissolved in water and it reacts with the aluminum, melting grease, soap, which clog drains. The fats saponification, due to the generated heat, change the grease into a soap-like substance, which is more easily rinsed down the drain. Ammonia gas is generated providing agitation and exposing the clog to fresh sodium hydroxide.

So a typical drain cleaner contains a metal hydroxide (20-60 %), an hypochlorite generator (20-40 %) and an effervescent system (10-40 %), a lubrificating agent (1-10 %) and a binding agent (1-10 %)[231,232].

An effervescent method to clean soiled dishes by hand washing was patented[232]. This method of cleaning comprises the addition of an effervescent product to a volume of water; the contacting volume of water with the effervescent product and the soiled dishes; their soaking, wiping and rinsing in contact with the volume of water and the effervescent product for a period of time.

5.1 Conclusions

The foaming agents and the effervescent materials background can be introduced in a prospective of future trends such as soaps and cleansings formulations that can be tested and introduced in the industry as proprietary know how.

The main raw materials used to produce an effervescent system (tablets or drain cleaners) were sodium carbonate, sodium bicarbonate as basic component and citric or fumaric acid as acidic component.

Every effervescent product, can contain functional molecules such as fragrance, essential oils, plant extracts, emollient materials, surfactants as emulsifiers and foamers, binders and inorganic materials.

The production process consists in two granulates methods that produces a wet granulation using two separate granulation steps for the alkaline and the acid components with a subsequent dry blending step. The blend is made in a high shear granulator, with subsequent drying, a single-pot or in a fluid bed spray granulator.

Some effervescent products such as tablets based on sugar alcohols or pearls, organic chlorine solid disinfectant, effervescent additives for calcium phosphate cements and drain cleaners, are present on the market.

The component concentrations for these latter products have to be considered an useful tool to do some industrial trials for fabrication of drain cleaners.

CONCLUSIONS

The structural analyses (FT-IR, NMR) conducted on the PHAs samples obtained from olive oil mills wastewater, confirmed that these materials are mainly consisting of PHB. The copolymeric nature was detected only for PAR-7 as shown by the double melting peak in its DSC trace.

TGA traces showed a series of degradation peaks connected with the components present in the samples. The residue recovered at 500 °C presented small values for all PAR samples and a drastically decrease for SAR-4 sample in the SAR series.

GPC experiments led us to know the average molecular weight and the polydispersion index for all samples. Peaks at higher retention time were evident in the traces and they were connected to the fermentation and/or the extraction method.

In regard of the LCA study, this gave a method for a comparative evaluation of the environmental impact associated to the PHA production according to the technology developed in POLYVER Project.

For the ligno-cellulosic materials, the percentage of each component was obtained by chemical analysis. The structural (FT-IR, SEM) and thermal properties (TGA, DSC) were investigated and led to conclude that the waxes were responsible for the thermal instability of the materials and that the acetylation process led to the material less thermally stable materials when compared to the pristine cellulose.

The thermal characterization of the blends based on PLA and Bionolle showed that the thermal stability increased with the Bn content, while the mechanical properties do not play any improvement when Bn content was superior at a 50 %.

SEM photomicrographs for the CA/PHB blends showed the presence of two phases with the CA particles dispersed in the PHB matrix.

The adhesion between CA and PHB increased with the cellulose acetate (CA) percentage.

The T_g from DSC experiments was evident only for CA/PHB (50/50) and CA/PHB (60/40).

WAXD pattern of CA/PHB blends exhibited the main peaks of a semi-crystalline material and the addition of cellulose acetate (CA) did not change the crystalline structure of PHB.

Ulva and ground rices dimensional distribution was assessed and it was found that their granulometry made them suitable for composite formulations.

TGA analysis gave useful information on the degradation temperature of all materials that was necessary to know for blending fibers and polymers.

The prepared laminates and composites were investigated for the structural, morphological, thermal and mechanical properties.

The obtained results for the ulva composites, were an improved adhesion at the composite interface between the polymer and the filler, a decrease in thermal stability with the increased filler content and mechanical properties in agreement with composites which become more fragile by increasing the algal biomass content.

The addition of an inorganic material improved the density of the produced items and the TGA analysis confirmed as expected an increase in the recovered residue amount at 500°C.

The reported background on the foaming agents and effervescent materials gives useful hints for the production of cleansing and drain cleaners formulations that are planned to be developed in a forthcoming doctorate thesis.

REFERENCES

[1] Takashi F., (1998) 'Processability and properties of aliphatic polyesters, BIONOLLE, synthetized by polycondensation reaction' *Polymer Degradation and Stability*, **59**, 209-214.

[2] Wu C.S., (2003) 'Physical properties and biodegradability of maleated-polycaprolactone/starch composite' *Polymer Degradation and Stability*, **80**, 127-134.

[3] Yasuniwa M., Iura K., Dan Y. (2007) 'Melting behaviour of poly(L-lactic acid): effects of crystallization temperature and time' *Polymer*, **48**, 5398-5407.

[4] Pillin I., Montrelay N., Grohens Y. (2006) 'Thermo-mechanical characterization of plasticized PLA: Is the miscibility the only significant factor?' *Polymer*, **47**, 4676-4682.

[5] Scandola M., Focarete M.L., Adamus G., Sikorska W., Baranowska I., Swierczek S., Gnatowski M., kowalczuk M., Jedlinski Z., (1997) 'Polymer blends of natural poly(3-hydroxybutyrate-co-3-hydroxyvalerate) and a synthetic atactic poly(3-hydroxybutyrate). Characterization and biodegradation studies' *Macromolecules*, **30**, 2568-2574.

[6] Wu C.S., (2006) 'Assessing biodegradability and mechanical, thermal and morphological properties of an acrylic acid-modified poly(3-hydroxybutyric acid)/wood flours biocomposite' *Journal of Applied Polymer Science*, **102**, 3565-3574.

[7] Tomaz Duarte M.A., Hugen R.G., Martins Sant'Anna E., Pezzin Testa A.P., Pezzin S.H., (2006) 'Thermal and mechanical behaviour of injection molded poly (3-hydroxybutyrate)/poly (ε-caprolactone) blends' *Materials Research*, **9**, 25-27.

[8] Persenaire O., Alexandre M., Degee P., Dubois P., (2001) 'Mechanism and kinetics of thermal degradation of poly (ε-caprolactone).' *Biomacromolecules*, **2**, 288-294.

[9] UNI EN ISO 1183-1, (2005) 'Methods for determining the density of non-cellular plastics. Part I: Immersion method, Liquid picnometer method and titration method.' Engineering Library, Pisa.

[10] Hocking P.J., (1995) 'Enzymatic degradability of poly (β-hydroxybutyrate) as a function of tacticity', *Pure Applied Chemistry A,* **32**, 889-894.

[11] Chiellini E., Cinelli P., Imam S.H., Mao L., (2001) 'Composites films based on poly(vinylalcohol) and lignocellulosic fibres: preparation and characterization in biorelated polymers

[12] ASTM Standard E104-02, (2002) "*Standard Practice for Maintaining Constant Relative Humidity by Means of Aqueous Solutions"*, ASTM International: West Conshohocken, PA, <www.astm.org>

[13] Cerqueira D.A., Filho G.R., and Meireles C.dS., (2007) 'Optimization of sugar cane bagasse cellulose acetylation', *Carbohydrate Polymer*, **69**, 597-582.

[14] Chiellini E., Cinelli P., Fernandes E.G., Kenawy E.R., and Lazzeri A., (2001) 'Gelatin-Based blends and composites. Morphology and thermal mechanical characterization', *Biomacromolecules*, **2**, 806-811.

[15] Doi Y, *Microbial Polyesters*, VCH Publishers, New York, (1990).

[16] Byrom D, *Plastics from Microbes. Microbial Synthesis of Polymers and Polymers Precursors*, Mobley DP, 5 (1994).

[17] http://inventabrasilnet.t5.com.br/plastico.htm.

[18] Dairy Industry Waste as Source For Sustainable Polymeric Material Production. ACRONYM: WHEYPOL
Contract n.: G5RD-CT-2001-00591, Project n.: GrD2-2000-30385

[19] Akita S., Einaga Y., Miyaki Y., Fujita H., (1976) *Macromolecules*, **9**, 774.

[20] Miyaki Y., Einaga Y., Hirosye T., Fujita H., (1977) *Macromolecules*, **10**, 1356.

[21] Csomorova K., Rychly J., Bakos D., Janigova I., (1994) 'The effect of inorganic additives on the decomposition of poly(beta-hydroxybutyrate) into volatile products' *Polymer Degradation and Stability*, **43**, 441-446.

[22] Janigova I., Lacik I., Chodak I., (2002) 'Thermal degradation of plasticized poly(3-hydroxybutyrate) investigated by DSC' *Polymer Degradation and Stability*, **77**, 35-41.

[23] Azuma Y., Yoshie N., Sakuray M., Inocue Y., Chujo R., (1992) 'Thermal behaviour and miscibility of poly(hydroxybutyrate)/poly(vinyl alcohol) blends' *Polymer*, **33**, 4763-4767.

[24] Sudesh K., Abe H., Doi Y., (2000) 'Synthesis, structure and properties of polyhydroxyalkanoates: biological polyesters' *Progress Polymer Science*, **25**, 1503-1555.

[25] Day M., Cooney J., Shaw K., Watts J., (1998) 'Thermal analysis of some environmentally degradable polymers' *Journal of Thermal Analysis and Calorimetry*, **52(2)**, 261-274.

[26] Chiellini E., Grillo Fernandes E., Pietrini M., Solaro R., (2003), *Macromol. Symp.*, **197**, 45.

[27] Xie W.P., Chen G., (2008), *Biochem. Engin. J.*, **38**, 384.

[28] Luo R., Chen J., Zhang L., Chen G., (2006), *Biochem. Engin. J.*, **32**, 218.

[29] Silverstein R. M., Webster F. X.,(1999), 'Identificazione Spettroscopica di Composti Organici', *I Ed. Italiana*, Casa Editrice Ambrosiana, Milano.

[30] Bayari S., Severcan F., Gursel I., Hasirci V., Alaeddinoglu G., (1998),'The FTIR Studies of the Poly(3-hydroxybutyrate) and Poly(3hydroxybutyrate-co-3-hydroxyvalerate)'. In: P.I. Harris, and D. Chapman, *New Biomedical Materials*, IOS Press, Amsterdam, 58.

[31] Nakanishi K., Solomon P.H., (1977), 'Infrared Absorption Spectroscopy', Holden-Day, Inc., San Francisco.

[32] Xu J., Guo B.H., Yang R., Wu Q., Chen G.Q., Zhang Z.M., (2002), *Polymer*, **43**, 6893.

[33] Roig A., Cayuela M.L., Sanchez-Monedero M.A., *Waste Manag.*, (2006), **26**, 960.

[34] Kapellakis I.E., Tsagarakis K.P., Crowther J.C., (2008), *Rev. Environ. Sci. Biotechnol.*, **7**, 1.

[35] CE Directives 271/1991, 676/1991.

[36] Raveendran K., Ganesh A., Khilar K.C., (1996), 'Pyrolysis characteristics of biomass and biomass components', *Fuel,* Vol. **75(8),** 987-998.

[37] Nassar M.M., Ashour E.A., Seddik S.V., (1998), ' Thermal characteristics of bagasse', *Energy Sources*, **20**, 831-837.

[38] Sun R.C., Sun X.F., Xiao B., (2002), 'Extraction and characterization of lyophilise extractives from rice straw. Spectroscopic and thermal analysis', *Journal of Wood Chemistry and Technology,* **22(1),** 1-9.

[39] Sun J.X., Sun X.F., Zhao H., Sun R.C., (2004), 'Isolation and characterization of cellulose from sugarcane bagasse', *Polymer Degradation and Stability,* **84**, 331-339.

[40] Bilba K., Ouensanga A., (1996), 'Fourier transform infrared spectroscopic study of thermal degradation of sugar cane bagasse', *Journal of Analytical and Applied Pyrolysis,* **38**, 61-73.

[41] Chen Y., (2005).

[42] Hanna A.A., Basta A.H., El-Saied H., and Abadir I.F., (1999), "Thermal properties of cellulose acetate and its complexes with some transition metals", *Polymer Degradation and Stability*, **63**, 293-296.

[43] Hoareau W., Trindade W.G., Siegmund B., Castellan A., and Frollini E., (2004), "Sugar cane bagasse and curaua lignins oxidized by chlorine dioxide and reacted with furfuryl alcohol: characterization and stability", *Polymer Degradation and Stability*, **86**, 567-576.

[44] Yang H., Yan R., Chen H., Lee D.H., and Zheng C., (2007), "Characterstics of hemicellulose, cellulose, and lignin pyrolysis", *Fuel*, **86**, 1781-1788.

[45] Sun J.X., Mao F.C., Sun X.F., and Sun R.C., (2004), "Comparative study of hemicelluloses isolated with alkaline peroxide from lignocellulosic materials", *Journal of Wood Chemistry and Technology*, **24 (3)**, 239-262.

[46] Cerqueira D.A., Filho G.R., Nascimento de Assuncao R.M., Meireles C.dS., Toledo L.C., Zeni M., Mello K., and Duarte J., (2008), "Characterization of cellulose triacetate membranes produced from sugar cane bagasse, using PEG 600 as additive", *Polymer Bulletin*, **60**, 397-404.

[47] Ifuku S., Nogi M., Abe K., Handa K., Nakatsubo F., and Yano H., (2007), "Surface modification of bacterial cellulose nanofibers for property enhancement of optically transparent composites: dependence on acetyl group DS", *Biomacromolecules*, **8**, 1973-1978.

[48] Samois E., Dart R.K., Dawkins J.V., (1997), "Preparation, characterization and biodegradation studies on cellulose acetates with varying degrees of substitution", *Polymer*, **38(12)**, 3045-3054.

[49] Hurtubise F.G., (1962), "The analytical and structural aspects of the infrared spectroscopy of cellulose acetate", *Tappi*, **45(6)**, 460-465.

[50] Sun J.X., Sun X.F., Sun R.C., Fowler P., Baird M.S., (2003), 'Inhomogeneities in the chemical structure of sugar cane bagasse lignin', *J. Agric. Food Chem*, **51**, 6719-6725.

[51] Xiao B., Sun X.F., Sun R., (2001), 'Chemical, structural and thermal characterizations of alkali-soluble lignins and hemicelluloses, and cellulose from maize stems, rye straw, and rice straw', *Polymer Degradation and Stability*, **74**, 307-319.

[52] Kohler S., Liebert T., Heinze T., (2008), 'Interactions of ionic liquids with polysaccharides. Pure cellulose nanoparticles from trimethylsilyl cellulose synthesized in ionic liquids', *Journal of Polymer Science: Part A: Polymer Chemistry*, **46**, 4070-4080.

[53] Shao Z., Li G., Xiong G., Yang W., (2002), 'Modified cellulose adsorption method for the synthesis of conducting perovskite powders for membrane application', *Powder Technology*, **122**, 26-33.

[54] Cerqueira D.A., Filho G.R., Da Silva Meireles C., (2007), 'Optimization of sugar cane bagasse cellulose acetylation', *Carbohydrate Polymers*, **69**, 579-582.

[55] Cerqueira D.A., Filho G.R., Assuncao R.M..N., (2006), 'A new value for the heat of fusion of a perfect crystal of cellulose acetate', *Polymer Bulletin*, **56**, 475-484.

[56] Filho G.R., Assuncao R.M.N., Vieira J.G., Meireles CdS., Cerqueira D.A., Da Silva Barud H., Ribeiro S.J.L., Messaddeq Y., (2007), 'Characterization of methylcellulose produced from sugar cane bagasse cellulose: crystallinity and thermal properties', **92**, 205-210.

[57] Auras R.A., Harte B., Selke S., Hernandez R., (2003), 'Mechanical, Physical, and Barrier Properties of Poly(lactide) Films', *Journal of Plastic Film & Sheet*, **19(2),** 123-135.

[58] Martino V.P., Ruseckaite R.A., Jimenez A., 'Processing and Mechanical Characterization of Plasticized Poly(lactide acid) Films

for Food Packaging', Proceeding of the 8th Polymers for Advanced Technologies International Symposium, Budapest, Hungary, 13-16 Settembre 2005.

[59] Inglis T.L., "An Improved Packaging Film from Polylactic Acid", Can. Pat. Appl. 2005 CA 2472420, 19pp.

[60] Auras R.A., Harte B., Selke S., (2004), 'An overview of Polylactides as Packaging Materials', *Macromolecular Bioscience*, **4(9),** 835-864.

[61] Auras RA, Singh SP, Singh JJ, (2005), 'Evaluation of Oriented Poly(lactide) Polymers vs. Existing PET and Oriented PS for Fresh Food Service Containers', *Packaging Technology & Science*, **18**(4), 207-216.

[62] Holm V.K., Ndoni S., Risbo J., (2006), 'The Stability of Poly(lactic acid) Packaging Films as Influenced by Humidity and Temperature', *Journal of Food Science*, **71(2),** E40-E44.

[63] Inomata I., (2005), 'Green Plastics with Advancing Reform. 1. The Prospects and the Theme of the Plant-Based Film Ecology', *Mitsubishi Plastics*, Inc., **34(11),** 30-32.

[64] Lagaron J.M., Cabedo L., Cava D., Feijoo J.L., Gavara R., Gimenez E., (2005), 'Improving Packaged Food Quality and Safety. Part 2: Nanocomposites', **22(10),** 994-998.

[65] Lim K., Mustapha A., (2003), 'Reduction of Escherichia Coli O157:H7 and Lactobacillus Plantarum Numbers on Fresh Beef by Polylactic Acid and Vacuum Packaging', *Journal of Food Science*, **68(4),** 1422-1427.

[66] Jacobsen S., Fritz H.G., Degee P., Dubois P., Jerome R., (2000), 'New Developments on the Ring Opening Polymerization of Polylactide', *Industrial Crops and Products*, **11(2-3),** 265-275.

[67] Aritake T., "Polylactic Acid Resin Compositions for Thermoforming, Polylactic Acid Resin Sheets for Thermoforming, and Thermoformed

Objects Obtained Therefrom", PCT Int. Appl. 2004 WO 2003-JP16642, 23 pp.

[68] Johnson M., Shivkumar S., Berlowitz-Tarrant L., (1996), 'Structure and properties of filamentous green algae', *Materials Science and Engineering* B, **38**, 103-108.

[69] Taddei P., Tinti A., Reggiani M., Fagnano C., (2005), 'In vitro mineralization of bioresorbable poly(ε-caprolactone)/apatite composites for bone tissue engineering: a vibrational and thermal investigation', *Journal of Molecular Structure*, 744-747, 135-143.

[70] Ali R., Iannace S., Nicolais L., (2003), 'Effects of processing conditions on the impregnation of glass fibre mat in extrusion/calendering and film stacking operations', *Composites Science and Technology,* **63**, 2217-2222.

[71] Wu C.S., (2003), 'Physical properties and biodegradability of maleated-polycaprolactone/starch composite', *Polymer Degradation and Stability*, **80**, 127-134.

[72] Wu C.S, (2006), *J. Appl. Polym. Sci.*, **102**, 3565–3574.

[73] Otey, F.H.; Mark, A.M.; Mehltretter C.L.; Russell, C.R. (1974) *Ind. Eng. Chem. Res*., **13**, 90-92.

[74] Lahalih, S.M.; Akashah, S.A.; Al-Hajjar, F.H., (1987), *Ind. Eng. Chem. Res.*, **26**, 2366-2372.

[75] Coffin, R.; Fishman, M.L.; Ly, T.V. (1996), *J. Appl. Polym. Sci.*, **57**, 71-79.

[76] Chen, L.; Imam, S.H.; Gordon, S.H.; Greene, R.V., (1997), *J. EnViron. Polym. Degrad.*, **5**, 111-117.

[77] Chiellini E., Cinelli P., Corti A., Kenawy E. R., Grillo- Fernandes E., Solaro R., (2000), *Macromol. Symp.* **152**, 83-94.

[78] Mao L., Imam S.H., Gordon S., Cinelli P., Chiellini E., (2000), *J. Polymers & Environment*, **8**, 205.

[79] Chiellini E., Cinelli P., Imam S.H., Mao L., (2001), *Biomacromolecules*, **2**, 1029.

[80] Chiellini E., Cinelli P., Grillo Fernandes E., Kenawy E.R., Lazzeri A., (2001), *Biomacromolecules,* **2**, 806.

[81] Cinelli P., Chiellini E., Lawton J.L., Imam S.H., (2006), *J. Polymer Research* **13**, 107-114

[82] Chiellini E., Cinelli P., Ilieva V.I., (2008), *Int. J. Materials and Product Technology*, **10(10)**…

[83] Paradossi G., Cavalieri F., Pizzoferrato L., Liquori A. M., (1999), *Int .J. Biol. Macromol.,* **25**, 309-315.

[84] Scandola M., Focarete M. L., Adamus G., Sikorska W., Baranowska I., Sa Wierczek S., Gnatowski M., Kowalczuk M., Ski Z. J., (1997) *Macromolecules,* **30**, 2568-2574.

[85] Averous L., Moro L., Dole P., Fringant C., (2000), 'Properties of thermoplastic blends: starch-polycaprolactone', *Polymer* **41**, 4157–4167.

[86] Duarte M. A. T, Hugen R. G., Martins E.S., Pezzin A. P. T., Pezzin S. H., (2006), *Materials Research*, **9(1),** 25-27.

[87] Mitchell C.A., Krishnamoorti R., (2005), 'Non-isothermal crystallization of in situ polymerized poly(ε-caprolactone) functionalized-SWNT nanocomposites', *Polymer,* **46**, 8796-8804.

[88] Singh R.P., Pandey J.K., Rutout D., Degee Ph., Dubois Ph., (2003), 'Biodegradation of poly(ε-caprolactone)/starch blends and composites in composting and culture environments: the effect of compatibilization on the inherent biodegradability of the host polymer', *Carbohydrate Research*, **338**, 1759-1769.

[89] Lepoittevin B., Devalckenaere M., Pantoustier N., Alexandre M., Kubies D., Calberg R., Jerome R., Dubois P., (2002), 'Poly(ε-caprolactone)/clay nanocomposites prepared by melt intercalation:

mechanical, thermal and rheological properties', *Polymer*, **43**, 4017-4023.

[90] Sorrentino A., Gorrasi G., Tortora M., Vittoria V., Costantino U., Marmottini F., Padella F., (2005), 'Incorporation of Mg-Al hydrotalcite into a biodegradable poly(ε-caprolactone) by high energy ball milling', *Polymer,* **46**, 1601-1608.

[91] Chen B., Sun K., (2005), 'Poly(ε-caprolactone)/hydroxyapatite composites: effects of particle size, molecular weight distribution and irradiation on interfacial interaction and properties', *Polymer Testing*, **24**, 64-70.

[92] Wu C.S., (2005), 'A comparison of the structure, thermal properties, and biodegradability of polycaprolactone/chitosan and acrylic acid grafted polycaprolactone/chitosan', *Polymer*, **46**, 147-155.

[93] Singh S., Mohanty A.K., (2007), 'Wood fiber reinforced bacterial bioplastic composites: Fabrication and performance evaluation', *Composites Science and Technology*, 1753-1763.

[94] Wu C.S., (2006), 'Assessing biodegradability and mechanical, thermal, and morphological properties of an acrylic acid-modified poly(3-hydroxybutyric acid)/wood flours biocomposite', *Journal of Applied Polymer Science*, **102**, 3565-3574.

[95] POLYVER Project

[96] Abayasinghe M, Suresh S, Perera P, Smith D., (2003), 'Synthesis and Characterization of Poly(ester amide)s Derived from Lactide and Depsipeptides', 55th Southeast Regional Meeting of the American Chemical Society, Atlanta, GA, United States, Washington.

[97] Aritake T, (2004), "Polylactic Acid Resin Compositions for Thermoforming, Polylactic Acid Resin Sheets for Thermoforming, and Thermoformed Objects Obtained Therefrom", PCT Int. Appl. 2004 WO 2003-JP16642, 23 pp.

[98] Auras R.A, Singh S.P, Singh J.J, (2005), "Evaluation of Oriented Poly(lactide) Polymers vs. Existing PET and Oriented PS for Fresh Food Service Containers", *Packaging Technology & Science*, **18(4),** 207-216.

[99] Auras R.A, Harte B, Selke S, (2004), "An overview of Polylactides as Packaging Materials", *Macromolecular Bioscience*, **4(9),** 835-864.

[100] Auras R.A, Harte B, Selke S, Hernandez R, (2003), "Mechanical, Physical, and Barrier Properties of Poly(lactide) Films", *Journal of Plastic Film & Sheet*, **19(2),** 123-135.

[101] Avella M, De Vlieger J.J, Errico M.E, Fisher S, Vacca P, Volpe M.G, (2005), "Biodagradable Starch/Clay Nanocomposites Films for Food Packaging Applications", *Food Chemistry*, **3**, 467-474.

[102] Bassam E. N, (2001), Renewable Energy for Rural Communities, *Renewable Energy*, **24**, 40.

[103] Bastioli C, Milizia T, Floridi G, Scaffidi Lallaro A, Cella G. D, Toisin M, "Biodegradable Aliphatic-Aromatic Polyesters Mostly on Azelaic acid, their Blends with other Biodegradable Polymers, and Uses", PCT Int. Appl. 2006 WO 2006-EP2673, 29pp.

[104] Sperling L. H, Carraher C. E, Polymers from Renewable resources in H. F Mark, N. M Bikales, C. G Overberger, G. Menges (eds.) Encyclopedia of Polymer Science and Engineering, Wiley, New York, 1988, **12**, 658-690.

[105] Bozel J. J ed, Chemicals and Materials from Renewable Resources, Proceedings of a Symposium held at the 218th National Meeting of the ACS in New Orleans, Louisiana, 22-26 August 1999, ACS Symp. Ser. 784, ACS, Washington D. C, USA, 226pp, 2001.

[106] Yu L, Dean K, Li L (2006), "Polymer Blends and Composites from Renewable Resources", *Progress Polymer Science*, **31**, 576-602.

[107] Mareschal F, Biodegradable Plastics Views of APME (Association of Plastics Manufacturers in Europe) in E. Chiellini, R. Solaro eds. Biodegradable Polymers and Plastics, Kluwer Academic/Plenum Publishers NY, pp.67-71, 2003.

[108] Warwel S, Bruse F, Demes C, Kunz M, Klaas M.R (2001), "Polymers and Surfactants on the Basis of Renewable Resources "*Chemosphere*, **43**, 39-48.

[109] Roper H, Renewable Raw Materials in Europe- Industrial Utilization of Starch and Sugar, NutraCos, May-June (2002), 37-44.

[110] Petersen K, Nielsen P.V, Olsen M.B (2001), "Physical and Mechanical Properties of Biobased Materials-Starch, Polylactate and Polyhydroxybutyrate", *Starch/Staerke*, **53(8),** 356-361.

[111] Pillin I, Montrelay N, Grohens Y (2006), "Thermo-Mechanical Characterization of Plasticized PLA: Is the Miscibility the Only Significant Factor?", *Polymer*, **47(13),** 4676-4682.

[112] Martino V.P, Ruseckaite R.A, Jimenez A, "Processing and Mechanical Characterization of Plasticized Poly(lactide acid) Films for Food Packaging", Proceeding of the 8th Polymers for Advanced Technologies International Symposium, Budapest, Hungary, 13-16 Settembre 2005.

[113] Cargill Dow LLC, Can. (2004), "That's wrap! Corn Yields a Natural Solution for Suistanable Food Packaging", *Canadian Chemical News*, **56(1),** 16-17.

[114] Holm V.K, Ndoni S, Risbo J (2006a), "The Stability of Poly(lactic acid) Packaging Films as Influenced by Humidity and Temperature", *Journal of Food Science*, **71(2),** E40-E44.

[115] Lagaron J.M, Cabedo L, Cava D, Feijoo J.L, Gavara R, Gimenez E (2005), "Improving Packaged Food Quality and Safety. Part 2: Nanocomposites", **22(10),** 994-998.

[116] Lim K, Mustapha A (2003), "Reduction of Escherichia Coli O157:H7 and Lactobacillus Plantarum Numbers on Fresh Beef by Polylactic Acid and Vacuum Packaging", *Journal of Food Science*, **68(4),** 1422-1427.

[117] Jacobsen S, Fritz H.G, Degee P, Dubois P, Jerome R (2000), "New Developments on the Ring Opening Polymerization of Polylactide", *Industrial Crops and Products*, **11(2-3),** 265-275.

[118] Fang J.M, Fowler P.A, Escrig C, Gonzalez R, Costa J.A, Chamudius L (2005), "Development of Biodegradable Laminate Films Derived from Naturally Occurring Carbohydrate Polymers", *Carbohydrate Polymers*, **60(1),** 39-42.

[119] Cabedo L, Feijoo J.L, Villanueva M.P, Lagaron J.M, Gimenez E (2006), "Optimization of Biodegradable Nanocomposites Based on PLA/PCL Blends for Food Packaging Applications", *Macromolecular Symposia*, **233**, 191-197.

[120] Choi W.Y, Lee C.M (2006), "Development of Biodegradable Hot-Melt Adhesive Based on Poly-ε-Caprolactone and Soy Protein Isolate for Food Packaging System", LWT- *Food Science and Technology*", **39(6),** 591-597.

[121] Haugaard V.K, Danielsen B, Bertelsen G (2003), "Impact of Polylactate and Poly(hydroxybutyrate) on Food Quality", *European Food Research and Technology*, **216(3),** 233-240.

[122] Rhim J.W, Mohanty K.A, Singh S.P, Ng, Perry K.W (2006), "Preparation and Properties of Biodegradable Multilayer Films Based on Soy Protein Isolate and Poly(lactide)", *Industrial & Engineering Chemistry Research*, **45(9),** 3059-3066.

[123] Yamane K, Kawakami Y, Hokari Y, "Biodegradable Multilayered Polyglycolic Acid Resin Sheet", PCT Int. Appl. 2006 WO 2003-JP6704, 22pp.

[124] Wang T, "Biodegradable Laminate Materials Containing Poly(lactic acid) and Polyvinyl Alcohol Outer Layers for Packaging Liquid Food and their Manufacture", 2002 CN 1359790, 6pp.

[125] Sato T, Yamane K, Wakabayashi J, Sato Tomoaki, Suzuki T, "Multilayer Sheet Made of Polyglycolic acid Resin", PCT Int. Appl. 2006 WO 2005-JP11261, 18pp.

[126] Cleveland C.S, Reighard T.S, "Biodegradable Paper-Based Cup or Package and Production Method", U.S. Pat. Appl. Publ.2006 US 2005-221175, 7pp.

[127] Bonutti P.M, "Biodegradable Packaging Materials", U. S. Pat. Appl., Publ. 2005 US 2005-123497, 15pp.

[128] Matsunaga A, Chikamasa N, Yoshida N, "Polylactic Acid-Based Long-Fiber Nonwoven Fabrics, Biodegradable Bags Containing the Same, and Manufacture Thereof", Jpn. Kokai Tokkyo koho 2006 JP 2005-232682, 21 pp.

[129] Sebastien F, Stephane G, Copinet A, Coma V (2006), "Novel Biodegradable Films Made from Chitosan and Poly(lactic acid) with Antifungal Properties Against Mycotoxinogen Strains", *Carbohydrate Polymers*, **65(2),** 185-193.

[130] Nakamura T, Iwazaki K, Kato M, Maruyama I, "Biodegradable Polylactic Acid Multylayer Film and Formation Process thereof", PCT Int. Appl. 2004 WO 2004-JP1236, 17pp.

[131] Wang T, "Composite Material for Packaging Food and its Production Process", 2001 CN 99-125782, 5pp.

[132] Li L, Kerry J.F, Kerry J.P (2005), "Selection of Optimum Extrusion Technology Parameters in the Manufacture of Edible/Biodegradable Packaging Films Derived from Food-Based Polymers", *J. of Food, Agricolture & Environment*, **3(3-4),** 51-58.

[133] Wang L, Shogren R, Carriere C (2000), "Preparation and Properties

of Thermoplastic Starch-Polyester Laminate Sheets by Coextrusion", *Polymer Engineering and Science*, **40(2),** 499-506.

[134] Steinka I, Morawska M, Rutkowska M, Kukulowicz A (2006), "The Influence of Biological Factors on Properties of Some Traditional and New Polymers Used for Fermented Food Packaging", *Journal of Food Engineering*, **77**, 771-775.

[135] Mori H, Iwasaki Y, Kobayashi Y, "Biodagradable Bags for Packaging Foods Available in High-Speed Production", PCT Int. Appl. 2002 WO 2002-JP858, 37pp.

[136] Oksman K, Skrifvars M, Selin J. F (2003), "Natural fibres as reinforcement in polylactic acid (PLA) composites", *Composites Science and Technology*, **63**, 1317-1324.

[137] Balan V., Sousa L. C., Chundawat S. P. S., Vismeh R., Jones A. D., and Dale B.E. (2008), "Mushroom spent straw: a potential substrate for an ethanol-based biorefinery", *J Ind Microbiol Biotechnol*, **35**, 293–301.

[138] Chen T., Breuil C., Carriere S., and Hatton J.V. (1994), *Tappi J.*, **77**, 235.

[139] Doherty W., Halley P., Edye L., Rogers D., Cardona F., Park Y., and Woo T. (2007), "Studies on polymers and composites from lignin and fiber derived from sugar cane", *Polym. Adv. Technol.*, **18,** 673-678.

[140] Gong R., Jin Y., Chen J., Hu Y., and Sun J. (2007), "Removal of basic dyes from aqueous solution by sorption on phosphoric acid modified rice straw", *Dyes and Pigments*, **73**, 332-337.

[141] Habibi Y., El-Zawawy W. K., Ibrahim M. M., Dufresne A. (2008), "Processing and characterization of reinforced polyethylene composites made with lignocellulosic fibers from Egyptian agro-industrial residues", *Composites Science and Technology*, **68**, 1877–1885.

[142] Barkalow D. G., Rowell R. M., and Young R. A. (1989), "A new approach for the production of cellulose acetate: acetylation of mechanical pulp with subsequent isolation of cellulose acetate by differential solubility", *Journal of Applied Polymer Science*, **37**, 1009-1018.

[143] Chen G.Q., Wu Q., Zhao K., Yu H.P., and Chan A. (2000), *Chin J. Polym. Sci.*, **18**, 389.

[144] Edgar K. J., Buchanan C. M., Debenham J. S., Rundquist P. A., Seiler B. D., and Shelton M. C. (2001), "Advances in cellulose ester performance and application", *Progress in Polymer Science*, **26**, 1605-1688.

[145] Gamez S., Gonzalez-Cabriales J. J., Ramirez J. A., Garrote G., and Vazquez M. (2006), *J. Food Eng.*, **74**, 78.

[146] Greco P., and Martuscelli E. (1989), *Polymer*, **30**, 1475.

[147] Inoue Y., and Yoshie N. (1992), *Prog. Polym. Sci.*, **17**, 571.

[148] Liu C.F., Sun R.C., Zhang A.P., and Ren J.L. (2007), *Carbohydrate Polymer*, **68**, 17.

[149] Luo R., Xu K., and Chen G.-Q. (2007), "Study of miscibility, crystallization, mechanical properties, and thermal stability of blends of poly(3-hydroxy butyrate) and poly(3-hydroxy butyrate-*co*-4-hydroxy butyrate)", *Journal of Applied Polymer Science*, **105**, 3402-3408.

[150] Meireles C.dS., Filho G.R., and Nascimento de Assuncao R.M. (2007), *Journal of Applied Polymer Science*, **104**, 909.

[151] Reverley A. (1985), in *Cellulose and its Derivatives*. Ed. J.F. Kennedy. Ellis Horwood, Chichester, Ch. 17, p. 211.

[152] Rodringues J. A. F. R., Parra D. F., and Lugao A. B. (2005), *J. Therm. Anal. Cal.*, **79,** 379.

[153] Sarrouh B. F., Silva S. S., Santos D. T., and Converti A. (2007), *Chem. Eng. Technol.*, **30**, 270.

[154] Steinmeier H. (2004), "Acetate manufacturing, process, and technology", *Macromolecular Symposia*, **208**, 49-60.

[155] Yang H., Li Z.S., Lu Z.Y., and Sun C.C. (2005), *Eur. Polym. J.*, **41**, 2956.

[156] Xu S., Luo R., Wu L., Xu K., Chen G.-Q. (2006), "Blending and characterizations of microbial poly(3-hydroxybutyrate) with dendrimers"**,** *Journal of Applied Polymer Science*, **102(4),** 3782-3790.

[157] Das P., Ganesh A,. and Wangikar P. (2004), Biomass and Bioenergy, **27,** 445-457.

[158] Philip S., Keshavarz T., Roy I (2007), "Polyhydroxyalkanoates: biodegradable polymers with a range of applications", *Journal of Chemical Technology and Biotechnology,* **82,** 233-247.

[159] Turning a Liability into an Asset: Landfill Methane Utilisation Potential in India, August 2008.

[160] LeVan S. L (1989), In: Schniewind, Arno P., ed. Concise Encyclopedia of Wood & Wood –Based Materials. Ist edition. Elmsford, NY: Pergamon Press: 271-273

[161] Alvarez V.A, Vazquez A (2004), "Thermal degradation of cellulose derivatives/starch blends and sisal fibre biocomposites", *Polymer Degradation and Stability*, **84**, 13-21.

[162] Sun J.X, Sun X.F, Sun R.C, Su Y.Q (2004), "Fractional extraction and structural characterization of sugarcane bagasse hemicelluloses", Carbohydrate Polymers, **56**, 195-204.

[163] Angelidaki I., Ellegaard L., Kioer Ahring B. (2003), "Applications of the Anaerobic Digestion Process'', *Advances in Biochemical Engineering/Biotechnology*, **82**, 1-33.

[164] Briassoulis D. (2004), ''An Overview on the Mechanical Behaviour of Biodegradable Agricultural Films'', *Journal of Polymers and the Environment*, **12**, 65-81.

[165] Narayan R., www.msu.edu/user/narayan.

[166] Functional Material Solutions 2007, 2008, 2009, 2010. Editor: Jari Koskinen, Graphic Design: Tuija Soininen, Copyright: VTT Technical Research Centre of Finland 2008.

[167] Grima S., Bellon-Maurel V., Feuilloley P., Silvestre F. (2002), ''Aerobic Biodegradation of Polymers in Solid-State Conditions: A Review of Environmental and Physicochemical Parameter Settings in Laboratory Simulations'', *Journal of Polymers and the Environment*, **8(4)**, 183-195.

[168] Gopinathan M. C., Sudhakaran R. (2009), ''Biofuels: opportunities and challenges in India'', *In Vitro Cell. Dev. Biol.-Plan*, **45**, 350-371.

[169] Rutz D.; Janseen R. Biofuel technology handbook. WIP Renewable Energies, Munich 2007.

[170] FAO (Food and Agriculture Organization) The state of food and agriculture 2008: Biofuels: Prospects, risks and opportunities. FAO, Rome2008.

[171] Martinot E. Renewables 2007—global status report.

[172] Dufey, A. (2006),''Biofuels production, trade and sustainable development: Emerging issues'', *Sustainable Markets Discussion Paper No. 2.*

[173] Koplow D. (2007), ''Biofuels—at what cost? Government support for ethanol and bio-diesel in the United States: 2007 update''. Global subsidies initiative of the International Institute for Sustainable Development.

[174] Kutas G.; Lindberg C.; Steenblik R. (2007), ''Biofuels—at what cost? Government support for ethanol and bio-diesel in the European

Union: 2007 update''. Global subsidies initiative of the International Institute for Sustainable Development.

[175] Steenblik R. (2007), ''Biofuels—at what cost? Government support for ethanol and bio-diesel in selected OECD countries: 2007 update''.

[176] Bailey, R. (2008), ''Another inconvenient truth''. *Oxfam briefing paper*. http://www.oxfam.org/pressroom/press release/2008-06-25/another-inconvenient-truth-biofuels-are-notanswer.

[177] IEA (International Energy Agency) World energy outlook 2007: China and India insights. OECD/IEA, Paris; 2007b. http://www. iea.org/textbase/npsum/WEO2007SUM.pdf.

[178] Worldwatch Institute Biofuels for transportation: Global potential and implications for sustainable agriculture and energy in the 21st century. Worldwatch Institute, Washington, DC; 2007. http://www.worldwatch.org/node/4078.

[179] Mitchell, D. (2008), ''A note on rising food prices. Policy research working paper, 4682''. The World Bank, Development Prospects Group; 2008. http://www wds.worldbank.org/external/default/WDSContentServer/WDSP/IB/2008/07/28/000020439_20080728103002/Rendered/PDF/WP4682.pdf.

[180] Searchinger T.; Heimlich R.; Houghton R. H.; Dong F.; Elobeid A.; Fabiosa J.; Togkoz S.; Hayes D.; Yu T. (2008), ''Use of US croplands for biofuels increases greenhouse gases through emissions from land use change''. *Science*, **319**, 1238–1240.

[181] World Bank Rising food prices: Policy options and World Bank response. World Bank, New York; 2008 http://siteresources.worldbank.org/NEWS/Resources/risingfoodprices_backgroundnote_apr08.pdf.

[182] Dufey A.; Vermeulen S.; Vorley B. (2007), ‘’Biofuels: Strategic choices for commodity dependent developing countries’’. Common Fund for Commodities, Amsterdam2007.

[183] Banse M.; Nowicki P.; Van Meijl H. (2008), ‘’Why are current food prices so high. In: Zuurbier P.; Van de Vooren J. (eds) Sugarcane ethanol: Contributions to climate change mitigation and the environment. Wageningen Academic, Wageningen, pp 227–248. http://library.wur.nl/way/bestanden/clc/1880664.pdf.

[184] DEFRA (Department for Environment, food and Rural Affairs) A sustainability analysis of the Brazilian Ethanol, UNICAMP www.unica.com.br/download.asp?mmdCode=1A3D48D9-99E6-4B81-A863-5B9837E9FE39; 2008.

[185] UNICA Sugarcane in Brazil sustainable energy and climate. UNICA, São Paulo; 2008a. http://english.unica.com.br/multimedia. UNICA Brazilian sugarcane ethanol: Get the facts rights and kill the myths. UNICA, São Paulo; 2008b. http://www.unica.com.br/download.asp.

[186] IEA (International Energy Agency) Renewables in global energy supply: An IEA fact sheet. OECD/IEA, Paris; 2007a. Available at: http://iea.org/textbase/papers/2006/renewable_factsheet.pdf.

[187] Swain S. N., Biswal S. M., Nanda P. K., Nayak P. L. (2004), ‘’Biodegradable Soy-Based Plastics: Opportunities and Challenges’’, *Journal of Polymers and the Environment*, **12(1)**, 35-42.

[188] Philip S., Keshavarz T., Roy I. (2007), ‘’Polyhydroxyalkanoates: biodegradable polymers with a range of applications’’, *Journal of Chemical Technology and Biotechnology,* **82**, 233-247.

[189] Wang Y.Z., Yang K.K., Wang X.L., Zhou Q., Zheng C.Y., Chen Z.F. (2004), ‘’Agricultural Application and Environmental Degradation of Photo-Biodegradable Polyethylene Mulching Films’’, *Journal of Polymers and the Environment,* **12(1)**, 7-10.

[190] Plastics Additives & Compounding September/October 2006, pp. 22-25.

[191] Ahmad M. (2004), ''Thermoplastic micro-spheres as foaming agents for wood plastic composites'', WPC 2004 Conference, Vienna, Austria.

[192] Plastics Additives & Compounding May 2002, pp.24-26.
www.epieurope.com/en/chemical-foaming-agents.php

[193] www.colormatrix.com/en/products/foaming-agents.html

[194] ''Protein foaming agent GreenFroth for light weight cellular concrete for foamed concrete'', www.greenfroth.com/index.php

[195] US Patent 5643510-''Producing foamed gypsum board using a foaming agent blend'',

[196] www.patentstorm.us/patents/5643510/fulltext.html

[197] http://njzhulijiang.en.made-in-china.com/product/ybOnJmdxVG

[198] www.westsenior.co.uk/additiveBlends.aspx

[199] ''OnCap Chemical Foaming Agents'', www.polyone.com

[200] Foaming Agents by Alqemia Group

[201] ''MILLIFOAM: Gypsum Foaming Agents'', www.huntsman.com

[202] AQF-2^{TM} Foaming Agent

[203] http//old.finintertrade.ru/en/materials/foaming/

[204] Choy et al., US Patent 4548649

[205] www.dr-luca.de/web/en/foaming_agent/

[206] www.lioncopolymer.com/prods_foamers.html

[207] ''Effervescent Technology Primer''.

[208] Lee R. E., ''Effervescent Tablets: Key Facts about Unique, Effective Dosage Form'', *Amerilab Technologies*.

[209] www.pharmpedia.com

[210] www.pharmpedia.com

[211] www.gea-ps.com/npsportal/cmsdoc.nsf/WebDoc/ndkw74tg54

[212,213] Smith M. W., ''Utilization of Effervescent Spray Technology to Eliminate Volatile and toxic Diluents'', *Science & Engineering: Adhesive Materials & Processes*, pp.5-10.

[214] ''Pearl Calcium Effervescent Tablets'', www.tootoo.com/d-rp11897375-Pearl_Calcium_Effervescent

[215] ''LiFizz- Effervescent Calcium Plus D-Strawberry Flavored'' www.zooscape.com/cgi-bin/maitred/GreenCanyon/questp4

[216] ''Tubes make effervescent energy tablets portable for consumers'', (2008), www.healthcare-packaging.com/archives/2008/01/tubes_m

[217] Zhang P., Li G.C., Zhang H.P., Yang L.C., Wu Y.P. (2009), ,'Preparation of porous polymer electrolyte by a microwave assisted effervescent disintegrable reaction'', *Electrochemistry Communications*, **11**, 161-164.

[218] ''Effervescent Plastics Promise More With Less'' http://blog.ecolect.net/2008/11/effervescent-plastics-promise-more

[219] ''Look for cooperation on erythritol effervescent tablets'' www.1biw.com/pj_view.aspx?id=6987

[220] ''Effervescent Chlorine Disinfectant Tablet'' www.made-in-china.com/china-products/productviewOiJn

[221] ''Investigation of an effervescent additive as porogenic agent for bone cement macroporosity'' www.find-health-articles.com/rec_pub_17264385-investigation

[222] ''Effervescent Dosage Manufacturing'' http://pharmtech.findpharma.com/pharmtech/Analytical/Effervescent

[223] ''Effervescent Creatine vs. Creatine Monohydrate'' www.illpumpyouup.com/articles/effervescent-creatine-vs-cre

[224] ''The value range'', www.oystar.manesty.com

[225] Wiwattanapatapee R., Chumthong A., Pengnoo A.,

Kanjanamaneesathian M., (2007), ‘’Effervescent fast-disintegrating bacterial formulation for biological control of rice sheath blight’’, *Journal of Controlled Release*, **119**, 229-235.

[226] Jakus J., Kriska T., Vanyur R., (2002), ’’Effect of multivitamins in an effervescent preparation on the respiratory burst of peritoneal macrophages in mice’’, *British Journal of Nutrition*, **87**, 501-508.

[227] Liang Z., Jingdong Y., Yibing H., Gang Z., (2004), ‘’Technological Research on Bioflavonoid Effervescent Tablet of Tartary Buckwheat’’, *Section F: Nutrition and Pharmacy*, pp.563-566.

[228] Li X. D., Pan W. S., Nie S. F., Wu L. J., (2004),’Studies on controlled release effervescent osmotic pump tablets from Traditional Chinese Medicine Compound Recipe’’, *Journal of Controlled Release*, **96**, 359-367.

[229] (WO/2004/020570) ‘’Effervescent Hot Tablet’’, www.wipo.int/pctdb/en/wo.jsp?WO=20044020570&IA=WO

[230] US Patent Office 2,999,293, patented Sept. 12, 1961

[231] (WO/2000/040688) ‘’Drain Cleaner’’, www.wipo.int/pctdb/en/wo.jsp?wo=2000040688&IA=US2

[232] ‘’Use of an effervescent product to clean soiled dishes by hand washing’’ www.freshpatent.com/Use-of-an-effervescent-product-to-cl

[233] Akiyama M., Tsuge T., Y. Doi Y., (2003), ‘Environmental life cycle comparison of polyhydroxyalkanoates produced from renewable carbon resources by bacterial fermentation’, *Polym. Degrad. Stab.*, **80**, 183.

[234] Harding K. G., Dennis J. S., Blottnitz H., Harrison S. T. L, (2007), *J. Biotechnol.*, **130**, 57.

[235] Harrison S.T.L., ‘*The Extraction and Purification of Alicaligens Eutrophus*, PhD Dissertation, Cambridge University (1990).

[236] Petkovica G., Engelsen C. J., Haoyad A. O., Breedveld G., (2004), 'Environmental impact from the use of recycled materials in road construction: a method for decision making in Norway', *Resources, Conservation and Recycling*, **42**, 249-264.

[237] Kim J., Yun S., Ounaies Z., (2006), 'Discovery of cellulose as a smart material', *Macromolecules*, **39**, 4202-4206.

[238] La Scala J., Wool R. P., (2005), 'Property analysis of triglyceride-based thermosets', *Polymer*, **46**, 61–69.

[239] Bansil R, Hermann HJ, Stauffer D., (1984), *Macromolecules*, **17**, 998–1004.

[240] Sahimi M, Arbabi S., (1993), Phys Rev B;**47**:703–12.